Effect of Inert Gas Discharge Time on Wood Crib Fires in Reduced-Scale and Full-Scale Experiments

by

Jonathan Zimak

A Thesis

Submitted to the Faculty

of the

WORCESTER POLYTECHNIC INSTITUTE

In partial fulfillment of the requirements for the

Degree of Master of Science

in

Fire Protection Engineering

April 2022

APPROVED:

_____

Professor Albert Simeoni, Major Thesis Adviser and Head of Department

_____

Professor Milosh Puchovsky, Major Thesis Adviser

_____

Professor James Urban, Committee Member

Abstract

Currently, the UL 2127, *Inert Gas Clean Agent Extinguishing System Units*, and FM 5600, *Clean Agent Extinguishing Systems*, standards are used to test inert gas suppression systems and to determine the minimum extinguishing concentration (MEC) for total-flooding suppression system applications. For Class A ordinary solid combustible test articles, both UL and FM standards follow equivalent methodologies; only UL will be referred to for brevity. In this standardized test, the article is placed within a 100 m^3 enclosure, burned, subjected to a suppression event over a certain discharge period, and then allowed to soak for 10 minutes before exposure to fresh air, checking for reignition, to determine the required MEC. The UL wood crib was selected as the sole test article to study over the UL plastic sheet arrays to simplify testing requirements and facilitate the study of re-ignition potential at the longer discharge period.

In 2012, the NFPA 2001, *Standard on Clean Agent Fire Extinguishing Systems*, was revised to allow a maximum 120 s discharge period for systems that protect Class A fire hazards with inert gases. Preliminary tests conducted using Class A articles indicate that this change in discharge period can potentially change the suppression dynamics, resulting in different listed MECs, and created confusion in the inert gas industry. Confusion around these changes and results arises from two primary sources. The first being the requirements of the UL 2127 only to achieve crib extinguishment and reignition prevention. The second is the issue where the selected discharge period is not reported on test results. By not publicizing the discharge period, it is impossible to understand if a lower listed value for MEC is due to a design advantage or from a change in extinction dynamics between the two discharge periods. To answer these questions and provide more clarity to the inert gas industry, the underlying physics of the extinction dynamics within the test enclosure and near the burning test article must be better understood.

In this work, a series of full-scale experiments were conducted to study the effect of discharge time over the extinction of a Class A test article following the methodology presented in the UL 2127 standard. During these experiments, the instrumentation was increased above UL requirements to capture the evolution of the article's mass and changes in the oxygen content, gas velocity, and temperature in the atmosphere that surrounds it. Additionally, a novel ¼ scale enclosure and crib were designed to replicate the full-scale suppression dynamics with significantly reduced resource demands for testing. The scaling of the crib was performed following the method proposed by Heskestad and Croce et al. The reduced-scale enclosure was designed such that the only change in burning rate would be from the discharge event itself.

The results obtained support the hypothesis that the fundamental changes in the suppression dynamics are caused by recirculating flows of agent and entrained air created during the high-pressure discharge. The impact of these recirculating flows, designated as bulk flows, alters the dynamics of the suppression event. The bulk flow effects, quantified by gas-phase velocity through the crib, were dependent on the agent discharge flow rate and were most prevalent at the full-scale test and 60 s discharge periods.

Furthermore, the change in discharge time from 60 to 120 s had a negligible effect on the average agent extinguishment concentration at both scales. No crib at either scale or discharge period reignited after suppression or when exposed to fresh air after the prescribed 10-minute soak period. The constant agent extinguishing concentration results indicate that any differences between approved and listed MEC are likely not related to the discharge period selection.

Acknowledgments

I would like to express my very great appreciation to my thesis advisors, Professor Albert Simeoni and Professor Milosh Puchovsky, for their guidance, mentorship, and intellectual expertise, and to Professor James Urban for participating as part of the evaluation committee. I also would like to thank, Ray Ranellone, Fredrick Brokaw, and Peter Guertin for their laboratory and construction support. Thanks to the entire WPI postdoc and student team who provided feedback at every stage of the project including Juan Cuevas, Ahmed O'Said, Reza Ziazi, Muthu Kumaran, Abhinandan Singh, and Weixuan Gong. Not without work!

Special thanks to Kidde-Fenwal Inc. for providing the topic of study, financially supporting the project, and for providing a team of experts to collaborate with including Jamie Pierce, Joe Senecal, Richard Lupien, Fred Penden, Peter Stokes, Mike Sandford, and John Kliem.

Table of Contents

List of Tables

List of Figures

List of Figures (cont.)

List of Figures (cont.)

List of Variables and Abbreviations

Variables and Greek Symbols	
A	area (m^2)
b	stick thickness (cm)
B	B number (-)
c	wood species constant (mg/ s $cm^{-1.5}$)
C	constant (-), coefficient (-), heat capacity (J/K), concentration (% Vol)
f	friction factor (.13)
F	ratio of the thermal diffusivity of Douglas-fir to the wood tested (-)
g	acceleration due to gravity (cm/s^2)
G	modified Froude number, crib geometry factor (-)
h	heat transfer coefficient (W/m^2K), height (m)
H	enclosure height (m), heat-transfer coefficient with mass flux (W/m^2K)
k	ratio of the mass flux of gases leaving to the mass flux entering a volume (-), thermal conductivity (W/m K), heat ratio (C_P/C_v)
K	agent-specific parameter (-)
K1	IG-100 constant (0.7997)
K2	IG-100 constants (.002927)
l	stick length (cm)
m	mass (kg or g)
n	number of sticks per layer (-)
N	number of Layers of sticks (-)
Nu	Nusselt number (-)
O_2	volume percent oxygen concentration (% Vol)
P	pressure (Pa), perimeter = 4S (cm)
Pr	Prandial number (-)
r	ratio (-)
R	gas law constant (8.314 J/mol K)
Re	Renolds number (-)
S	spacing between sticks (cm)
t	time since ignition (s)
Δt	discharge period (s)
T	temperature (K or ºC)
v	velocity (m/s)
v	stoichiometric coefficient of oxygen in the balanced chemical Eq. (-)
V	volume (m^3)
w	mass flowrate through the orifice (kg/s)
X	inert gas concentration (volume percent)
ε	emissivity (.25)
σ	Stefan–Boltzmann constant ($5.670\times10{-}8$ $W\cdot m^{-2}\cdot K^{-4}$)
λ	ratio of mass flux of fuel and products leaving to mass flux of air entering (-)
γ	fuel-to-air mass ratio for the gaseous reactions that take place in the crib (-)
Ψ	drag coefficient (-)
ρ	density (g/cm^3)

Variables and Greek Symbols (cont.)	
τ	characteristic response time for a thermocouple (s)
u	dynamic viscosity (N s/m^2 *10-6)
φ	porosity factor (cm$^{-1.1}$ or cm)

Subscripts	
V	ventilation opening
S	exposed surface of the wooden sticks
v	vertical shafts in the crib, vent
sp	Spalding's B number
p	constant pressure
g	gas
d	discharge
a	agent
c	crib, crib shafts, critical
tc	thermocouple
CF	critical flow
o	initial condition
(f)	final
(s)	starting
eq	equivalence
E	enclosure
s	gas specific
TC	thermocouple
$Gross$	Gross' porosity
Heskestad	Heskestad's porosity

Superscripts	
$\dot{()}$	Per unit time

Abbreviations	
AP	agent parameter (-)
DIOM	Design, Installation, Operation, and Maintenance Manual
fn	A function of
HRR	Het release rate
LPC	Loss Prevention Council
SFPE	Society of Fire Protection Engineers
MC	Moisture content
MLR	Mass loss rate
NFPA	National Fire Protection Association
UL	Underwriters Laboratory
WPI	Worcester Polytechnic Institute

1.0 Introduction

Water-based fire suppression systems such as sprinklers and water sprays are not suitable for use in all types of occupancies. This incompatibility is often due to the chemical nature of the protected assets or when the cost of damage due to discharged water is too high [1]. Total flooding clean agents are often used in these scenarios. These agents are electrically nonconducting and leave no residue after discharge.

Halon 1301 was used as the main fire suppression agent until 1993 when the Montreal Protocol banned ozone-depleting agents. Since its ban, 15 major clean agents have been commercialized for firefighting purposes as a replacement to halon, with 8 approved for use in normally occupied spaces including the inert gas IG-100, nitrogen. Nitrogen poses significant advantages as a halon replacement, as it is naturally occurring, has zero global warming potential, and does not thermally decompose [2]. Nitrogen suppression research is becoming more popular in support of the airline industry as it phases out the installation of halon fixed fire suppression systems in new aircraft cargo compartments by 2040 [3]. Nitrogen has also been recently studied for use in hybrid extinguishing systems combined with water mist sprays [4].

The two common extinction mechanisms for clean agent suppression are oxygen and temperature reduction [5]. During the discharge of the suppressing agent, there is a reduction in the oxygen concentration Halocarbon clean agents like Halon 1301 suppress fires through a combination of chemical and physical mechanisms that reduce the flame temperature below levels required to continue the combustion reaction [1]. Inert gasses such as Nitrogen and Argon extinguish fires by reducing the oxygen concentration below the required flammability limit. This decrease of oxygen is accompanied by an increase of the agent species which increases the heat capacity of the local atmosphere, eventually reducing the flame temperature below sustainable

levels. The agent quantity needed to suppress combustion is the minimum extinguishing concentration (MEC) and is often defined as the minimum concentration of inert gas necessary to suppress a cup-burner flame [6–8]. The MEC is then used by system manufacturers as a baseline to define the design concentrations for suppression systems designed to protect a variety of different commodity classifications [7].

Currently, inert gas suppression systems are tested in a 100 m^3 enclosure as per UL 2127, *Inert Gas Clean Agent Extinguishing System Units*, and FM 5600, *Clean Agent Extinguishing Systems,* to determine an appropriate minimum agent extinguishing concentration used for the design of the installed systems [9,10]. The UL 2127 Standard and FM 5600 Standard test inert gas system discharges in the same manner. The two extinguishing test methods are assumed to be equivalent through this thesis and the name UL 2127 is used for brevity.

When first issued in 1997 the UL 2127 Standard tested inert gas extinguishing systems over a strict 60 s discharge period as required by NFPA 2001, *Standard on Clean Agent Fire Extinguishing Systems* [9]. In 2012, NFPA 2001 changed its requirements to allow a maximum 120 s discharge period to reduce overpressure effects, nozzle noise, and required installation pipe schedule [7]. Currently, system manufacturers have been allowed to choose the time it takes to release the suppressing agent to typically be either 60 s or 120 s per NFPA 2001. The change in discharge time has led to testing results that surprise industry experts, including the project sponsor Kidde-Fenwal Inc., and create confusion in the inert gas industry.

The confusion arises from two main sources. The first source of confusion revolves around the requirements of the UL 2127 Class A extinguishing tests which only requires extinction of a test article and confirmation that the test article is no longer a threat after exposure to fresh air. By only looking at these two metrics, the intermediary extinction dynamics are often overlooked in

favor of finding better solutions to pass the UL 2127 tests. The second is an issue that arises in the reporting of the approved MEC where the discharge duration is not reported. By not publicizing the discharge period, it is impossible to understand if a lower listed value for MEC is due to a commercial system design advantage or from a shift in extinction dynamics that changes between the two discharge periods. To answer these questions and provide more clarity to the inert gas industry, the underlying physics of the extinction dynamics must be better understood within the test enclosure and near the combusting test article.

The UL 2127 test utilizes 4 types of test articles for Class A fires, the wood crib and three different plastic sheet arrays. To successfully pass the extinguishing test, all four articles must be tested and extinguished. For simplicity, only one type of test article was selected for study, the wood crib. Wood cribs were selected over the plastic sheet arrays because they are inexpensive and exhibit both flaming and smoldering combustion, making it highly effective as a surrogate for real-world materials in testing [11].The use of wood cribs presents the unique protection goal of requiring suppression and reignition prevention, unlike the plastic sheet arrays which are not monitored for reignition per the UL 2127 test method [9]. At the time of test article selection, wood crib reignition was hypothesized to be a major contributing factor to the test result discrepancy between discharge periods due to assumed larger agent leakage at the longer discharge period. [2]

Wood cribs often reach a quasi-steady state burning rate quickly and maintain it for a large portion of the burn [12]. Wood cribs are much better test articles than a simple pile of sticks as methodical stacking allows for a greater surface and burning area. The constant stick spacing allows for an increase in ventilation area and oxygen flow into the crib. The multitude of adjacent stick members allow for sufficient stick to stick reradiation which creates a period of constant heat release rate controlled by the stick spacing [13]. Because of their burning characteristics,

versatility, and reproducibility, wood cribs have become a favorite test article for various types of fire testing [14]. Additionally, there is an abundance of available literature on wood cribs dating back to the 1930's to support scaling [13,15–23].

Two drawbacks of the full-scale UL 2127 extinguishing test are its size and resource requirements. The 100 m^3 enclosure is logistically impractical for many laboratories and each test requires the discharge of 3 very large (120 kg) compressed gas cylinders. Running many of these tests would create numerous logistical and resourcing issues which would reduce efficiency and prevent the study of all the parameters of interest. Because of these issues, the decision was made to draw on the available literature of wood cribs and scale down the crib and enclosure. The scaled enclosure and crib are intended to create an efficient extinguishing test data collection method that is representative of the full scale.

The goals of this thesis are twofold. The first one is to identify the extinction dynamic differences between a 60-s and 120-s discharge period and analyze the effects of different discharge times on the agent extinguishing concentrations. To study the extinction dynamics, a variety of additional instrumentation such as thermocouples and gas phase velocity sensors will be placed in the near field of the wood crib to record how the agent interacts with the burning wood crib during discharge.

The second objective is to validate the use of a reduced-scale crib and enclosure for replicability of the full-scale and applicability for future testing. The reduced scale crib and enclosure will drastically reduce the resource demands and allow a greater range of variables to be studied. Additionally, the design of a reduced scale test will potentially be a powerful tool for the entire clean agent community.

2.0 Literature Review

The literature review section contains eight subsections dedicated to wood cribs including three additional subsections for mass loss rate calculation methods that will be used during the scaling analysis. The UL 2127 and FM 5600 extinguishment tests are described at the end of this section.

2.1 Wood Cribs: A General Overview

Wood cribs are an array of regular, three-dimensional sticks, as depicted below in Fig. 1. Each stick has a square cross-section, b, and a length, l, significantly larger than its thickness [24]. The sticks are arranged with uniform edge-to-edge spacing on each layer, S. Each layer is laid 90 degrees, as shown below, to the previous layer and often attached with a staple or nail to prevent the sticks from moving during testing [9]. The total number of layers, N, defines how tall the crib will be.

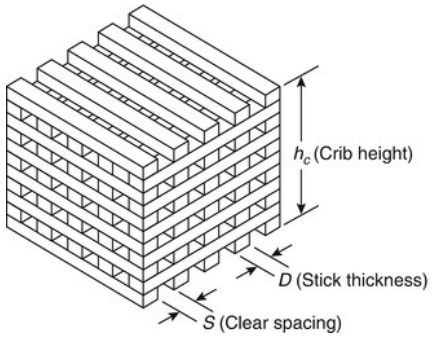

Figure 1: A wood crib three-dimensional view, extracted from [24]

The burning rate of wood cribs is based on the physical makeup of the wood sticks, wood crib construction, ignition characteristics, and the enclosure variables [25]. The physical makeup of the wood sticks includes moisture content, dimension, and type of wood. The wood crib construction defines the effective combustion surface area and includes factors such as how many sticks, how close the sticks are, and the number of layers. Ignition characteristics include where, how, and over

what period the crib is ignited. Enclosure variables can include enclosure geometry, air supply, ventilation parameters, external reradiation effects, and atmospheric oxygen content.

Wood cribs are described as porous fuels. As such, the heat and mass transfer that accompanies the combustion process occurs both within the crib's boundaries and above the crib [11]. Advective transport, or bulk motion transportation, allows the crib to transfer products of combustion as a burning front within the crib from bottom to top. As the crib burns, atmospheric air is drawn into the crib, mixes and supports the combustion reaction, and then is carried upward by buoyancy through the vertical shafts and exhausted at the top of the crib, as shown in Fig. 2 below. While traveling up the vertical shafts, the hot gasses transfer heat to other crib members which aid in the further pyrolysis of more fuels [11]. This gas exchange phenomenon is restricted by the porosity of the crib, discussed later. The products of combustion are transported through convection and radiation to the surrounding atmosphere and enclosure once out of the crib.

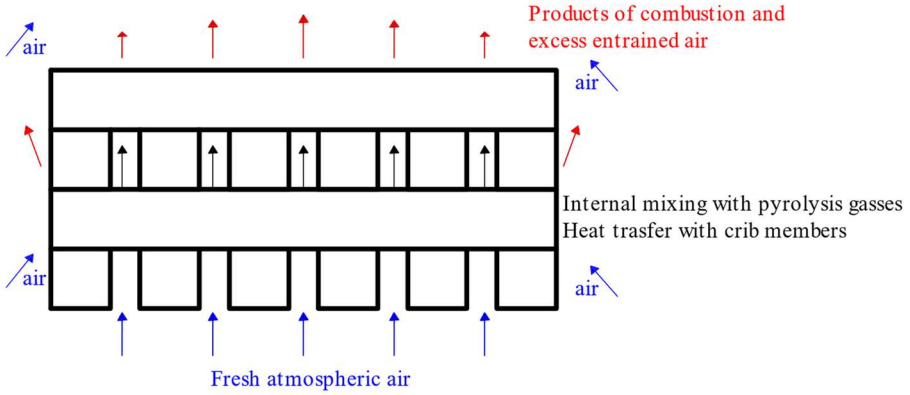

Figure 2: Crib burning visualization.

As the cribs can self-sustain combustion, there is no need for external heat or radiant energy sources once ignited [12]. A well-designed wood crib has a marked advantage over a simple pile of sticks as its increased surface area allows for a greater burning area and more reradiation which

can be controlled by selection of stick spacing [13]. Wood cribs often reach a quasi-steady state burning rate quickly and maintain the burning rate for a large portion of the burn as shown by the constant slop of the crib mass 200 s after the pan fire subsides to 800 s where the first crib members start to fall from the test stand with a straight line fit over this period in Fig. 3, below. Because of the burning characteristics, versatility, and reproducibility, wood cribs became a favorite test article for various types of fire testing [7,9,13,26].

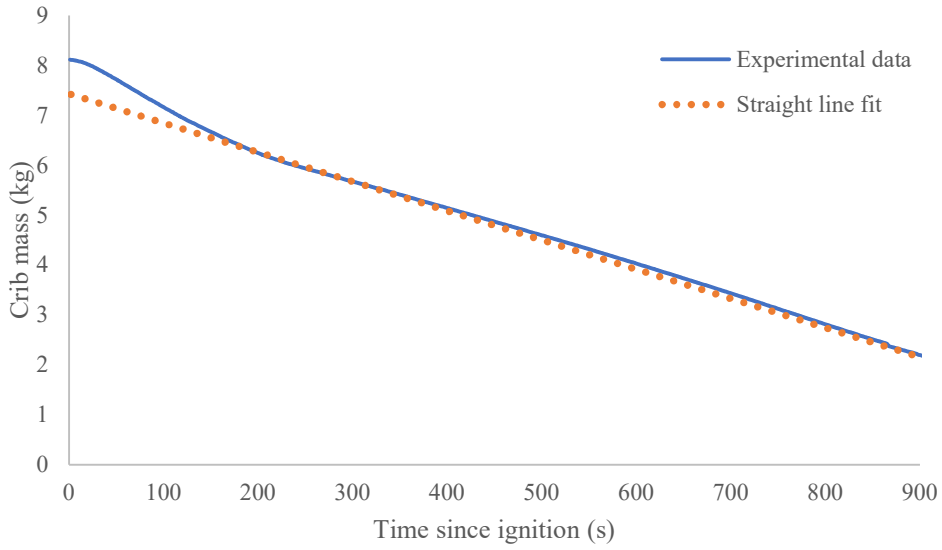

Figure 3: UL 2127 full scale crib mass for an example free burning test

2.2 Wood Crib Use as Test Articles

Wood cribs are used in a variety of test methods and experimental designs as they offer a well-studied, cheap, and reproducible source for heat, radiation, and smoke that is often representative of common fire threats. Often, the tests will look to standardize some variables such as construction, moisture, mass, or durability based on the objectives and intent of the test.

The National Fire Protection Association references the term “wood crib” in 25 of its Codes, Standards, and Guides available online, often in annex text, because of the previously

mentioned desirable characteristics. Noteworthy references include NFPA 13: *Standard for the Installation of Sprinkler Systems*, 2016 Edition states that sprinklers intended to protect specific hazards or construction features are only allowed if they are evaluated against an intended hazard, typically a 350 lb (159 kg) wood crib [27]. NFPA 502: *Standard for Road Tunnels, Bridges, and Other Limited Access Highways*, 2017 Edition references wood crib tests conducted in the Netherlands to provide designers with sample historical data [28]. In these tests, wood cribs were loaded into vehicles to assess the effectiveness of sprinklers during a tunnel fire scenario involving various vehicles. NFPA 251: *Standard Methods of Tests of Fire Resistance of Building Construction and Materials* previously required a 1285 lb (583 kg) wood crib that created a uniform time-temperature exposure on interior walls [29]. This test was later retired and replaced by the gas heater of ASTM E119 and UL 263 [30].

Underwriters Laboratory, UL, uses wood cribs in three standards: UL 711, UL 1626, and UL 1715, as sources of standardized combustion products in addition to UL 2127 which is discussed in detail later. UL 711, *Rating and Fire Testing of Fire Extinguishers*, tests portable fire extinguishers against wood cribs [31]. The cribs are specifically sized and arranged to create a fire threat that must be extinguished by the fire extinguisher before it's empty. The test is unique as it requires that a certain percentage of the crib's total mass is lost before the extinguisher is operated. The specified mass loss percentage ensures a uniform and reproducible fire threat to test extinguishers against. UL 1626, *Residential Sprinklers for Fire Protection Service*, uses a 2.5 to 3.2 kg crib comprised of 4 layers of 4 boards [32]. Unique to this test is the conditioning of the crib before ignition, as it is required to be conditioned in a 104 ^{o}C chamber for 24 to 72 h and then placed in a plastic bag for 4 h to return to ambient temperature. The conditioning ensures both constant moisture content and prevents excess energy from the heated

wood members from creating discrepancies in the burning rate. UL 1715, *Standard for Fire Test of Interior Finish Material,* utilizes an exactly 30-lb (13.6 kg) 10-tiered wood crib cured at 120 ºF (49 ºC) until at a constant weight [33]. Conditioned strips are added to the crib to ensure the 30-lb limit is met. Unique to this test is the specified method of fastening the wood members together. The Standard specifically calls for 8d nails or 1.25-by-1-inch staples to hold the wood member together whereas most other standards just mention that the cribs must be held together with no further details provided. Additionally, this crib is not ignited by a pool fire like the previously mentioned test, but rather by a pound of fluffed, shredded wood excelsior with 4 oz (3 mL) of ethyl alcohol.

2.3 Wood Crib Ignition

The crib ignition for suppression testing is only important to bring the crib to a steady state burning rate quickly and repeatably. Ignition method of the crib depends on the test method and criteria of the study. Often, cribs are ignited with a small pan of flammable liquids, sized to accomplish the test goals of ignition. Such ignition has occurred at the crib edges, the crib center, and the crib base center to study flame propagation and growth rates [16,17,21]. In some methods, the whole crib can be submerged into a flammable liquid and allowed to drain [20]. Additionally, small cribs may be stuffed with acetone or other flammable liquid-soaked cotton balls that are evenly distributed throughout the crib.

A large pan can be used for a uniform ignition when the initial growth rate in the crib is not of concern such as when the crib is used for extinguishment testing [9,10]. A uniform ignition will cause the entire crib to ignite within the smallest window possible.

2.4 Wood Crib Mass Loss Rate Calculations

The following models for burning rate, mass loss of the test article per unit time, or MLR in an enclosure. Often, the enclosure involved a vent, and the cribs were used to study the burning rate as affected by a vent at some height. Such is the case with the Gross, Block, and Heskestad models [13,15,26]. Each of these three models utilizes a porosity factor, or ratio of open spaces to spaces occupied by the wooden sticks. Additionally, these models are independent of time and are used to calculate a steady state burning rate.

Babrauskas investigated different burning rates in three distinct regimes: surface control, porosity control, and ventilation control. A factor for each regime is calculated and the smallest of the regimes controls the burning rate. Additionally, the Babrauskas' model allows the integration of the time variable for unsteady state burning. While these models predict burning rates in an enclosure or in the open, Babrauskas et al. mention that there is little difference in burning rate when not enclosure ventilation controlled [24]. Therefore, if adequate enclosure ventilation exists, as in the UL 2127 test method, a wood crib burning in an enclosure will exhibit the same behavior as one burning in the open. This is especially true for smaller fires.

McAllister and Finney [19,20] investigated burning rate based solely on porosity. Their test included a multitude of cribs at a constant Heskestad porosity with varying L/b values and geometries. They concluded that the Heskestad correlation is best suited for wood cribs with stick thicknesses of 0.32 cm ($1/8^{th}$ an inch) or greater as the Block model of porosity both was less accurate at predicting their collected data.

2.4.1 Gross's Model

One of the first studies of burring rate for wood cribs was accomplished by Gross [13]. Gross used kiln-dried grade D Douglas Fir lumber with a moisture content of around 9.2%. Each

of the cribs was typically 10 levels high and had a stick length equal to 10 times the stick width. Heptane or alcohol was used to ignite the cribs such that the ratio of fuel rate to crib weight was 8%. This allowed the liquid to completely burn before heavily influencing the wood crib burning rate.

Gross identified that for some wood cribs the burning rate is determined by the rate of gas exchange into and out of the crib [13]. This factor was defined as the porosity factor, φ and is the ratio of actual to theoretical rates of airflow. The theoretical airflow rate was assumed to be proportional to the rate of volume change and the actual gas velocity exchanged in the crib is proportional to the square root of the heigh of a pile. This relationship was defined below, in Eq. 1.

$$\varphi_{Gross} = \frac{actual\ air\ flow}{theoretica\ \ air\ flow} = N^{.5} b^{1.1} \frac{A_v}{A_s} \qquad Eq.\ 1$$

The total exposed surface area of the sticks, A_s, can be calculated below [13,18].

$$A_s = 4blNn[1 - \frac{b}{2l}\left(n - 1 - \frac{n}{N}\right)] \qquad Eq.\ 2$$

Again, b is the stick width, l is the stick length, N is the total number of layers, and n is the number of sticks per layer. The area of the vertical shafts, A_v, is calculated below.

$$A_v = (l - nb)^2 \qquad Eq.\ 3$$

Gross concluded that for fires considered diffusion-limited, or where the rate of burning is proportional to the porosity factor, the burning rate or mass loss rate, MLR or $\dot{m}$, can be calculated below thought Eq. 4 [13,20]

$$F * \dot{m} * b = fn(N^{.5} b^{1.1} \frac{A_v}{A_s}) \qquad Eq.\ 4$$

Where F is the ratio of thermal diffusivities to relate a wood species to that of Douglas-fir, a dimensionless value equal to 1 for Douglas fir. A big outcome of Gross's study was the definition of three burning regions based on crib porosity, shown in Fig. 4 from Gross, below [13].

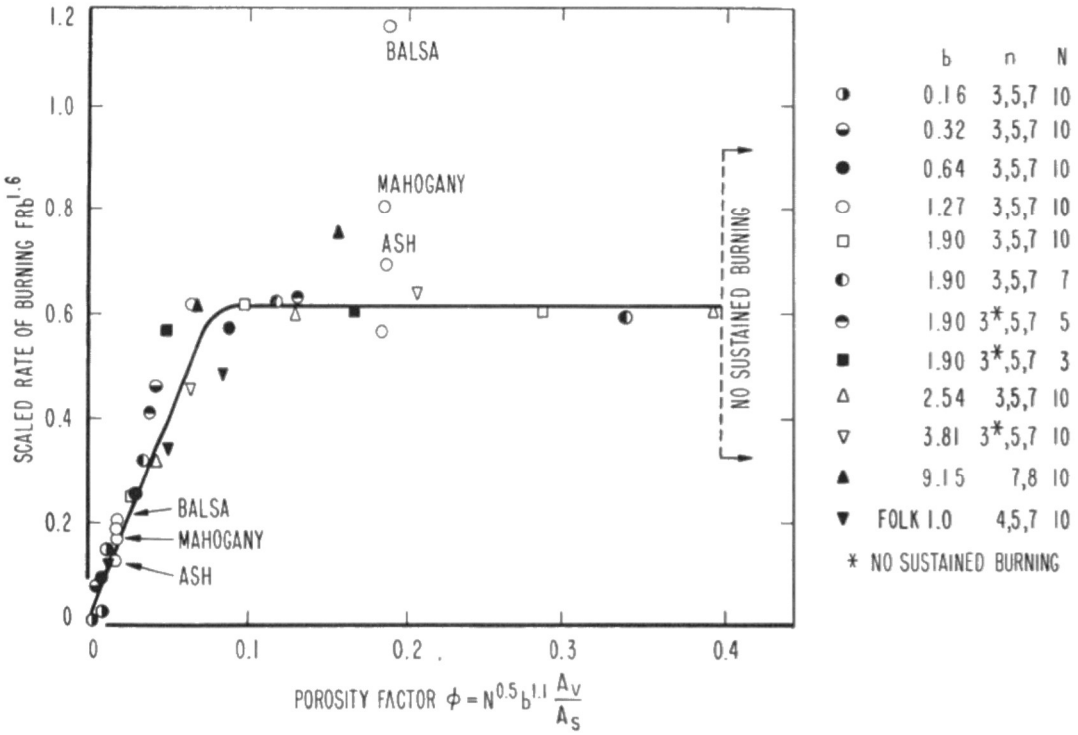

Figure 4: Gross's Effect of Porosity on the Scale Burning Rate, extracted from [13]

The three regions correspond to the three slopes or regions in the figure above. The first region consisted of low porosity cribs considered diffusion-limited where the scaled rate of burning is nearly proportional to the porosity factor. In this region, the increase in ventilation allows for a greater influx of air and therefore an increased rate of burning. The second region is the horizontal line in Fig. 4 which is the free combustion regime. Here, the scaled burning rate is independent of the porosity factor. The last region is the non-sustained combustion where the increased open air in the crib prevents adequate reradiation and no sustained combustion.

2.4.2 Block's Model

Block then built upon Gross's model of the wood cribs by thinking of the cribs as very rough-walled, porous tubes and two different burning regimes [26]. The densely packed burning regime is based on a single tube with a friction factor, f, found to be 0.13. Block included the conservation of mass, momentum, and energy in his burning rate Eq. 5, presented below.

$$\frac{\dot{m}}{A_s} = \frac{1}{2} * f * \rho \left\{ \frac{(\rho_o - \rho)}{\rho} g * h_c \right\}^{0.5} \frac{(\lambda - 1)}{\lambda} \frac{G}{\Psi} \qquad \textit{Eq. 5}$$

Where ρ is the density of air in the vertical shafts in g/cm^3 and ρ is the density of air in g/cm^3. g is the gravitational acceleration constant and h_c is the height of the crib in cm. λ is the ratio of the mass flux of fuel and products leaving a volume to the mass flux of air entering. The modified Froude number, G, is calculated through Eq. 6 below.

$$G = \left\{ \Psi^{-1} \left[\frac{1 - e^{-\Psi}}{1 - \left(\frac{\rho}{\rho_o}\right)^2 \lambda^{-2} e^{-\Psi}} \right] \right\}^{0.5} \qquad \textit{Eq. 6}$$

And the drag coefficient, ψ, is calculated through Eq. 7 below [20].

$$\Psi = \left(\frac{P_c h_c f}{2 A_v} \right) = \left(\frac{4 s h_c f}{2 s^2} \right) = 2 \frac{h_c}{s} f \qquad \textit{Eq. 7}$$

where P_c is the perimeter of vertical shaft, equal to 4 times the stick spacing, s, in cm. The ratio of gas mass flux leaving to air entering λ can be calculated through Eq. 8 below.

$$\frac{(\lambda - 1)}{\lambda} = \frac{B}{(B+1) + \Psi^{-1} \left(\frac{2}{1 + \frac{\rho}{\rho_o} \lambda^{-1}} \right)} \qquad \textit{Eq. 8}$$

where B, the enthalpy ratio is evaluated below.

$$B = \frac{H_c \gamma - c_p (T_s - T_0)}{H_c} \qquad \textit{Eq. 9}$$

Where c_p is the heat capacity, and T_0 and T_s are the ambient and surface temperatures, respectively. H_c is the heat-transfer coefficient.

The friction factor was found experimentally to be independent of the Renolds number as the number was assumed to be sufficiently high. Additionally, several cribs with a range of Renolds numbers representative of those used for the burns were tested by Block in a wind tunnel to confirm the selection.

2.4.3 Heskestad's Model

Seeing as how the Block model was calculation intensive, Heskestad furthered these models and defined a new porosity factor based instead on the spacing of stick instead of the number of layers, shown below in Eq. 10 [15].

$$\varphi_{\text{Heskestad}} = s^{.5} b^{.5} \frac{A_v}{A_s} \qquad \textit{Eq. 10}$$

This porosity assumes that the mass flow of air through the crib is instead proportional to $A_v S^{1/2}$ instead of $A_v h_c^{1/2}$ as identified by Block. The burning rate Eq. then becomes Eq. 11, where $\dot{m}$ is the steady-state MLR rate in g/s which occurs between 80% to 55% of the original crib weight.

$$\frac{\dot{m}}{A_s b^{-0.5}} = fn\left[\left(\frac{A_v}{A_s}\right)\right] s^{0.5} b^{0.5} \qquad \text{Eq. 11}$$

McAllister and Finney used the below empirical correlation, Eq. 12, to calculate MLR based on the Heskestad's model and available data [20].

$$\frac{10^3 \dot{m}}{C_p * A_s b^{-0.5}} = 1 - exp\left[-50\left(\frac{A_v}{A_s}\right)\right] s^{0.5} b^{0.5} \qquad \text{Eq. 12}$$

The above correlation, Eq. 12, was found to work well for l/b values less than or equal to 36 but the calculated MLR falls below by 7% to 19% for l/b equal to 48, and 40% below for l/b equal to

96. This is due to a change in observable flaming patterns where cribs no longer burned uniformly, but rather from the edges of the crib inward Similar behavior was also observed for the densely packed cribs with low porosity. The correlation was tested for Heskestad porosities between 0.053 and 0.13 and a variety of vertical gaps between ignition pan and crib base.

Additionally, McAllister and Finney identified the flame height above the crib is proportional to the Heskestad porosity [20]. This was expected as the turbulent flame height was depended on the ratio of the burning rate to the airflow through the crib, not on top of the crib as prior thought.

2.4.4 Babrauskas' Model

Babrauskas studied wood cribs ignited uniformly and concluded that the burning rate is limited by either the fuel surface, crib porosity, or enclosure ventilation [24]. A crib can switch limits as burning continues and the crib's porosity increases. In general, the limiting mass loss rate will best model the crib burning behavior. For fuel surface control, the burning rate is limited by the surface area of the wood members, and the below Eq. 13 is used to calculate the MLR of the crib.

$$\dot{m} = \frac{4}{D} m_o v_p \left(\frac{m}{m_o}\right)^{1/2} \qquad \textit{Eq. 13}$$

$$m = m_o - \sum_i^t m_\iota(\dot{t}_\iota)\Delta t \qquad \textit{Eq. 14}$$

The MLR for a crib that is controlled by porosity, is shown below in Eq. 15.

$$\dot{m} = 4.4 * 10^{-4} \frac{S}{h_c} \frac{m_o}{D} \qquad \textit{Eq. 15}$$

The MLR for a crib that is controlled by ventilation control, such as an open window in an enclosure, is shown below in Eq. 16.

$$\dot{m} = 0.12 A_v \sqrt{h_v} \qquad \textit{Eq. 16}$$

Where A_v is the vent area and h_v is the height of the vent. For a wood crib burning freely, the porosity and fuel surface are the only possible controls. Once in an enclosure, the wood crib may be limited by the amount of fresh air or oxygen in the enclosure and therefore become ventilation controlled. Either way, the mass loss rate can then be multiplied by the heat of combustion of wood, assumed to be 12 * 10^3 kJ/kg for Douglas fir, and yield a heat release rate [34].

2.5 The Effect of Layout on Wood Crib Mass Loss Rate

Obach and Weckman [35] investigated the effects of different crib layouts with constant geometry and porosity, but with cribs stacked in different arrangements on MLR. Their findings indicated that two identical cribs placed side by side and ignited uniformly exhibit the same heat release, MLR, and burning rate behavior as that of a single crib of equal length. That is, the value of a crib's MLR is dependent linearly on the length of the crib, assuming constant construction parameters and modular cribs can be combined to target a goal MLR. Additionally, when two identical cribs are stacked vertically, the MLR will be greater compared to the two cribs stacked horizontally. The correlation between stacking and adjacent placement was not further quantified but is interesting to note when scaling and designing crib fires.

2.6 The UL 2127 and FM 5600 Extinguishing Test

Both the UL 2127 and FM 5600 tests for class A fire extinguishment are remarkably similar, if not the same. For brevity, whenever the UL 2127 standard is mentioned, the FM 5600 standard is also implied.

The UL 2127 Class A extinguishment test wood crib requires 24 spruce or fir lumber sticks that are 2-by-2-inch nominal width and 18 inches long, as shown below in Fig. 5 [9]. The

actual dimensions of sticks are 1.5 by 1.5 inches by 18 inches and the final wood crib dimensions are 18 by 18 by 6 inches. Each of the 4 layers contains 6 sticks that are spaced 1.8 inches apart edge to edge. These dimensions correspond to a Heskestad porosity of 0.153 cm. UL specifies that the wood must be between 9 and 13 percent moisture content, which ensures a significant amount of the bound water that could affect the crib burning rate is removed before testing.

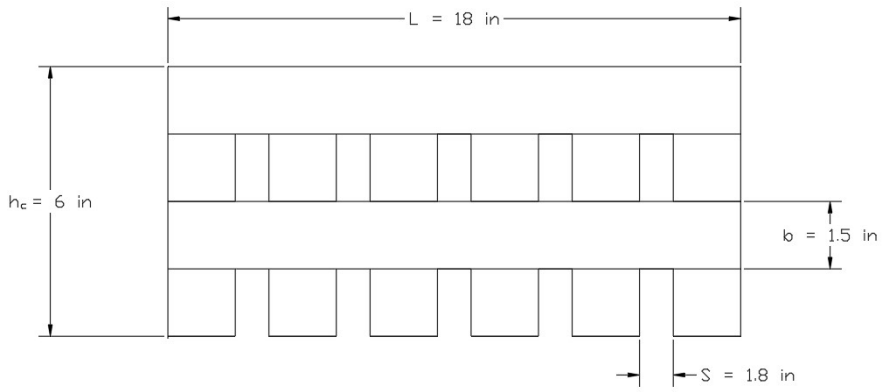

Figure 5: The UL 2127 wood crib and dimensions

The crib is ignited from its base with 0.4 gallons (1.5 L) of commercial-grade heptane that must burn freely under the crib for 3 to 3.5 min. The heptane is placed in a 19-by-19-inch (48-by-48-cm) square pan that is at least 4 inches (10 cm) tall. The distance between the top of the heptane pan and the wood crib is 12 (30 cm) inches. The heptane is ignited, and the wood crib can burn for 6 min before being subject to a discharge event.

The UL 2127 Class A fire Extinguishment tests measure the oxygen concentration at 3 locations in the enclosure and require that observation be made to confirm visual extinguishment of the test article post-discharge and before the end of the 10-minute soak period. The tests assumed that any reduction in oxygen concentration is due to the addition of the inert gas agent [10]. The concentration of agent, C_a, at a point of known oxygen concentrations can then be calculated through Eq. 17, below.

$$C_a = 100 * \left(1 - \frac{O_{2(f)}}{O_{2(s)}}\right) \qquad \textit{Eq. 17}$$

While the fuel mass is required to be recorded for the set of polymeric materials, it is not required for the wood crib.

2.7 Reignition

NFPA 2001 defines two types of combustion that occur in solid fuels which can occur together or lead to one another [7]. The most readily recalled combustion type, flaming combustion, involves the volatile gases resulting from the decomposition of fuel. As these gases react and further decompose, they break down chemically to release more heat. The second type of combustion is smoldering, or glowing combustion, which occurs when the reaction is at or on the fuel surface. While flaming combustion can be immediately extinguished with generally low levels of clean agent, smoldering combustion may not. Further, a slow heat release rate is characteristic of smoldering combustion and under the right circumstances can lead to reignition and flaming combustion. Therefore, it is necessary for the inert gas extinguishing test to address both flaming and smoldering combustion.

The 10-minute soak time post-discharge is intended to ensure that clean agents can suppress smoldering combustion and prevent the reintroduction of flaming combustion. The hold time is intended to simulate the response time for emergency personal and confirms that the systems are designed safely [34].

2.8 Wood Crib Scaling Calculations

Three methods were selected for scaling the wood crib test article, presented in the Methods chapter. Two methods, that of Heskestad [15] and Block [26], require additional background which is presented in the following subsections.

2.8.1 Heskestad's Scaling Calculations

From earlier, Eq. 11, it is known that for free-burning cribs, the burning rate is just a function of the crib porosity so long as adequate natural ventilation is supplied. To translate the free-burning wood crib model into an enclosure burning model, Heskestad suggested utilizing a ratio of enclosure burning to free-burning, $\frac{\dot{m}}{\dot{m}_r}$, where $\dot{m}_r$ is the free-burning MLR, shown below through Eq. 18 [15].

$$\frac{\dot{m}}{\dot{m}_r} = fn\left(\varphi, G, \frac{A_v {h_v}^{0.5}}{\dot{m}_r}\right) \qquad \textit{Eq. 18}$$

In the above Eq., G relates to the relative geometry such as crib length or height, A_{vent} is the vent area, and h is the height of the vent. Additionally, the temperature deviation from ambient and product of combustion species scale with the above factors. This model does not account for changes in moisture content or wood species that could affect the burning rate. While the free-burning cribs are not intended to burn in ventilation-controlled enclosure, this method is unique as the crib construction parameters are all dependent on an external factor, the enclosure height, and not the original full-scale crib construction as in the other methods.

To design the wood cribs, factors such as N, l, and b must be obtained. As the above Heskestad model is designed for enclosures, the enclosure height, H, is chosen as the scaling parameter. Under constant porosity and enclosure geometrics, the free burn rate scales proportionally to the mass flow of air through a vent, the vent area times height, which is also proportional to $H^{5/2}$.

$$\dot{m} \propto H^{5/2} \qquad \textit{Eq. 19}$$

Because the cribs scale under constant porosity, combining Eq.s 18 and 19 yields a proportionality between the vent area factors and the height of the enclosure, shown below in Eq. 20.

$$A_v S^{1/2} \propto \mathrm{H}^{5/2} \qquad \textit{Eq. 20}$$

Again, maintaining a constant geometric construction or porosity, the height of the crib and stick length both scales linearly with the enclosure height, H.

$$l \propto h_c \propto \mathrm{H} \qquad \textit{Eq. 21}$$

Croce et al. [18] applied Heskestad's method and simplified the scaling down the construction parameters, below, as a power-law relationship with the enclosure height, H.

$$\frac{b\prime}{2} + l' + n' = N' = 5/2 \qquad \textit{Eq. 22}$$

$$2l' + \frac{b\prime}{2} = 5/2 \qquad \textit{Eq. 23}$$

$$l' = n' + b' \qquad \textit{Eq. 24}$$

$$b' + N' = 1 \qquad \textit{Eq. 25}$$

$$l' = 1 \qquad \textit{Eq. 26}$$

The scaling relationships can then be derived and consolidated as follows through Eq. 27.

$$b \propto H^{\frac{1}{2}};\ l \propto H^{\frac{9}{8}};\ N \propto H^{\frac{1}{2}};\ n \propto H^{\frac{5}{8}} \qquad \textit{Eq. 27}$$

The above proportionalities were shown to accurately design cribs so long as the porosity and enclosure geometry is held constant, and the crib free-burning rate is properly scaled. The model has been proven to be correlated well within 20% error for various crib constructions and scales.

2.8.2 Block Scaling Calculations

As the spacing between the stick increases into the free-burning domain, the wood crib is better approximated as several individual burning sticks. This MLR, $\dot{m}$, can be approximated by turbulent free convective boundaries rather than a set of vertical tubes, as defined by Eq. 28 below.

$$\frac{\dot{m}}{A_s} = \left(\frac{H_c}{C_p}\right) B_{sp} = \left(\frac{H_c'}{C_p}\right) \ln(1 + B_{sp}) = \; cb^{-0.5} \qquad \textit{Eq. 28}$$

B_{sp} is a derived though the Spalding B number and is the ratio of enthalpy difference between the fluid outside the boundary layer and the energy required to pyrolyze a unit mass of fuel. The variables H_c and H_c' represent the heat transfer coefficients for the crib geometry for mass transfer and zero mass flux respectively. B_{sp} is dependent on the physical fuel properties and crib geometry and is proportional to the negative square route of the stick thickness times a constant relating to the crib species, c. Values for c vary between 0.87 and 1.33 mg/ s $cm^{-1.5}$ depending on the type of wood species, its density, and moisture content [26].

Values of C for various species of wood

	C, mg/ (sec $cm^{1.5}$)	ρ(dry), g/cm^3	M, %
Ponderosa pine	1.03	0.500	7.9
Ponderosa pine	1.07	0.345	7.7
Birch	1.30	0.630	7.3
Idaho pine	0.87	0.405	8.1
Maple	1.33	0.555	7.6
Oak	1.33	0.700	6.8
Redwood	0.86	0.335	7.7
Sugar pine	0.88	0.330	7.3
Western hemlock	0.96	0.565	7.6
Whitewood	1.11	0.425	6.9

Table 1: Block's species factor c for different wood species, extracted from [26]

As values for spruce or fir lumber were not defined by Block, the value of 1.11 was assumed for fir or spruce lumber as whitewood is of similar density to fir lumber and as the average of the available values.

3.0 Methodology

The methodology section is comprised of the scaling methods, experimental protocols, and instrumentation quantification.

The scaling approach taken is sequential. First, several free-burning crib scaling methods will be presented. These methods are used to create several wood cribs studied with a free burning protocol intended to identify the appropriate scaling of the wood crib. After this, the reduced scale enclosure must be designed to ensure negligible enclosure effects on the burning rate of the wood crib.

The design of the discharge event section is included for situation awareness. Due to the complexity of designing discharges and software requirements, all systems were designed by Kidde-Fenwal, Inc. The three experimental protocols included after are for the free burning and two extinguishing tests scales.

The Instrumentation quantification section includes all necessary calculation, corrections, and errors of the data acquisition tools.

3.1 Methods for Scaling Wood Cribs

There are a variety of ways to scale physical phenomenon. Regardless of the method, all relevant variables are identified and evaluated. The variables of most importance, the dominant variables, and those with the greatest impact on the model are selected to control experimentally [14]. As such, it is not required to control every variable when scaling. Often, the dominant variables are arranged into nondimensional groups creating scaling dependencies on groups of variables, not any individual variable.

The method used by Quintiere utilizes a variety of conservation equations to scale fires for numerous applications [14]. Conservation of mass, momentum, energy, heat loss, chemical species, and others are included. Quintiere then summarized these correlations into 22 dimensionless groups and 9 dimensionless variables. While these variables are very helpful for general fire scaling, the reduced design flexibility limited the application to this project. Porosity is instead used because of its success as in previous studies stated in the literature review to scale the MLR of the wood cribs and select the reduced scale crib [15,18,20–22,26,36].

Three wood crib specific scaling methodologies are originally selected to create an initial pool of reduced-scale cribs to identify the necessary characteristics of the reduced scale crib. Each model varies ether the porosity, geometry such as N and n values, or l/b ratio. From each model, two or three crib geometries are selected to test. Each crib geometry is selected based such that the widths of the sticks, b, are from a constant pool of 1 cm, 1.5 cm, and 2 cm where possible to ease the initial crib construction burden.

3.1.1 Heskestad Scaling

The Heskestad model scales based on enclosure size. To maintain uniform enclosure geometry, the full-scale enclosure size must be defined. To meet the 100 m^3 requirement for UL 2127, the minimum enclosure size utilizing 4 ft high sheeting is 17.25 x 17.25 x 12 ft. With the Heskestad proportionality statements presented earlier, Eq. 27, a new enclosure height can be selected, and the crib construction parameters of N, n, l, and b can be calculated according to Eq. 30.

$$\frac{X'}{X} = \left(\frac{H'}{H}\right)^m \qquad \textit{Eq. 29}$$

Where X represents the crib construction parameter and m is the proportionality exponent stated earlier in Eq. 29 and H' is the full-scale enclosure height of 12 ft. The reduced scale enclosure height, H, is systematically changed to yield a b value close to one of the common values from earlier. Values of N and n are rounded to the nearest whole numbers. The stick length is increased slightly to account for changes in N and n such that the porosity is within 5% of the desired full-scale porosity. Final crib construction parameters for the Heskestad method are below in Table 2.

TABLE 2: Heskestad scaled selected free-burning test cribs.

H (ft)	B (cm)	(cm)	N/n	Porosity
9.2	3	23.5	3/4	0.15
5.7	2	13	3/3	0.15

3.1.2 Constant Porosity and Geometry Scaling

Cribs scaled under constant porosity and geometry would look exactly like the full-scale crib, except with thinner and shorter stick members. Based on the burning rate Eq. 11 from earlier, the free-burning rate of a wood crib is only a function of its porosity and geometry when not in a ventilation-controlled enclosure [15]. Under constant geometry values for N and n; the free-burning rate is just dependent on the length of the wooden sticks, l, and their width, b. By charting the relationship between stick length and width for a constant porosity value of 0.152, N of 4, and n of 6; the following correlation is developed for constant porosity and geometry scaling, shown below in Fig. 6.

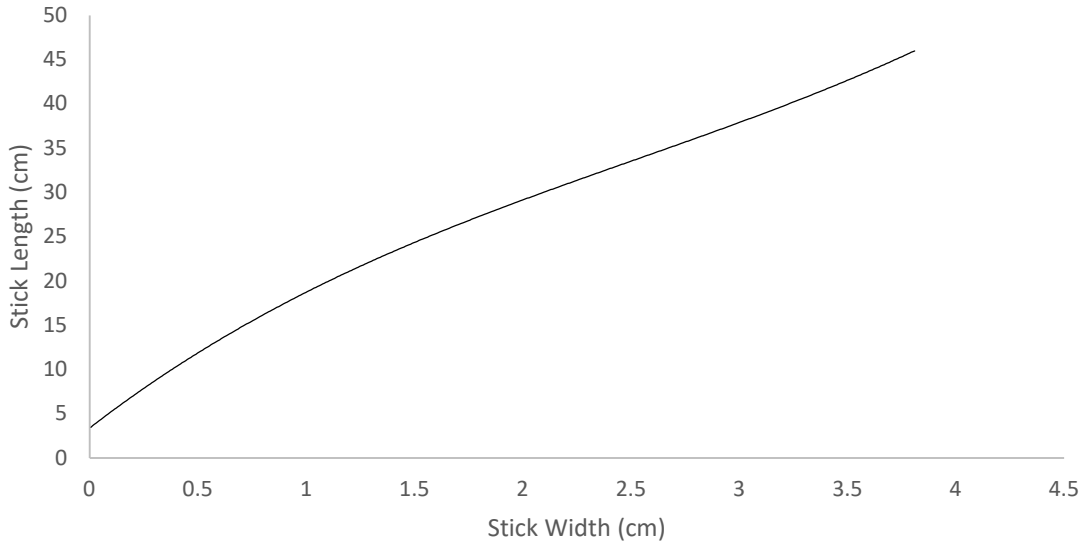

Figure 6: Derived empirical correlation for stick length given stick width under constant porosity =0.153, N = 4, and n = 6.

The general Eq., below, is derived by fitting a polynomial expression to the curve.

$$b = 0.5414 * l^3 - 4.0826 * l^2 + 18.884 * l + 3.3609 \qquad Eq.\ 30$$

b is chosen from the stock pool and the length is rounded to the nearest 0.5 cm, which has little impact on the porosity of the crib. Selected cribs for free burning constant porosity and geometry scaling are consolidated below, Table 3.

Table 3: Constant porosity and geometry selected free-burning test cribs.

b (cm)	l (cm)	N/n	Porosity (cm)
2.5	33.75	4/6	0.15
2	29	4/6	0.15
1.5	24	4/6	0.16

3.1.3 Block Scaling

The block model for scaling the cribs assumes the cribs will maintain an open packed arrangement and scales based on burning rate, Eq. 28. Assuming the crib is always in the open-

packed regime, then the ratio of the full-scale burning rate to that of the reduced-scale crib is shown below in Eq. 31.

$$\left(\frac{\dot{m}}{A_s}\right)_{full} \Big/ \left(\frac{\dot{m}}{A_s}\right)_{scale} = c * b_{full}{}^{-0.5} \Big/ c * b_{scale}{}^{-0.5} \qquad Eq.\ 31$$

As each of the cribs will be made of the same material, the wood species constant c value cancels out, yielding the below equation.

$$\frac{\dot{m}_{full}}{\dot{m}_{scale}} \frac{A_s(scale)}{A_s(full)} = b_{full}{}^{-0.5} \Big/ b_{scale}{}^{-0.5} \qquad Eq.\ 32$$

Where $A_{s(full)}$ and b_{full} are the values for the full-scale UL 2127 crib of 14280 cm^2 and 3.81 cm, respectively. By selecting a burning rate ratio of 1/2, the following geometry is identified. The length is assumed to be 12 times the width in alignment with the full-scale crib ratio. Block model selected free-burning test cribs are consolidated below, Table 4.

Table 4: Block model selected free-burning test crib parameters.

$\frac{\dot{m}_{scale}}{\dot{m}_{full}}$	b (cm)	l (cm)	N/n	Porosity
0.5	2.4	28.8	4/6	.153

3.2 Uniform Ignition Scaling

The UL 2127 class A suppression test requires that the cribs be ignited uniformly from a 2.5 ft^2 square pan at least 4 inches high and 12 inches below the base of the crib [9]. The size of the pan is 19 by 19 inches and extends a half in inch all directions around the base of the wooden crib, ensuring a uniform ignition. The 0.4 gallons of commercial-grade heptane used must provide a 3-to-3.5-minute burn time as per UL 2127. Ethanol alcohol is used in substitution for heptane to prevent cost and sourcing issues. This substitution has been made before for wood

cribs as the pan liquid only serves the purpose of uniformly igniting the crib [13]. Several trials are conducted, and the amount of alcohol is reduced to 850 mL for the full UL 2127 scale in a 19-inch (48 cm) square pan and 180 mL in the 12-inch (30 cm) square pan at the reduced-scaled. Both volumes provide a 3 to 3.5-minute burn time required by UL 2127. The burn time was not reduced at the small scale to replicate the full UL 2127 extinguishing test method timeline.

3.3 Enclosure Scaling

The next scaling step is the design of an enclosure to act as a fixed volume for the discharge event. An important aspect of the enclosure is that it prevents agent loss during both the discharge and the hold period [1]. This enclosure volume must both be minimalized for ease of testing but also be large enough to provide an adequate amount of oxygen to the crib and not affect the MLR. The goal size is a 75% volume reduction such that the reduced enclosure could be utilized without the need for a large hood for laboratory smoke extraction.

UL 2127 states that the full-scale enclosure must be greater than 100 m^3 with a minimum wall length of 13.1 ft (4 m) and a minimum ceiling of 11.5 ft (3.5 m). The smallest regular square enclosure with a height a multiple of 4 ft (1.2 m), the height of a sheet of plywood, which can be made is 17.25 ft by 17.25 ft by 12 ft high (5.25 by 5.25 by 3.7 m), which surpasses the UL 2127 minimum size with 3571 ft^3 or 101 m^3.

The question was raised on how the original UL 2127 test enclosure size was selected, and if a similar method could be used to calculate the reduced-scale size. Not much is officially known about the original 100 m^3 selection and many in the industry who were asked assumed that the size was just the scale on an enclosure that was readily available.

An attempt was made to identify the scaling source of the 100 m^3 enclosure. Some historical perspective can be made by looking into the predating Loss Prevention Council (LPC) manual from 1996 and the predecessor Standard, UL 1058, *Halogenated Agent Extinguishing System Units*. An extinguishing agent enclosure size was cited at 96.45 m^3 from the LPC, such that an inert gas system provider would need two nozzles to protect the space [37]. Shortly after and before the 1996 publication, the requirements of the LPC were relaxed such that one discharge nozzle can be used if it does not spray directly onto the fire. It is known that the UL 1058 enclosure size was increased to 100 m^3 with a minimum horizontal dimension of 4 meters around the same time [38]. This increase was to limit the amount of oxygen depletion in the enclosure and increase the distance between the system nozzle and the test fires. Since then, the 100 m^3 enclosure became an industry standard. When FM 5600 was first published in 2008 the scale was kept maintaining consistency and prevented the need to reevaluate current systems on the market [39].

Without a clear rational for enclosure size selection, the reduced scale enclosure size was then selected according to oxygen consumption. At its basics, the chemical Eq. of combustion can be described below [14].

$$Fuel + O_2 \rightarrow Products \qquad RXN\ 1$$

For wood products, the mean molecular formula is often only comprised of carbon, oxygen, and hydrogen, such as $CH_{1.7}O_{0.74}N_{0.002}$ for Douglas Fir [34,40]. With a relationship between the fuel chemical compounds and oxygen defined an idealized complete, or stoichiometric, relationship can be derived called the mass oxygen-to-fuel ratio, r, which represents the maximum possible conversion of the fuel to products as shown below in Eq. 33.

$$r = \frac{m_{O2}}{m_{Fuel}} = \frac{v_O M_O}{M_{Fuel}} \qquad Eq.\ 33$$

Where v_O, is the stoichiometric coefficient of oxygen in the balanced chemical Eq. m_{O2} is the mass of O_2, and m_{Fuel} is the mass of the fuel. For Douglas Fir, r is equal to 1.32 and for pine or oak, r is equal to 1.21 and 1.35 respectively [34]. The equivalence ratio, r_{eq}, is then equal to the mass ratio of available fuel to oxygen multiplied by the mass oxygen-to-fuel ratio, below.

$$r_{eq} = \frac{m_{available\ fuel}}{m_{available\ O2}} * r \qquad Eq.\ 34$$

When r_{eq} is less than 1, the system has burned all the available fuel and has leftover oxygen which is called fuel lean [14]. When r_{eq} is greater than 1, there is excess unburnt fuel and insufficient oxygen, commonly called fuel rich. In an idealized 100% efficient system, all the fuel and oxygen would combust leaving only products when the r_{eq} is equal to 1, below.

$$m_{O2} = m_{Fuel} * \mathrm{r} \qquad Eq.\ 35$$

As a demonstration of the fuel to oxygen ratio in the full-scale enclosure the amount of oxygen required to completely combust one UL 2127 full-scale crib can be calculated. The full-scale UL 2127 wood crib has a total wood member volume of 972 in^3 (16000 cm^3). Assuming a density of 32 lbs/ft^3 (513 kg/m^3) [41], the crib would weigh 18 lb (8 kg). Assuming 21% oxygen in the air, and a constant density of 0.074887 lb/ft^3 (1.225 kg/m^3) at the UL test temperature of 70 ºF (21 ºC) and 1 atm, the 100 m^3or 3531.5 ft^3, enclosure contains roughly 55.54 lb (25 kg) of oxygen. Utilizing fuel and oxygen masses calculated above and the r value of 1.32 into Eq. 35, a r_{eq} of 0.43 can be calculated. This indicates that there is enough oxygen in a sealed full-scale UL 2127 enclosure to completely burn 2.3 theoretical wood cribs, ignoring the effects of reduced oxygen concentration on combustion.

The enclosure is designed to have a minimal impact on the burning rate of the crib before discharge and vent all products of combustion. The theoretically scaled enclosure only needs to supply sufficient oxygen for the crib up to 120 s of flaming combustion during the discharge period. From Eq. 28, an estimate of the steady-state mass loss rate for the UL 2127 wooden crib can be calculated to be 8.12 g/s. Over the maximum 120-s discharge period, the crib can burn a maximum of 975 grams or 2.15 lb. This equates to a minimum oxygen mass of 2.84 lb (1.27 kg) through Eq. 35, and 5 m^3or 181 ft^3 of atmosphere at ambient conditions. This represents the smallest compartment that can be theoretically constructed which would allow for a 120-s steady state crib burn time, not accounting for the reaction effects of combustion in a reduced oxygen content environment.

Rasbash & Langford studied the effects of burning cribs under reduced oxygen concentration conditions and identified the minimum oxygen concentration by volume that a wood crib can burn steadily in is 18% oxygen and that 11.3% O_2 is the theoretical minimum percentage of oxygen required to continue an idealized combustion reaction of wood within an atmosphere of higher nitrogen concentration [42]. This method assumed that the wood volatiles have simplified chemical formula and a heat of combustion of 4000 cal/g. While any reduction in oxygen will affect the steady state burning rate of a wooden test article, the change between 20% and 21 % O_2 only creates slight changes in crib combustion [42].

As the UL test methodology requires that the testing enclosure is within 0.5% of atmospheric oxygen content of 20.9 percent oxygen by volume, this variance can be used as the acceptable maximum change in oxygen concentration for the scalable enclosure. As 0.5% O_2 is less than the Rasbash & Langford limit for observable changes, there be a minimal effect on the combustion of the wood crib.

For a full-scale 120-s burn time that requires 181 ft^3 of atmosphere, from above, the enclosure atmospheric volume would need to be 7584 ft^3 or 196 m^3 to limit a 0.5% change in average oxygen content. Interestingly, this method is 98% accurate at calculating the enclosure size for a 60-s discharge period, 98 m^3, as prescribed by the original UL 2127 Standard of 100 m^3.

When scaling the enclosure for the smaller cribs for oxygen availability, Eq. 35 and Eq. 28 can be used with several substitutions for the masses and densities of air such that the minimum enclosure that will tolerate a less than 0.5% oxygen content drop over a Δt burn time for a chosen crib can be calculated below in Eq. 36.

$$V_{Enclosure} = \frac{\Delta t * C * b^{-0.5} * A_S * r}{0.005 * p_{O_2}} \qquad \textit{Eq. 36}$$

In the above Eq., p_{O_2} is the density of oxygen assumed to be 0.001309 g/cm^3 at 21 ºC and 1 atm, and $V_{Enclosure}$ is in cm^3.

The reduced scale enclosure size was then calculated to be 22 m^3 through Eq. 36. During the free burns, the reduced scale crib was identified to have a slightly lower recorded MLR at 1.2 g/s than the calculated Block method 1.9 g/s. The slightly lower observed MLR is likely due to an error in the assumed wood species c value used in the calculation and not the other measurable crib construction parameter inputs. The values for Douglas fir were not available and needed to be assumed. Based on experimental results from the full and reduced scale, a c value of 0.72 would be more appropriate for the dried Douglas fir used. Using the observed MLR of the reduced scale crib, an enclosure size of 14.5 m^3 could have been calculated, As the calculation method through Eq. 36 was more conservative, the value of 22 m^3 was used for the reduced scale enclosure size.

3.4 Discharge Event Design and Scaling

The first step in clean agent system design is to determine the design concentration [1]. This value is dependent on the chosen agent, agent discharge method, and a safety factor. NFPA 2001 [7] requires a minimum safety factor of 20 %, whereas the ISO [43] minimum is 30 % for class A threats. For nitrogen, or IG-100, the base concentration used to start the design of system is based on the cup burner test and relates to the ability to extinguish a pool of heptane at 32.6% agent [7]. The volume of inert gas required for a specified volume, V, can then be calculated below, through Eq. 37 [6,7,44].

$$\mathrm{X} = 2.303 * \frac{\mathrm{V}}{S} * \log\left(\frac{100}{100-\mathrm{C}}\right) * V_s \qquad \textit{Eq. 37}$$

Where X is the volume of inert gas required at 70 °F, V_s is the specific volume at 70 °F or calculated through the ideal gas law with nitrogen having a molecular weight of 0.028 kg/mol, calculated below [1,44]. S is the volume in the protected area at ambient temperature

$$s = \frac{R*T}{P*M} = \mathrm{k}_1 + \mathrm{k}_2 * \mathrm{T} \qquad \textit{Eq. 38}$$

Where R is the gas law constant, 8.314 J/mol-K, T is the temperature in K, P is the average nozzle pressure in Pa, and M is the molecular weight in kg/mol. k_1 and k_2 are constants, 0.7997 and 0.002927 respectively for nitrogen [1]. These calculations assume the agent is discharged into a compartment and becomes well mixed.

For agent discharge flow through an orifice, the system is considered to be either critical or subcritical flow, depending on the ratio of upstream to downstream pressure, r_c.

$$r_c = \frac{P_2}{P_1} \qquad \textit{Eq. 39}$$

Where P_2 is the downstream pressure at ambient conditions and P1 is the upstream pressure. The criticality of flow determines the nozzle calculation method. For nitrogen, IG-100, r_c, is found to be 0.528 [44]. As the intended test methodology will store and discharge the inert agent at relatively high pressures, well above 30.14 psia (208 kpa), the discharge event can be assumed to be totally in the supercritical regime. In practice, much of the agent has been observed to have been discharged before the system falls into the subcritical regime [44]. For critical flow, the mass flow rate can be calculated as

$$w = K_{CF} * C_d * d^2 * \frac{P}{\sqrt{T}} * AP \qquad \textit{Eq. 40}$$

In the above Eq. 40, w is the mass flowrate through the orifice in kg/s, K_{CF} is an agent-specific parameter, C_d is a discharge coefficient, d is the diameter of the orifice in meters, and AP is an agent parameter that is only a function of agent properties, defined as [44].

$$\text{AP} = \sqrt{K * M}\left[\left(\frac{2}{k_a+1}\right)^{\frac{k_a+1}{2(k_a-1)}}\right] \qquad \textit{Eq. 41}$$

The agent specific flow parameter is K, and k_a value is the specific heat ratio, C_p/C_v, which for IG-100 is 1.4 and M is the molecular weight in kg/mol. The other agent-specific parameter K_{CF} is 0.0313 for IG-100 and can be calculated below [44].

$$K_{CF} = \frac{\rho \cdot AP}{4\sqrt{R}} \qquad \textit{Eq. 42}$$

The discharge coefficient, Cd, is equal to 0.93 and is assumed to be constant for critical flow. For nitrogen, the supercritical orifice flow can then be calculated below, Eq. 43.

$$w = 0.00451 * d^2 \cdot \frac{P}{\sqrt{T}} \qquad \textit{Eq. 43}$$

When combined with the agent quality over a set discharge time, the equation becomes the orifice diameter as a function of enclosure size and properties, below.

$$d^2 = \frac{\mathrm{V}*\log(\frac{100}{100-\mathrm{C}})}{S*\Delta t*0.00451} * \frac{\sqrt{T}}{\mathrm{P}} \qquad Eq.\ 44$$

Where P and T are the average pressure and temperature at the entrance of the orifice plate.

Because the values of P and T change over the discharge time, it is ideal to utilize a computer program to calculate the orifice size and pressure profile for a given enclosure size. Because of the complexity of discharge design requires proprietary software to properly design the discharge system, no discharge calculations were performed by in the scope of this report. Each discharge system was designed by Kidde-Fenwal, Inc. through their proprietary software. The piping schedule and pipe arrangements were provided for each scale. Each discharge system was tested without a test article before suppression experimentation to ensure the goal agent design concertation is obtained within the enclosure.

3.5 Experimental Setups

Three different experimental setups are utilized. The free burning setup only includes the crib, stand, and instrumentation, but no enclosure. The reduced scale and full scale have the same setups at the free burning, but with the addition of an enclosure and discharge system.

All instruments used through the free-burning, reduced-scale, and full-scale enclosure testing are sampled at a frequency of 1 Hz. All data is recorded through a NI® data acquisition system. All recorded data is rounded to eighter 2 decimal places or 4 significant figures, whatever is smaller, for ease of data transfer and analysis. All experiments are visually recorded with a combination of DLSR type and GoPro cameras. The mass balanced used in each test

protocol is an Adams® Cruiser Bench Checkweighing Scales: CKT 32UH, with an internal error of 0.2 g.

Four 2.54 cm orifice bidirectional probes are located in the near field of the crib: directly above the crib, 1 foot above the center of the crib, directly below the center of the crib, and in a side pore of the crib. Probes are connected to Omega® Differential Pressure Transmitters with a set range of 0.25 in H20, 62 Pa, and an accuracy of 0.01 in H20, or 2.5 Pa. Each bidirectional probe was collocated with a thermocouple.

K-type exposed junction thermocouples were used through the experimentation with two different gages, all welded in-house. All thermocouples in and around the crib have an average caliper measured bead diameter of 1 mm, which is consistent with the approximation of double the wire diameter of 0.5 mm. Two 0.5 mm bead diameter thermocouples are used in the full-scale testing to record ceiling layer gas temperatures. The thinner thermocouples were chosen for their smaller thermal inertia to provide a better response time outside of the flame zone. Thermocouples in the wood crib are changed once the fiberglass insulation is burned through, or roughly every 3 tests. In the full-scale testing, thermocouples wires leading to an exposed bead not located in the crib are shielded with a 5 mm outer diameter aluminum tube to prevent excessive wear.

Three oxygen sensors, labeled K1, K2, and K3, are long-life electrochemical oxygen sensors produced by Nova®. The sensors have a T90 response time of 8-10 s for 90% of step-change and a resolution of 0.1% oxygen. The accuracy reported by the manufacturer is with 1% of the full-scale, or 0.25% oxygen [45]. The sensors were calibrated by the manufacture within the past year and are spanned before each test such that the output oxygen reading is 20.9% at

atmospheric conditions. An internal in-line filter scrubbed large particulates before the sensor input.

The paramagnetic oxygen analyzer, labeled as O_2, is a Servo-Mex® 4200 industrial gas analyzer. Its manufacturer reported intrinsic error is less than 0.15% O_2 with a T90 response time of fewer than 15 s at the operational flow rate of 100ml/min. The sensor's resolution is 0.01 percent oxygen, and the analyzer is zeroed each day with pure nitrogen and spanned with atmospheric air at 20.95% oxygen content. The in-line sample preparation consisted of a cold trap and calcium sulfate anhydrous chemical drying agent to remove water vapor, coarse particulate and a HEPA filter to remove solids, and a soda-lime CO/CO_2 scrubber.

The CO and CO_2 gas analyzer, labeled CO and CO_2 respectively, is a Servo-Mex® IR/gfx gas analyzer that samples both the CO and CO_2 content. The manufacturer reported T90 response time is less than 15 s for the unit and a resolution of 0.01 percent CO/CO_2. Each sensor in the unit is calibrated each testing day with nitrogen and spanned with CO/CO_2 calibration gas at 424 PPM and 3768 PPM respectively. The in-line sample preparation consisted of a cold trap and Calcium Sulfate Anhydrous chemical drying agent to remove water vapor and a coarse particulate filter with a HEPA filter to remove solids.

Calibration and corrections necessary for the above instrumentation is presented in Annex B, including the dynamic pressure to velocity conversion for the bidirectional probes, emissivity and thermal inertia correction for the thermocouples, and gas sensors delay times.

3.5.1 Free Burning Cribs Test Setup

Each of the 11 free burning cribs tested are placed on a metal stand with an open bottom roughly 36 inches above the floor on a mass balance. A shelf is placed under the crib where an

ethanol filled pan is placed. The distance between the top of the pan and the bottom of the crib is maintained at twice the height of the crib to replicate the UL 2127 test conditions. 4 bidirectional probes and several thermocouples are placed in and around the crib to record temperature and velocity data, as shown for an example crib in Fig. 7 below.

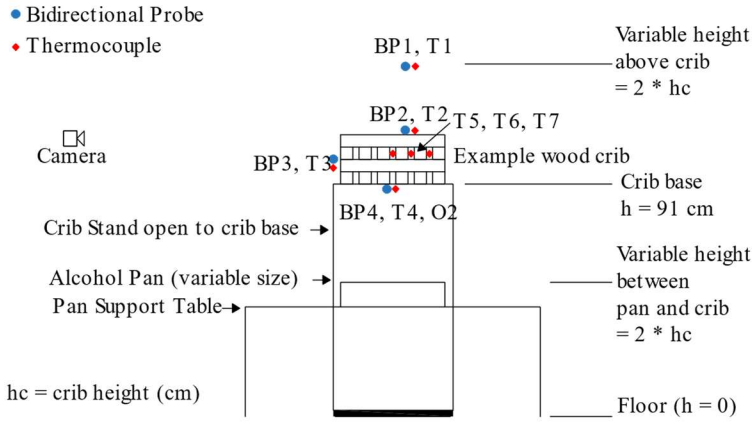

Figure 7: Free-burning test setup and instrumentation locations.

3.5.2 Reduced Scale Setup

The reduced-scale enclosure is built with interior dimensions of 3.6 m by 3.6 m by 2.4 m tall for a total volume of 22.28 m^3. The enclosure, shown below in Fig. 8, is framed with 2x4 inch lumber, and sheathed with ¾ in (2 cm) poplar plywood sheathing. All cracks between plywood sheets and instrumentation inlets are sealed twice with closed-cell urethane foam to ensure an airtight seal. The enclosure is built on top of a laboratory platform and had a ¾-inch CDX plywood floor made with tight construction.

Figure 8: Picture of reduced -scale enclosure during construction.

The reduced-scale enclosure had a single 23-inch by 23-inch (58 by 58 cm) buoyancy-driven vent in the corner of the ceiling and a single 36-inch by 8-foot (91 by 244 cm) outward opening door provided access to and observation of the enclosure, as shown in Fig. 9. The door is sealed with ½-inch (1.3 cm) gasketing and locked directly into the frame of the enclosure. The schematic for reduced-scale enclosure design and oxygen sampling is below.

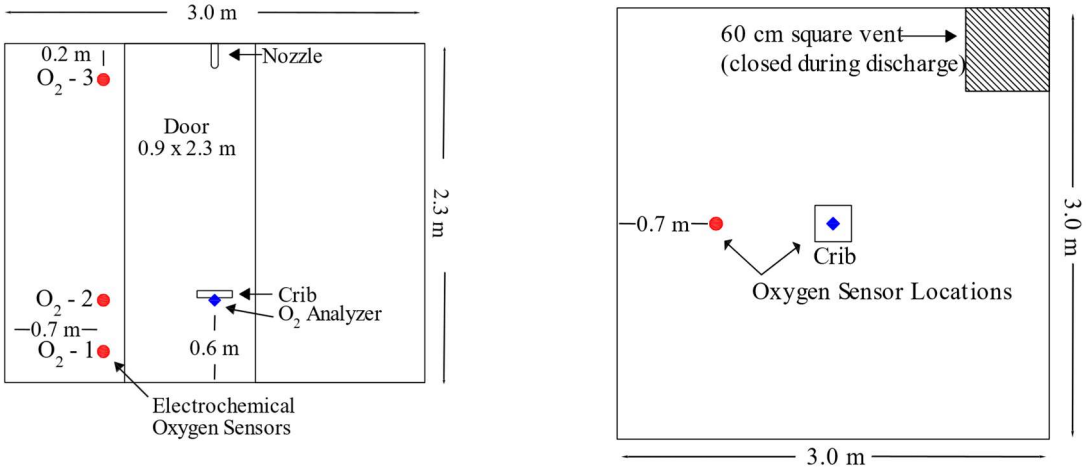

(a) (b)

Figure 9: Reduced-scale elevation's view (a) and arial view schematic (b) and detailing location and size of vent and oxygen sampling probes in relation to the crib and the enclosure.

Four oxygen sensors, three electrochemical and a paramagnetic oxygen analyzer Servo-Mex® O_2 combination CO and CO2, are in the enclosure. The three electrochemical sensors, K1, K2, and K3, are located at the UL 2127 specified locations equidistant between the crib and enclosure wall and vertically at heights of 10% of the vertical rise, at a height equivalent to that of the base of the crib, and 90% of the vertical rise. The Servo-Mex® O_2 analyzer sampling port also drew samples for CO and CO_2 analysis. Eight thermocouples are placed in and around the crib with four bidirectional probes for temperature and velocity measurements, shown below in Fig. 10.

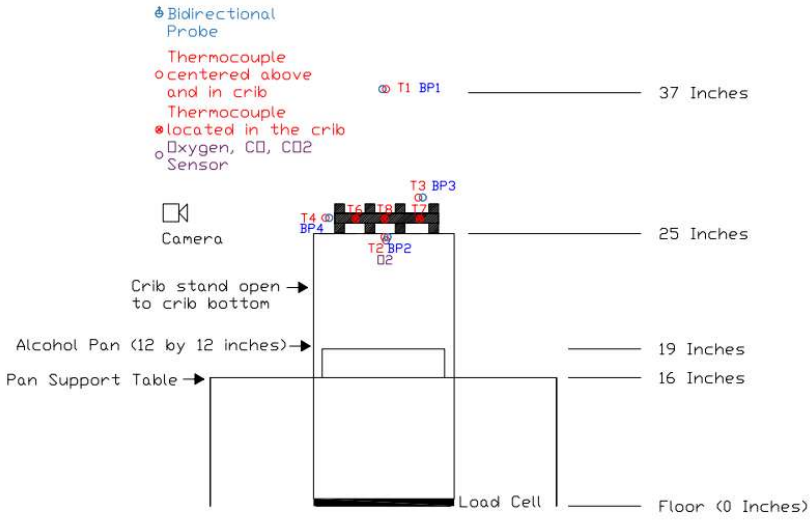

Figure 10: Reduced-scale test stand and instrumentation.

The IG-100 gas is provided by a single 80 L compressed gas cylinder at 200 bar, as shown below in Fig. 11. All charged cylinders were provided and set to 200 bar by Kidde-Fenwal, Inc. The cylinders are 185 cm tall and 27 cm in diameter. Empty cylinder weighed on average 227 lbs (103 kg) and full cylinders weighed between 273 lbs (124 kg) and 278.5 lbs (126).

Figure 11: Picture of IG-100 tanks, red, next to type K tanks, green and brown, for scale.

6 min after pan ignition the discharge event begins. A Kidde® fire protection releasing unit, shown below, opens an internal solenoid valve, which in turn opens the tank to the pipe network.

Figure 12: Rendering of Kidde® Releasing unit, obtained from [46]

Once the tank is open, the gas flows freely through the pipe network to the nozzle. The reduced-scale pipe network created through Kidde® pipe network software consisted of 9.5 ft (2.9 m) of ½-inch pipe and two 90-degree elbows, shown in the schematics of Fig. 13 below.

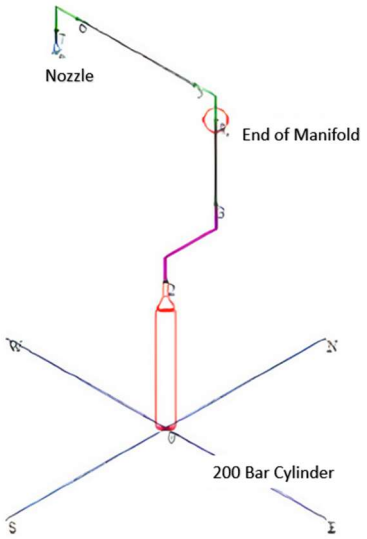

Figure 13: Kidde designed reduced-scale pipe network from bottle, red cylinder, to nozzle.

All pipe fittings are Class 400 lb malleable iron fittings as per the requirements of NFPA 2001, 2015 Edition, Sections 2-2.3 and A2-2.3.1. Pipes are mounted to the enclosure every 5.5 ft (1.7 m) as per the Kidde Design, Operation, Instillation, and Maintenance Manual [46].

The rate of discharge and gas flow rate is throttled only at the nozzle through the orifice plate. The orifice plate, labeled 2 on the below Fig. 14, is located within the nozzle body and could be changed out between discharge tests.

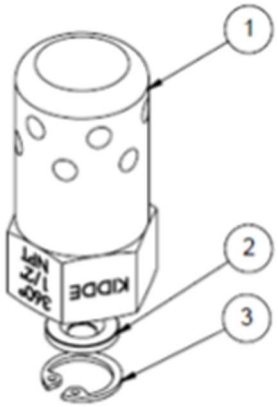

Figure 14: Kidde discharge nozzle body, 1, orifice plate, 2, and retainer ring, 3, obtained from [47]

Ten reduced-scale experiments, five for each discharge period, are conducted, as shown in **Error! Reference source not found.**, below.

Table 5. Experimental matrix for reduced-scale suppression tests.

Test #	Discharge Period (s)	Orifice Plate Diameter (mm)	Average Crib Mass (kg)	Average Mass of Agent Discharged (kg)
R4, R6, R7, R8, R59	60	4.5	1.06 ± 0.07	11.5 ± 1.4
R11, R12, R13, R14, R15	120	3	0.95 ± 0.04	11.1 ± 0.4

3.5.2 Full Scale Setup

The large-scale enclosure is built to have interior dimensions of 17 ft 2 in (5.23 m) by 17 ft 1 in (5.21 m) by 12-ft (3.66 m) tall for a total volume of 100.6 m^3, compliant with the UL 2127 Standard. The enclosure is framed with 2x4 lumber reinforced 1/3 and 2/3 of the vertical rise with additional 2x4s. 2x6 inch reinforcing cross beams are added along the floor to connect the bottom of the walls to prevent movement of the walls during discharge. The enclosure is sheathed with primary ¾-inch (2 cm) poplar plywood sheathing on the walls and 3/8-inch (1 cm) CDX plywood on the ceiling. All cracks between plywood sheets or instrumentation inlets are sealed twice on the outside and once on the inside with closed-cell urethane foam to ensure an airtight seal.

A 34 inch by 8 ft (86 cm by 2.44 m) door is centered on the main wall to provide access, visual observation, and ventilation makeup air during preburn, as shown in Fig. 15 below. The door is sealed within 15 s before discharge with 1-inch by 1/8-inch (2.5 cm by 1 cm) gasketing and latched twice at 1/3 and 2/3 of the vertical rise of the door directly into the building frame. The door is installed to open inward to provide a better seal during discharge.

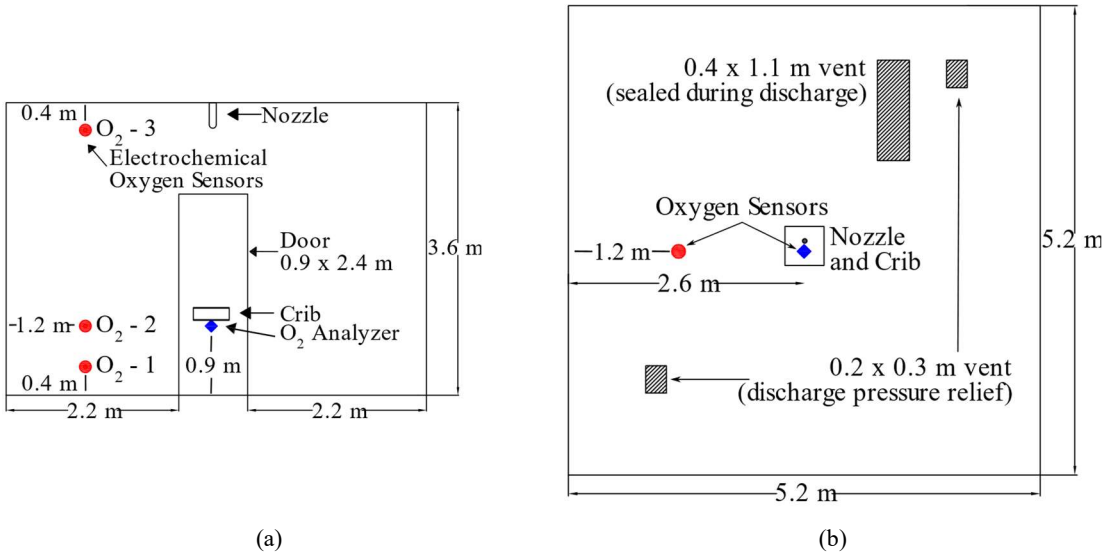

Figure. 15. Full-scale enclosure (a) elevation view (b) plan view, detailing the enclosure construction, ventilation location, and UL 2127 oxygen sampling locations.

Two types of vents on the roof provided ventilation during the preburn period before discharge, shown below in Fig. 16. A 36 x 111 cm buoyancy-driven flap is left open during preburn to exhaust the bulk products of combustion out of the enclosure, Fig. 16 (a). The flap is open at ignition and closed with a pull cord. The flap is sealed 15 s before discharge with 1 inch by 1/8-inch (2.5 cm by 1 cm) gasketing. An additional 9-by-12-inch (23 by 30 cm) forced convection vent which utilized a box fan mounted above the roof rafters to draw air from inside the enclosure out assisted the exhaust of lower temperature gasses, Fig. 16 (b). The area between the

fan and vent is encased to provide a better flow through the vent, which is measured with a hot wire anemometer to be on average 2.5 m/s.

(a) (b)

Figure 16: Picture of 36 x 111 cm buoyancy-driven flap (a) used to evacuate the combustion products pre-discharge on the full-scale enclosure ceiling. Picture of 9-by-12-inch forced convection vent (b) on the full-scale ceiling.

The full-scale discharge piping arrangement layout was provided by Kidde-Fenwal, Inc. and designed with their proprietary pipe network design software, shown below in Fig. 17.

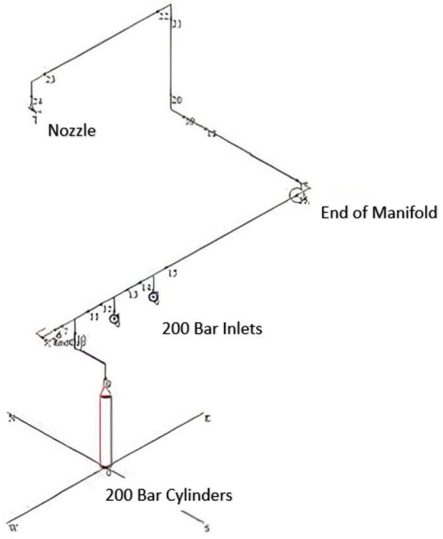

Figure 17: Kidde designed full- scale tank and pipe layout with specifications.

Three tanks, indicated by the circles on the above Fig. 17, on a one-inch schedule 40 steel pipe manifold provided the IG-100 gas. The manifold then ran horizontally 10 ft (3 m) to a right angle, and then 6 ft (1.8 m) across the front of the enclosure. The pipe is then reduced to ¾ inch diameter schedule 40 piping. Another 16 ft (4.9 m) of ¾-inch pipe with three additional right angles ran from the reduction to the nozzle mounted 5 inches below the ceiling in the center of the enclosure. All fittings are Class 400 lb malleable iron fittings as per the requirements of NFPA 2001, 2015 Edition, Sections 2-2.3 and A2-2.3.1. Pipes are mounted to the encloser at least every 5.5 ft as per Kidde-Fenwal, Inc. [46].

During discharge, cameras recorded several views of the crib to visually obtain the time of extinguishment. 7 thermocouples and 4 bidirectional probes recorded temperature and velocity data around the crib. Additionally, the same four oxygen sensors as the reduced-scale are in the enclosure including the Servo-Mex® 2 inches (5 cm) below the base of the crib, detailed below in Fig. 18.

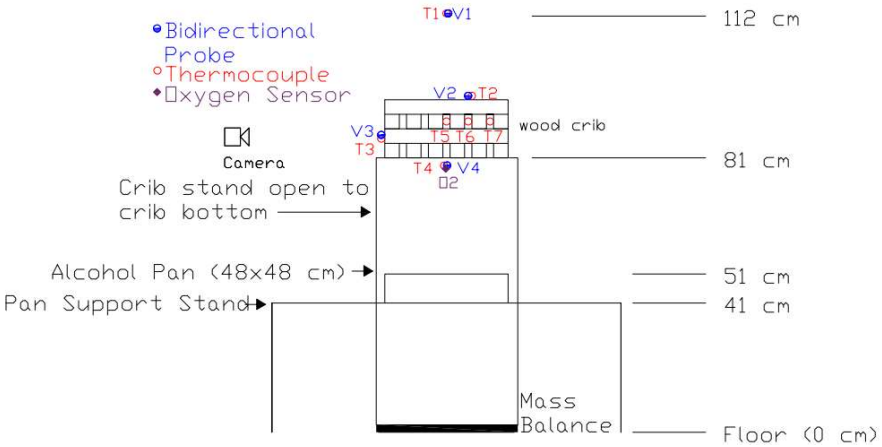

Figure 18: Instrumentation location and setup dimensions for the full-scale

Seven tests are conducted at the full scale. Before testing, cribs are dried by a portable heater to remove excess water content and checked before testing to ensure a moisture content

between 9 and 13 percent as per UL 2127 [9]. Moisture content is sampled at the center of each stick member at the top of the crib and all six members are averaged for the final crib moisture content. Test parameters for the full-scale testing are detailed below in Table 6.

Table 6: Full-scale Tests Experimental Matrix

Test	Discharge Period (s)	Orifice Plate Diameter (mm)	Original Mass of Crib (kg)	Mass of Agent Used (Lbs)
F1	60	13.5	7.477	114
F2	60	13.5	7.091	119
F3	120	8.5	7.244	121.5
F4	120	8	6.978	112.5
F5	120	7.5	6.978	106.5
F6	60	13	7.070	105
F7	120	7	6.613	108

3.6 Experimental Protocols

Two types of experimental protocols are followed during testing: one for free burning cribs and another for both scales of the extinguishment tests. The protocol for the extinguishment tests is almost identical for both scales and is presented in a single subsection.

3.6.1 Free Burning Cribs Test Protocols

The free-burning tests are conducted in the open, without an enclosure, and in the ambient lab environment. Cribs are dried at 70-degree Fahrenheit for a month before testing to decrease moisture content. Before ignition, the average moisture content of the crib, crib mass, and temperature is recorded. Moisture content is recorded by a General Tools MMD4E Digital Moisture Meter with an accuracy of ±3% water content and a resolution of 0.1%. Six readings are taken across the top row of stick members and averaged for the crib moisture content. All reduced-scale cribs are ignited by at least 180 mL of alcohol to ensure a uniform ignition without completely burning through the cribs before reaching a steady state burning rate. Pans are selected from an available laboratory stock such that the pan area is slightly larger than the

footprint of the crib. When possible, pans are square except the 9-inch diameter round pan. Each of the three UL 2127 full-scale cribs are ignited by a 19-by-19-inch square pan with 4-inch-high sides as per UL 2127 [9,10]. Each full-scale UL 2127 crib are ignited by a different amount of alcohol to get a baseline for standard equivalency. The test variables for each crib are summarized below, Table 7.

Table 7: Test variables for the free burning cribs

Crib (N,n,b,l)	Average Moisture Content (%)	Pan Size (inches)	Ethanol Ignition Amount (mL)
4,6,3.8,45.7	6.91	19” x 19”	1500
4,6,3.8,45.7	6.28	19” x 19”	1000
4,6,3.8,45.7	---	19” x 19”	400
4,6,2.5,33.75	6.40	19” x 19”	450
4,6,2,29	7.15	9” diameter	180
4,6,1.5x1,28.8	6.48	9” diameter	180
4,6,1.5,24	7.59	12” x 12”	180
3,3,2,13	7.40	12” x 12”	180
3,4,3,23.5	5.94	12” x 12”	180
4,6,2.4,28.8	6.10	12” x 12”	180

Cribs are allowed to burn until disintegration as defined by the first stick member falling off the stand. The air is assumed to be 20.9% oxygen and the internal lab temperature is relatively constant at 21 ^{o}C.

3.6.2 Full and Reduced Scale Extinguishment Test Protocols

The full-scale and reduced-scale experiments were conducted per UL 2127. The protocol is presented below, along with the results of an exemplary experiment, Fig. 19.

- Each full-scale wood crib was dried using an electric convective heater for at least 12h to an average moisture content between 9 and 13% and then stored in a doubled-up and sealed polyethylene bag. The reduced-scale wood cribs were conditioned in a drying oven at 95ºC for at least 12h. The average dry masses of the full- and reduced-scale cribs were 7.06 ± 0.27 kg and 1.0 ± 0.08 kg, respectively.

- 6 min before the start of discharge and with all the vents and door of the compartment open, a pan with ethanol was ignited under the crib at a distance of twice the crib height. The wood crib ignited and began burning briefly assisted by the pan fire for 3.5 min.
- Once ignited, the crib was allowed to burn freely in the enclosure until a steady state was achieved. This condition was confirmed by evaluating the average mass-loss rate over a one-minute period. From preliminary experiments, it was found that a period of 6 min was sufficient to ensure that the crib reached steady-state burning.
- During this initial period, the door and the vents remained open, allowing for the evacuation of the combustion products and the supply of fresh air. Despite this, it was found that the oxygen concentration within the compartment decreased slightly due to the partial accumulation of combustion products but that it remained within the 0.5% of original oxygen concentration limit.
- After reaching steady-state burning and 15 s before the start of discharge, the ceiling vents and door were closed. The fan used to exhaust preburn gasses at the full scale is turned off. 50 lb of weight is transferred to the reduced scale ceiling vent before discharge to ensure a tight seal. The beginning of the discharge is shown by the vertical red line in Fig. 19.
- Shortly after the start of discharge, the average oxygen concentration began to drop, the velocity at the top of the crib increased, and the crib mass and dropped due to the effects of the bulk flow. As the oxygen concentration approached the extinguishing concentration, the crib top velocity and mass approached a steady-state value as shown in Fig. 19.
- Extinction was defined by visual observation of flame disappearance and consistently occurred at the end of the discharge period for the full-scale tests. Shortly after crib extinguishment and

the end of discharge (t =120 s for Fig. 19), the velocity, mass, and oxygen concentration values stabilized. Then, the oxygen concentration slowly increased as fresh air leaked in and the agent mixture leaked out and began to stratify toward the upper portion of the enclosures.

- Ten min after the end of discharge, the enclosure vents and door were opened and a fan was turned on facing into the enclosure to allow fresh air to enter the enclosure, and the crib was checked for signs of reignition.

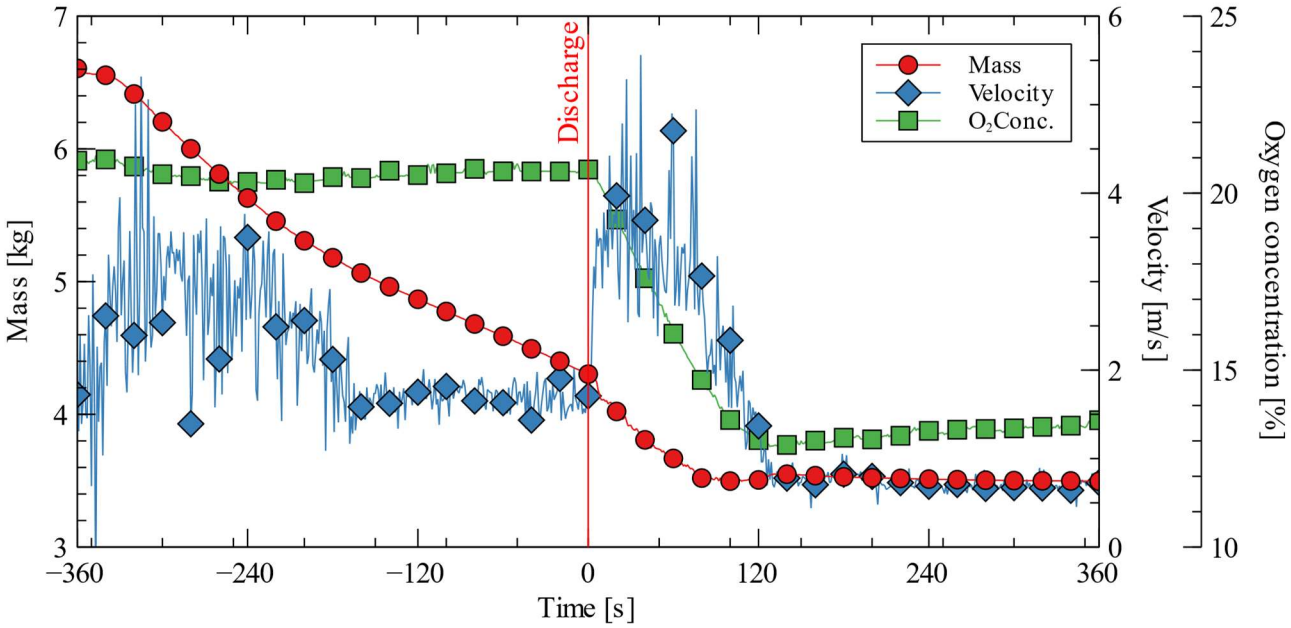

Figure 19: Typical experiment (full-scale test F7).

4.0 Results and Discussion

The results section is broken down into several subsections based on the original statement of work and the objectives of this study. The free-burning test results are presented first followed by the results of the full-scale and reduced-scale extinguishing tests, which are broken down phases of the discharge testing timeline: ignition, preburn, discharge, extinction, soak period. The discharge section is further broken down by instrument type: oxygen sensors used to calculate the percent agent, gas phase velocity, gas phase temperature, and crib mass. The differences between scale and discharge period are discussed at the end of each sub section.

4.1 Free-burning Crib Experiment Results

Cribs from each of the three previously mentioned methods for scaling cribs are burned on a mass balance to identify the best method for scaling the test article. The MLR is the average mass loss over the steady-state burn length. The length of steady-state burning is defined by a constant MLR for at least 10 s post pan burnout to the point where the MLR is no longer constant over a 10 s period or the crib members fall from the testing stand. The representative MLR, or MLR divided by initial mass, is used to gage cribs of different scales against each other. Cribs with a high representative MLR burn a larger percentage of their mass per s. As a result, these cribs often have short steady-state burn times and relatively high MLR for their size, as shown in Table 8, below.

Table 8: Free-burning crib results

Crib (N, n, b, l)	MLR (g/s)	Steady State Burn Length (s)	MLR/M_0 (1/s)[a] [Representative MLR]
3, 3, 2, 13	0.5	200	2.31
3, 4, 3, 23.5	1.2	600	0.84
4, 6, 1.5, 24	1.7	175	3.14
4, 6, 1.5x1, 28.8[b]	2.2	160	3.03
4, 6, 2, 29	2.4	120	3.43
4, 6, 2.4, 28.8	2.7	230	1.92
4, 6, 2.5, 33.75	3.1	475	1.28
4, 6, 3.8, 45.7[c]	5.4	660	0.66

[a] representative MLR is calculated to gauge what percentage of the cribs mass is lost every s
[b] crib sticks are rectangular cut to 1.5 by 1 cm to lengthen the steady-state burn time
[c] The UL 2127 full-scale crib, an average of 3 free burns

As stated earlier, the 3, 4, 3, 23.5 crib designed by the enclosure height Heskestad methodology is ultimately selected for its long steady-state burning period and similar representative MLR to that of the UL 2127 scale crib with construction parameters 4, 6, 3.8, 45.7. These reduced scale characteristics are achieved by reducing the number of layers and sticks per layer but increasing the stick thickness and therefore the crib surface area. The thicker crib sticks also deteriorate much slower, allowing for a sizable steady-state burn period to test in. While the representative MLR is 25% larger than the full-scale UL 2127 crib, the change is slight compared to the other reduced-scale options.

4.2 Ignition Results

Each full-scale and reduced-scale crib used for suppression testing is ignited with a pan of alcohol sized slightly larger than that of the crib to ensure a uniform ignition. The only purpose of the pan fire is to bring the crib to a steady state burning rate. At the full scale, the flames from the pan fire quickly reach the crib height and began igniting the bottom row of

sticks. After an average of 20 s, the bottom of the crib is ignited as observed by flames on the crib, and a significant change in crib mass loss rate. Around 40 s, the crib becomes fully involved in combustion as defined by visual observation of developed flames, an inflection of MLR, and a maximum flame temperature above the crib, shown below in Fig. 20. The original spike in mass-loss rate during the first 10 s can be attributed to entrained air and ancillary forces pushing up on the mass assembly right after pan ignition.

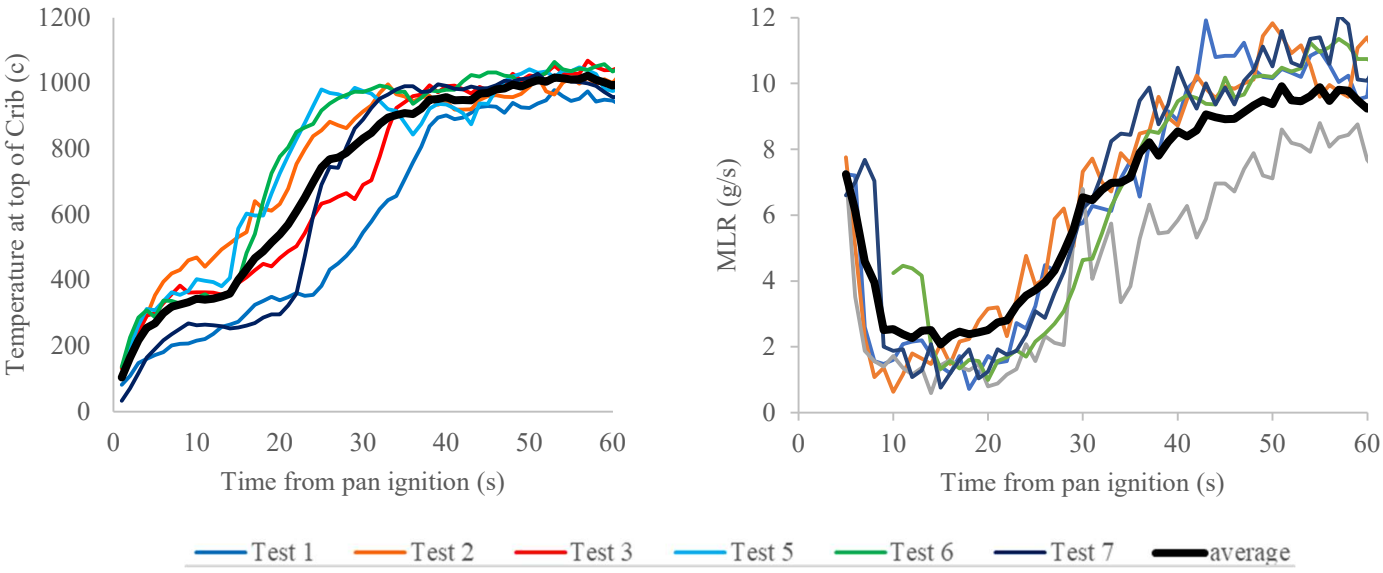

Figure 20: Full-scale Temperature of a central crib pore at TC 2 (left) and mass loss rate (MLR) of the crib (right) immediately after ignition. MLR data is shown with a moving period average of 5 s.

Visual observation of the crib over the first 55 s is shown below in Fig. 21. Of note is the 5th frame 20 s from pan ignition where flame first engulfs the entire crib and defined crib base ignition and the flame shape in the 9th frame after 40 s which is used to define full crib involvement.

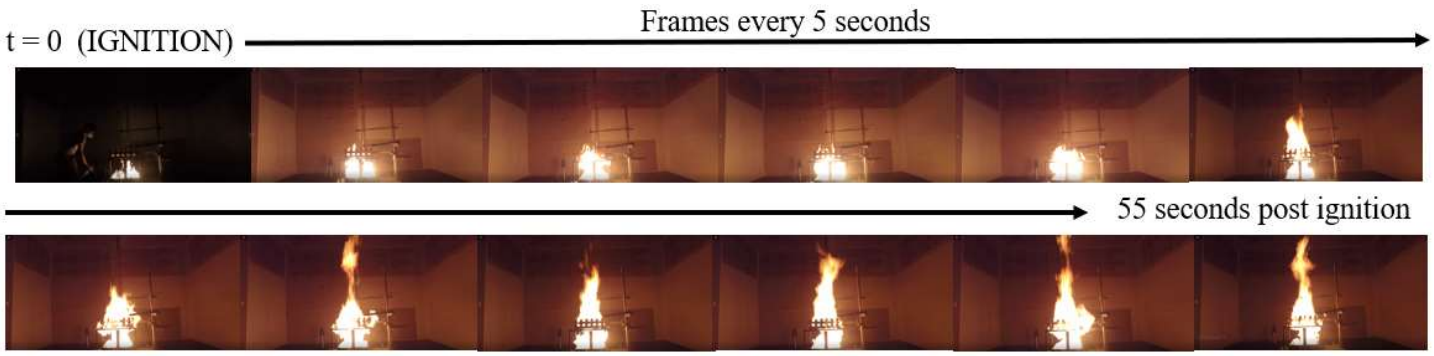

Fig. 21: Full-scale crib ignition frames at a frequency of 5 s over the first 55 s from pan ignition.

The reduced-scale cribs are observed to have an average crib base ignition at 6 s and complete crib involvement at 14 s, as shown in Fig. 22 below. Two main phenomena assisted the quicker crib ignition. First, the reduced-scale cribs are dried in an oven that removed essentially all the free moisture content in the wood making ignition easier. S, the cribs are significantly smaller and required less time for flames to spread to the corners of the crib.

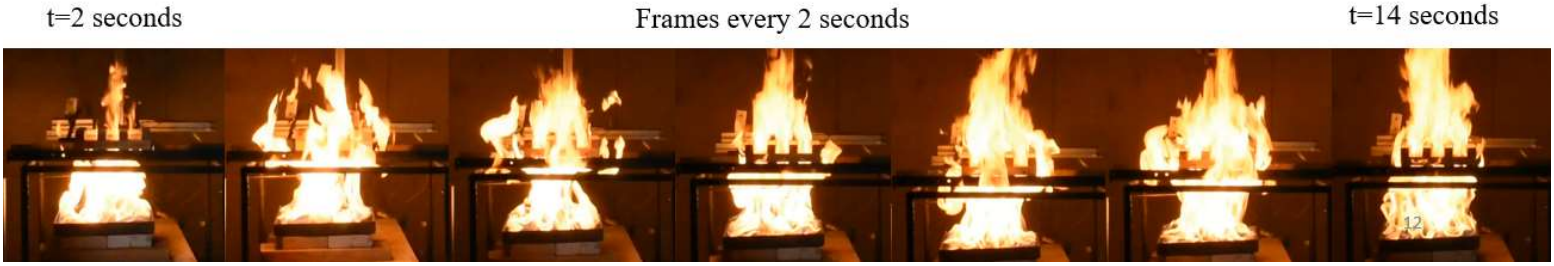

Figure 22: Reduced-scale crib ignition frames at a frequency of 2 s over the first 14 s from pan ignition.

The reduced-scale mass loss during discharge is unable to define ignition because of the alcohol pan fire air entrainment forces on the mass assembly. The temperature data is averaged for each discharge period as repeatability between the tests is demonstrated, shown below in Fig. 23. Averaged crib temperature data confirms that the crib is fully involved at 20 s post pan ignition.

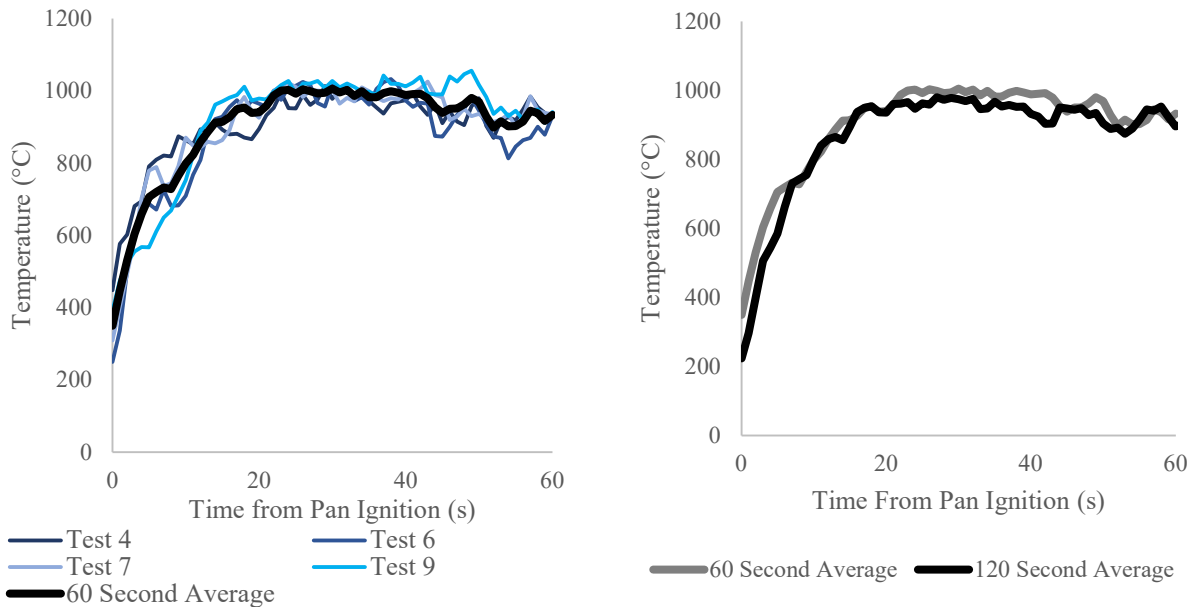

Figure 23: Reduced-scale crib ignition temperature profiles at T5 for all reduce scale 60-s test (left) and averages for both discharge periods (right) for the first minute after pan ignition.

4.3 Preburn Results

Once the alcohol pan burnt out after 3.5 min, the crib quickly reached steady state burning characteristics. In general, the 60 s period before discharge is used when calculating steady state burning behaviors. Steady state is defined by having approximately constant MLR, crib temperature, measured at T5, and gas velocity through the crib measured at V2. Full-scale mass loss data is present below in Fig. 24.

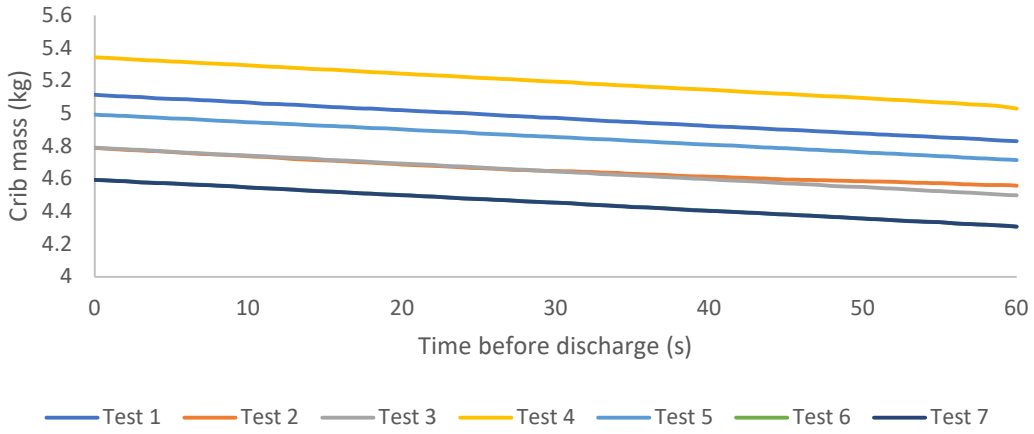

Figure 24: Full-scale crib mass before discharge.

The straight-line slope of the mass via least squares is obtained for each test to calculate the crib's mass loss rate, MLR. The MLR is obtained by calculating the rate of change across the 60 s period immediately before discharge for each scale. As each crib starts with a slightly different initial mass, the absolute crib mass varies slightly with little effect on slope for each crib. HRR is calculated by multiplying the MLR by the heat of combustion of Douglas fir, 17.7 kJ/g [14]. Consolidated steady state burning rate characteristics for the 60 s before discharge is below, Table 9.

Table 9: Steady state burning characteristics of the full and reduced scale cribs

	MLR (g/s)	HRR (kW)	Velocity at top of crib (m/s)	Central Crib Temperature at TC8 (°C)
Full-scale	4.7 ± 0.24	68.5 ± 3.5	1.6 ± 0.1	478 ± 23
Reduced-scale	1.13 ± 0.09	16.6 ± 1.6	.35 ± 0.2	406 ± 42

Mass loss rates were slightly lower than the free-burning conditions. This change is hypothesized to have originated from either the change in wood feedstock, the change in drying conditions between the free burns and suppression testing, or unexpected enclosure effects on the wooden crib. After pan burnout, the oxygen content in the enclosure quickly returned to near ambient

conditions, so a change in the quality of the wood feedstock used to construct the cribs is expected over ventilation effects from the enclosure.

4.4 Discharge Results

The discharge section is broken down by instrument type: oxygen sensors used to calculate the agent concentration, gas phase velocity, gas phase temperature, and crib mass. The differences between scale and discharge period are discussed at the end of each sub section. Bulk flow is introduced in the velocity subsection.

4.4.1 Agent Concentration Curves During Discharge

Understanding how the oxygen concentration changes during discharge at different locations in the enclosure became an important aspect in understanding the crib suppression dynamics. Oxygen concentration at each sampled location for the duration of an typical test is presented below in Fig. 25.

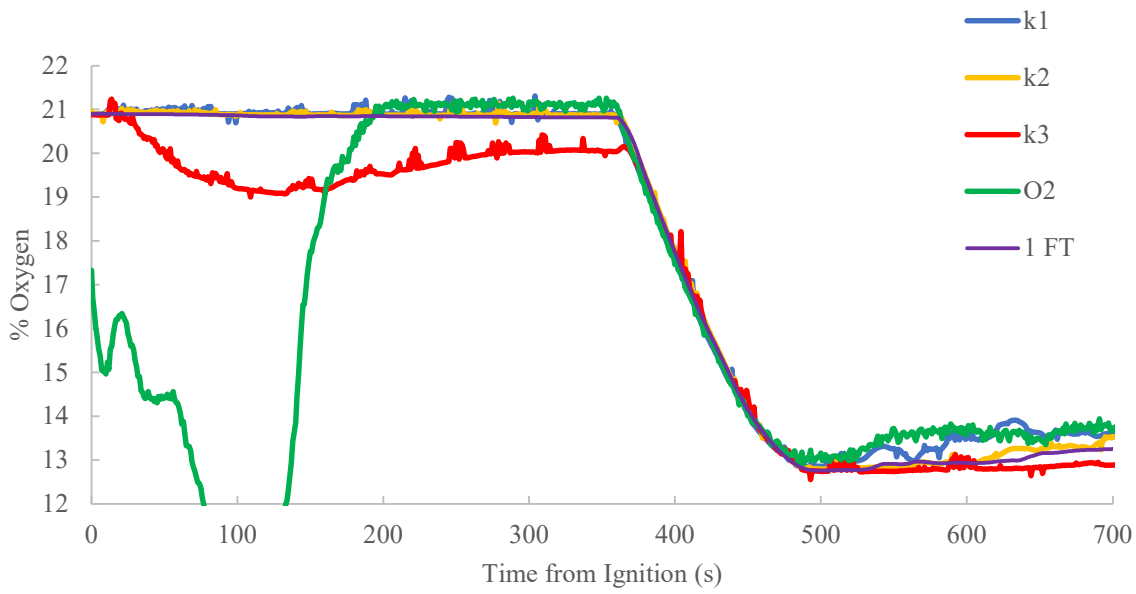

Figure 25: Exemplary Full-scale Test 7 oxygen concentration at 5 measured locations from pan ignition, t=0.

The initial drop in oxygen content observed by the O_2 sensors, the green line in Fig. 25, is due to the pan ignition and is present in all tests because the sampling location is located within the alcohol pan flame. It is important to note that after the pan burns out, the oxygen content at this location quickly returns to ambient conditions. The drop in oxygen content of the K3 sensors is due to the products of combustion collecting at the top of the enclosure. While every effort is made to vent these products before the start of discharge to obtain a deviation of less than 0.5% oxygen content from ambient, this is not always achieved. The effects on extinguishment results are hypothesized to be slight as the upper layer oxygen centration is constantly close to the UL standards. Additional vents should be added to the future full-scale enclosure, and it is suggested that the vent be in a more central location at the top of the enclosure such that a rising plume exits the enclosure roof before interacting with the ceiling. This contact with the ceiling likely cooled the products of combustion and hindered the buoyant flow through the rooftop ventilation.

During the discharge period, all the oxygen sensors track the same progress within the instrumental error, as shown below in Fig. 26. The consistent oxygen concentration trend regardless of the sensor location across all the full-scale testing supports the conclusion that during discharge, the agent concentration within the enclosure is uniformly dispersed. There is an observed average 5 s transition period during some tests where the K3 sensor near the top of the enclosure read slightly higher due to the presence of additional products of combustion. This uniform mixing assumption is only valid during discharge, as the agent will start to disperse and diffuse out of the enclosure after discharge, which is discussed later in the results chapter.

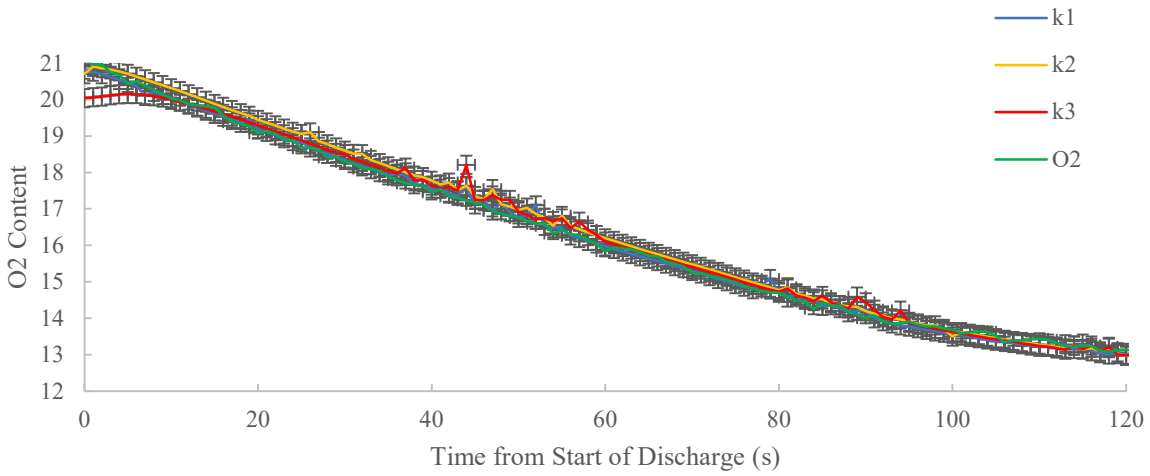

Figure 26: Full-scale Test 7 oxygen concentration at 5 measured locations during a 120-s discharge. Error bars indicate the instrumental error and calculated delay time uncertainty.

These same trends are observable at a 60-s discharge, shown below in Fig. 27, indicating the uniform mixing assumption is valid for both discharge periods at the full scale.

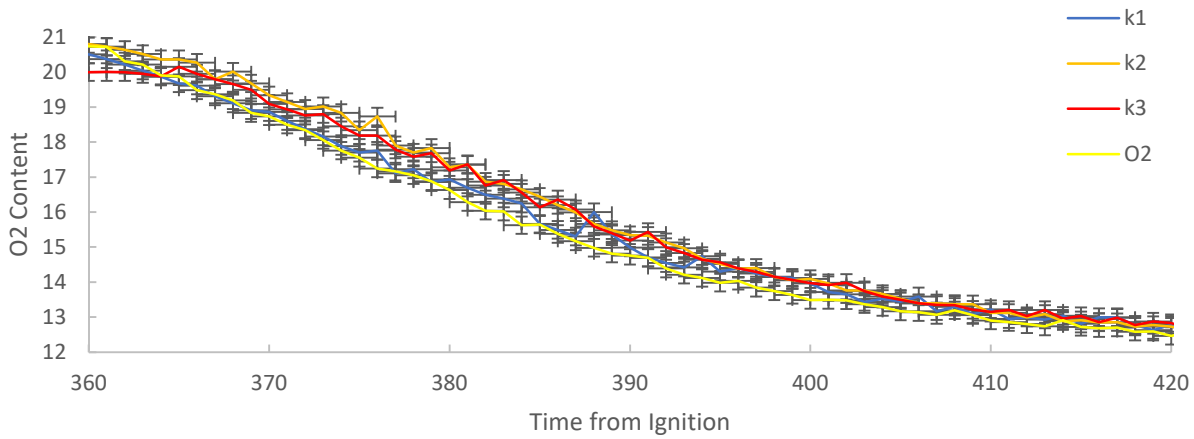

Figure 27: Full-scale Test 2 oxygen concentration at 4 measured locations during a 60-s discharge. Error bars indicate the instrumental error and calculated delay time uncertainty.

The 60-s discharges had slightly more variation in oxygen concentration at the various sampling location. However, each of the oxygen concentration curves falls within the span of instrumental error.

Similar oxygen concentration results are visible at the reduced scale, indicating success in discharge scaling, as shown through the Test 15, 120-s reduced scale discharge test shown below in Fig. 28. Because more agent tanks are available at the reduced-scale and initial orifice plate selections are accurate, the final concentration of oxygen is slightly higher, indicating less agent, than the full-scale tests which released more nitrogen than originally intended.

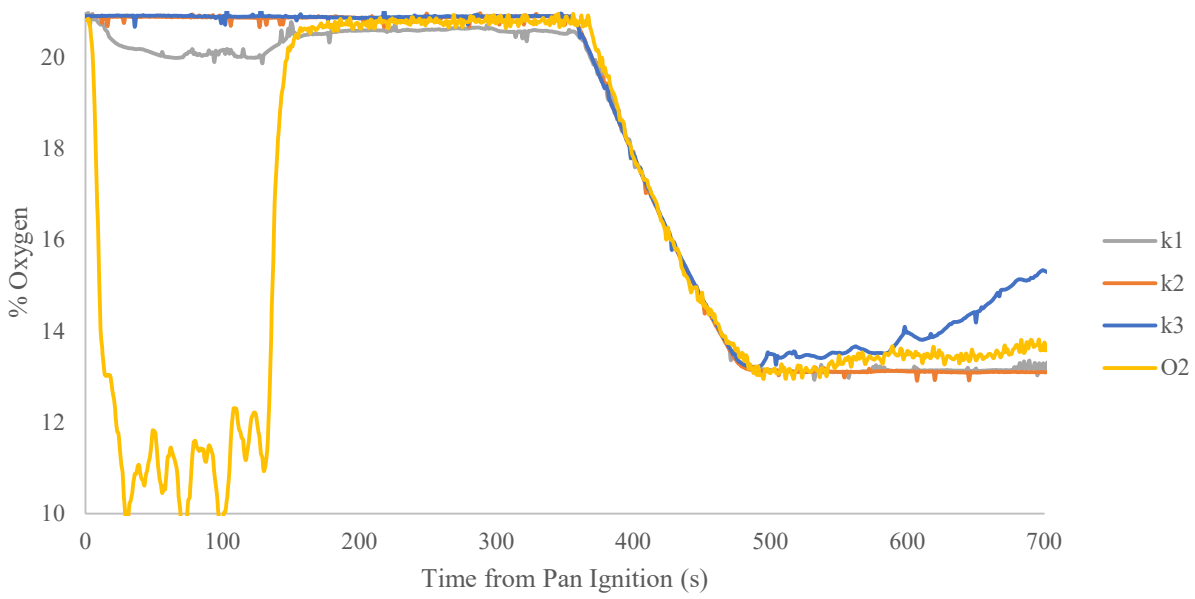

Figure 28: Reduced-scale Test 15 oxygen concentration at 4 measured locations from pan ignition, t=0.

The reduced-scale enclosure ventilation is adequately designed, and the products of combustion are allowed to vent from the enclosure and the upper layer oxygen sensor, K3, returns to within 0.5% ambient oxygen concentration before discharge. Again, the O_2 sensor oxygen content drops during the first 3.5 min before discharge as the alcohol pan fire burns. The oxygen concentration returns to ambient conditions shortly after pan extinction and long before the start of discharge, shown below in Fig. 29.

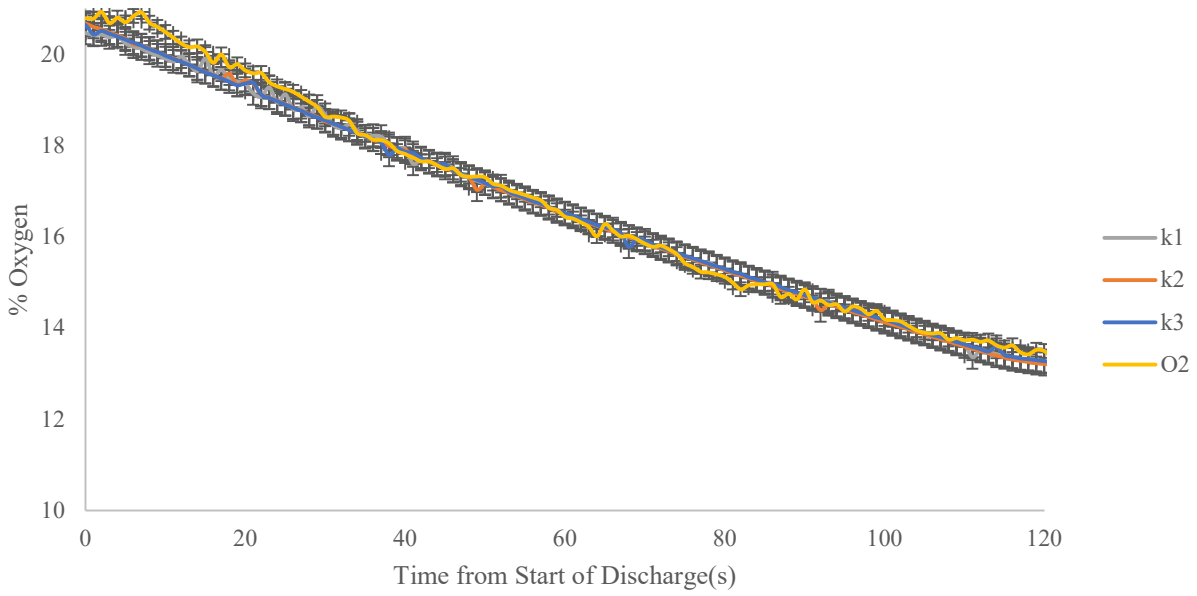

Figure 29: Reduced-scale Test 15 oxygen concentration at the 3 UL mandated oxygen sensor locations (K1 is the highest of the three) and at the base of the crib (O2) during a 120-s discharge. Error bars indicate the instrumental error and calculated delay time uncertainty.

The reduced-scale 120-s discharge also has a similar agent concentration profile as the full-scale and further supports the uniform agent mixing assumption during discharge. The inlet line for the O_2 did have a leak during data collection for the first few tests. This leak led to higher-than-expected oxygen concentration levels at the base of the crib. Data collect before the leak correction was removed.

The rate of agent increase in the enclosure is measured by a decrease in oxygen concentration, Eq. 17. The rate of agent increase is of utmost importance to identify changes in discharge time for both scales. Ideally, the agent rate of rise for a 120-s discharge will be half of that for the 60-s discharge as both periods are designed to discharge the same amount of agent. To compare discharge periods, the % discharge completion parameter is used, which is equal to the time since the start of discharge divided by the total discharge time. With this method, 50% discharge will be equal to 30 s for the shorter discharge period and 60 s for the longer discharge

period. Fig. 30 below shows all the full-scale average oxygen concentration curves. Of note is the variable orifice plate selection used at the full scale due to calibration issues of the full-scale discharge systems. As a result, all full-scale suppression tests utilized a different orifice plate except for the original two tests run twice to confirm deviation from the calculated outcomes.

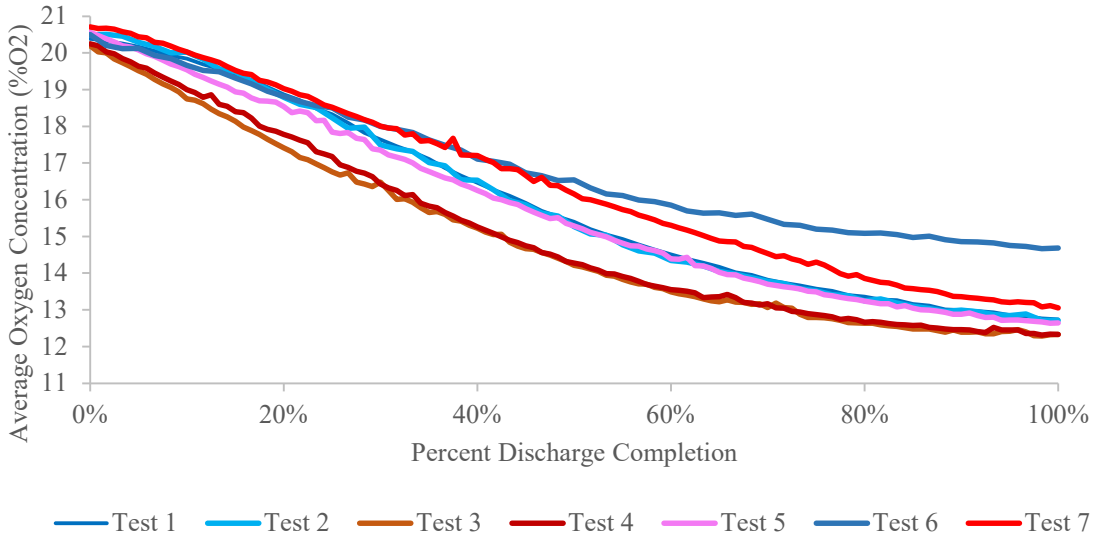

Figure 30: Full-scale oxygen concentration curves for 60 s and 120-s discharges

Of note is the fact that all full-scale discharges approached the same final agent concentration regardless of curve shape. While the orifice plate did vary, the total amount of discharge agent only varied a range of 16.5 lb (7.5 kg), or ± 7.3% of the average agent discharged between all the tests. Additionally, the average amount of total agent discharge over the 60- and 120-s discharge tests is 113 lbs and 112 lbs (51 kg), respectively. To compare the two discharge periods, the average of the three 60 s tests and four 120 s tests is used as the average amounts of agent discharged are the same.

The assumption in agent calculation that all the oxygen reduction is from the discharged agent is confirmed through two observations. The first is minimal deviation between oxygen

sensors that did and did not filter out CO and CO_2. The second is through the observation of the CO and CO_2 concentration under the crib during discharge, shown below in Fig. 31 for both scales.

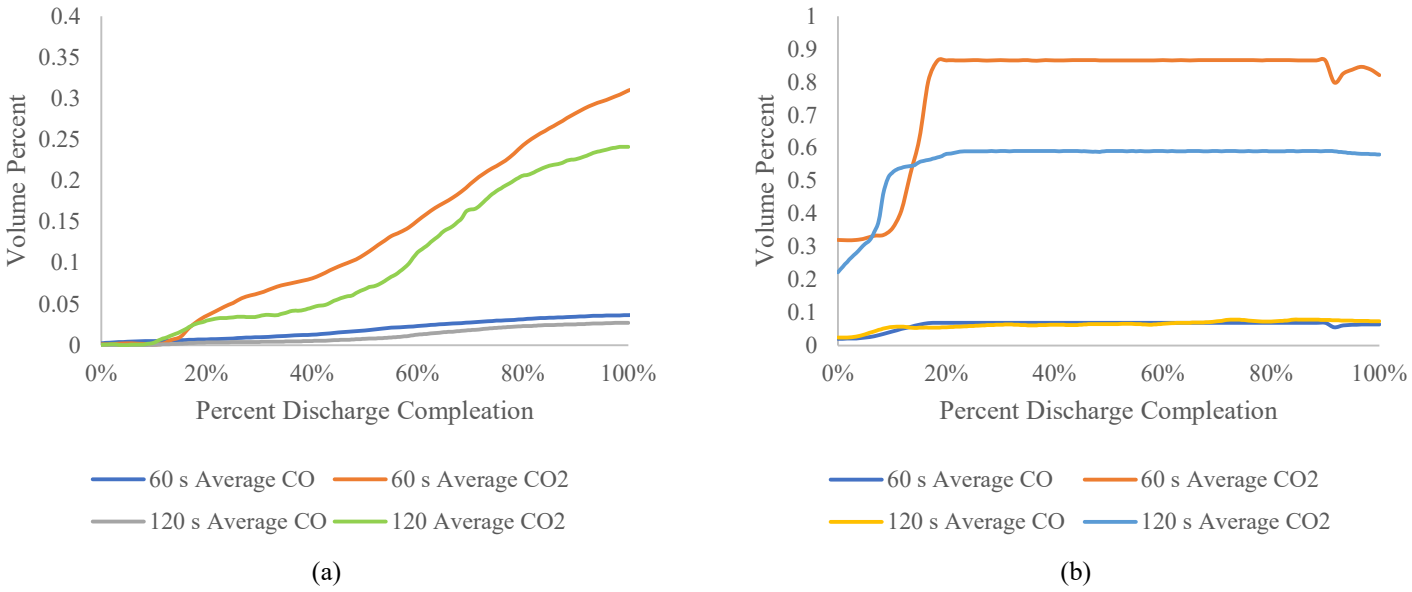

Figure 31: Average full-scale CO and CO_2, a, and reduced-scale, b, concentrations taken from under the crib during discharge.

While the concentration of CO_2 does rise through discharge, the volumetric fraction is still significantly lower than that of the added agent, and therefore is assumed to have a negligible interference with percent agent calculation. The agent concentration curves during discharge are averaged for each discharge period, shown below in Fig. 32, with the Test 6 data being removed due to an error in recorded oxygen concentration. The Test 6 error caused abnormally high oxygen concentrations during the second half of discharge which would have prevented the extinction of the crib which occurred anyways.

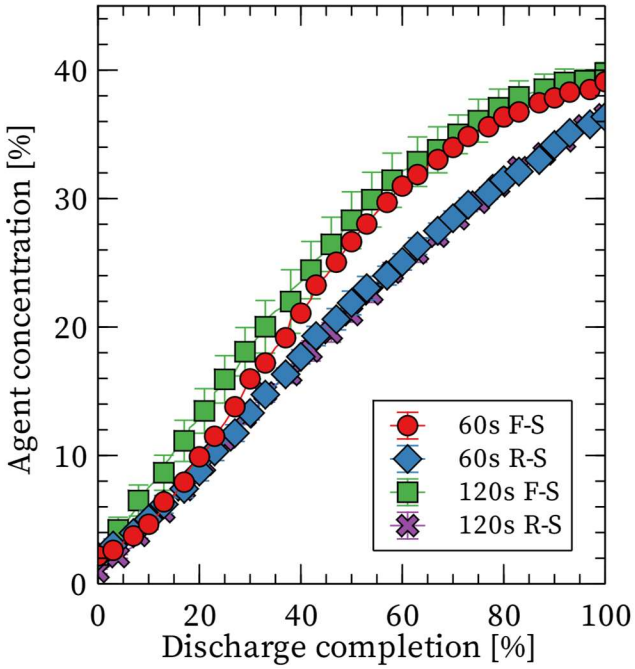

Figure 32: Average agent concentrations over percent discharge completion for both discharge periods and scales. Error bars indicate uncertainty.

The differences observed between the full-scale and reduced-scale curve shapes arise from the unexpected scaling reliance on the set size and pressure of the agent discharge bottles. Three agent bottles are used at the full-scale and are almost fully depleted at the end of the experiment. One bottle is used for the reduced scale and is only 2/3 depleted. The smaller the depletion ratio, the more linear the slope of agent concentration will be as demonstrated by the reduced scale results. For the full-scale and reduced-scale curves to better match, the ratio of percent agent used in the bottles to enclosure volume must be closer. It is important to note that regardless of agent concentration curve shape, suppression of the crib is still achieved at a constant oxygen concentration across all the tests.

4.4.2 Crib Gas Phase Velocity During Discharge: Introduction to Bulk Flow Effects

Gas phase velocity is recorded at four locations: one foot above the crib, directly above a crib pore, below the central crib pore, and horizontally in a side pore of the crib. In general,

velocity measurements, shown below in Fig. 33, at the base of the crib and at the side pore of the crib during discharge are sporadic and approached 0 m/s.

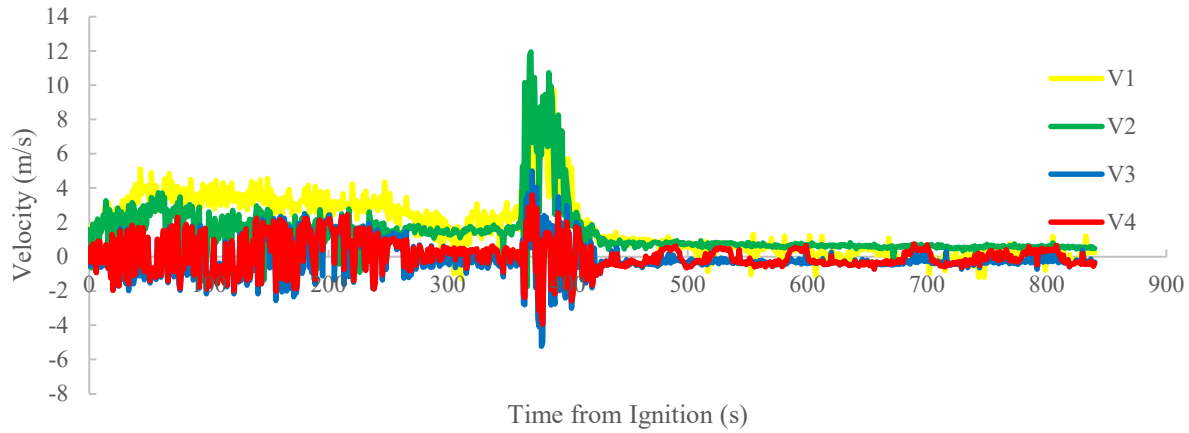

Figure 33: Full-scale Test 1 bidirectional probe velocity readings for an entire experiment starting at pan ignition, t=0.

Velocity measurements one foot above the crib, V1, and at the top of the crib, V2, provided much more interesting results due to significant deviation from steady state. The location at the top of the crib, V2, is selected for comparison between the discharge periods as it best represents the velocity through the test article. These individual full-scale trials are averaged for each discharge period, shown below. The %-discharge completion metric again allows for the comparison of 60-s to 120-s discharge periods, below in Fig. 33.

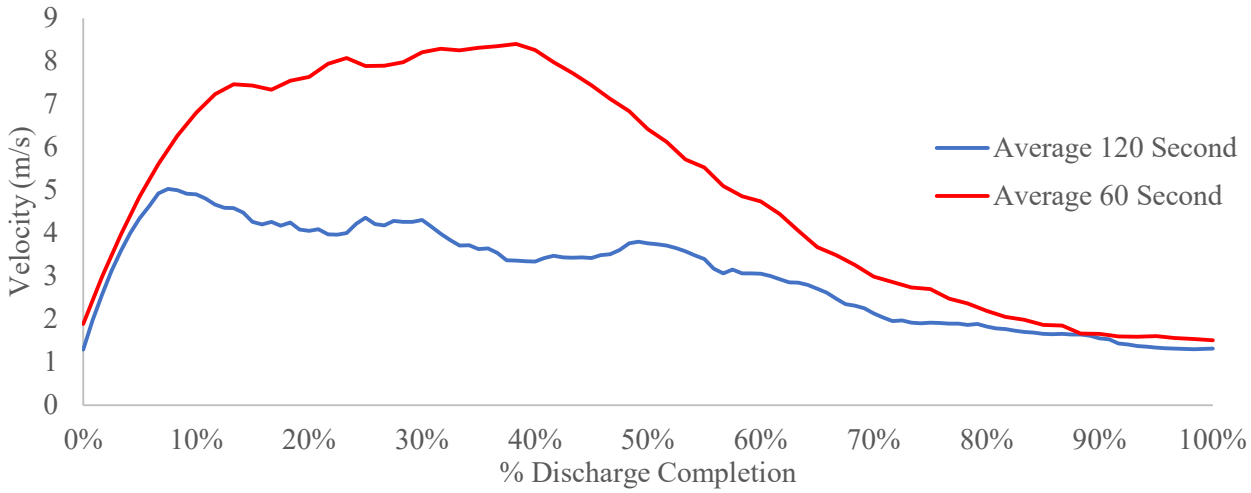

Figure 34: Full-scale average velocity profiles through a central crib pore taken one inch above the crib during discharge

During discharge at both scales, a significant amount of additional gases flow through the crib compared to the steady-state velocity of 1.6 m/s. Unlike the steady-state velocity which is only a result of the buoyant flows from the flaming crib, the velocity during discharge is a combination of the buoyant flows and added bulk flow from discharge. The added effects of bulk flow are much higher in the 60-s test because twice as much agent is discharged for the same time.

Several velocity curve characteristics are of interesting note. The first is the constant slope between the 60- and 120-s discharges during the first 10% to 15% of the discharge. During this period, the gasses within the enclosure are hypothesized to begin the formation of the bulk flow currents, discussed later in this section. The constant slopes are an indication that these currents are both interacting uniformly with the crib and increasing in a manner dependent on the discharge. The second characteristic is the overall shape of the curves. The 60-s discharge velocities increase rapidly to a point, maintain a relatively steady velocity, and then decrease while the 120-s velocities peak and then gradually decrease. The decrease of velocity is likely a function of the reduction in bottle pressure which affects how much agent is discharged from the

nozzle. It is known from earlier that because the agent concentration curves are similar for each full-scale discharge period, the amount of agent discharged over that period must be similar. Therefore, there must be some additional currently unaccounted for discharge parameter that controls the velocity of the bulk flow currents, which is currently hypothesized to be the faster depletion and changes in pressure of the nitrogen tanks. As tank pressure is not monitored and no instrumentation recorded nozzle effects, additional information and study are required to better understand the impact of the discharge velocities on velocity through the crib.

Another takeaway from the velocity curves is the final velocity at the end of discharge which approximates the original steady-state velocity. As the crib is no longer combusting at the end of discharge, the recorded velocity must be a combination of the buoyancy from the hot crib members and some additional bulk flow currents.

The effects of bulk flow are best envisioned as the enclosure dynamics resulting from the high-pressure agent discharged through the nozzle into a fixed volume enclosure which causes flows of agent and entrained gas mixtures. After leaving the nozzle at high velocities, the flows are shaped by the geometry of the enclosure and the mixture creates a recirculating profile of moving gasses, referred to as bulk flow. This flow would start at the nozzle, be shaped by the enclosure, pushed downward by the walls, and then pushed up by the floor, as visualized below in Fig. 35.

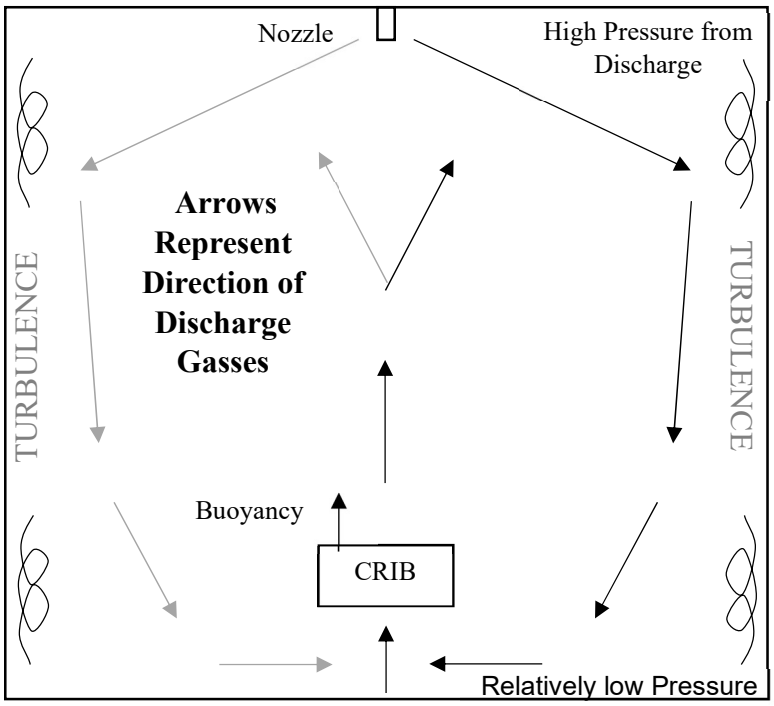

Figure: 35 Hypothesized bulk flow visualization.

The bulk flow hypothesis is supported by the increase in velocity through the crib and the changes in recorded mass and temperature which are discussed in a later section. Bulk flow is related to the amount of agent discharged into the enclosure per time. As such, the strongest effects of bulk flow are observed at the 60-s discharges and the full-scale. The effects of bulk flow are significantly weaker at the reduced scale due to the reduced amount of agent discharged. This hypothesis is based such that the relative strength of the bulk flow effects as quantified by the magnitude of deviation from crib steady-state burning is a function of the mass flow of agent into the enclosure.

Additional research must be conducted to confirm the above bulk flow hypothesis. Regardless of the actual profiles of the bulk flows within the enclosure, there are significant interactions as presented through this and the following sections between the discharge event and the test article. Characterization of the flows during discharge with and without a wood crib

would help better elaborate on how the agent and entrained gas mixtures interact with the enclosure. Instrumentation would likely include several additional bidirectional probes oriented vertically around the crib and several additional gas velocity measuring devices around the enclosure.

4.4.3 Crib Gas Phase Temperature During Discharge

During discharge, the effects of bulk flow greatly influence the recorded temperature in and around the crib, shown below in Fig. 36. As mentioned earlier, all temperatures are corrected to account for radiation losses and thermal inertia. An exemplary single test profile of all recorded temperatures is presented below.

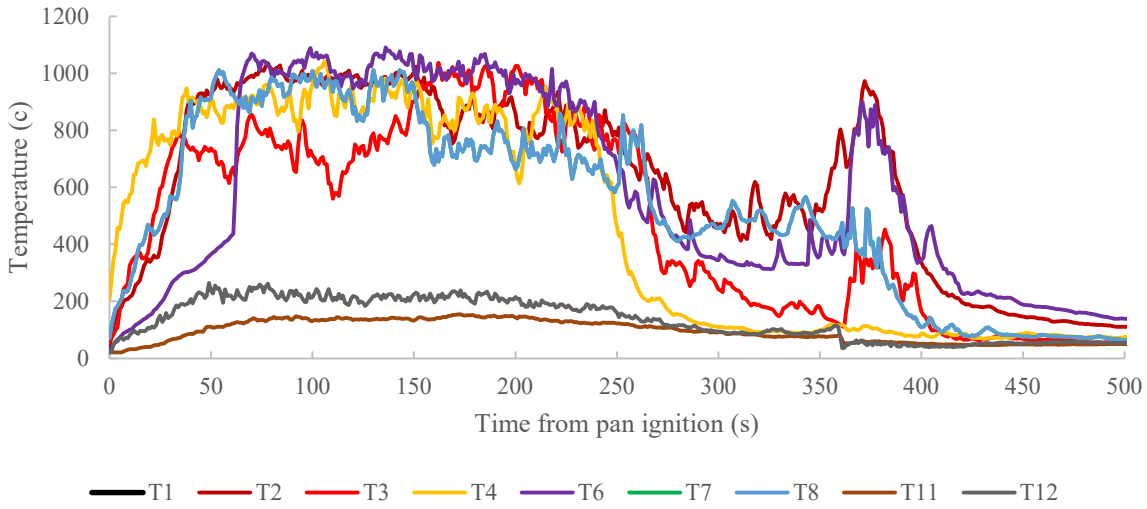

Figure 36: Full-scale Test 1, a 60-s discharge that occurred 360 s after pan ignition, t=0, thermocouple corrected temperature profiles for a whole suppression test.

Almost all the recorded temperatures exhibited a rapid increase in temperature during the first few seconds of discharge. During the period, erratic flame movements out of the crib are observed which explains why the thermocouple located on the side of the crib, T6, recorded a higher temperature. The temperature of the centrally located thermocouple in the crib, T6, and the thermocouple on the top of the crib, T2, spiked and then gradually decreased until extinction.

Due to the erratic behavior of the flames and the bulk flow, thermocouples not placed within the crib would sometimes read an ambient temperature and made comparisons between scales and discharge periods difficult. Good temperature profile repeatability is achieved for both scales using the centrally located thermocouple, T6, shown below. An average profile is also created for each scale and discharge period, shown below for the reduced scale in Fig. 37 and the full scale in Fig. 38.

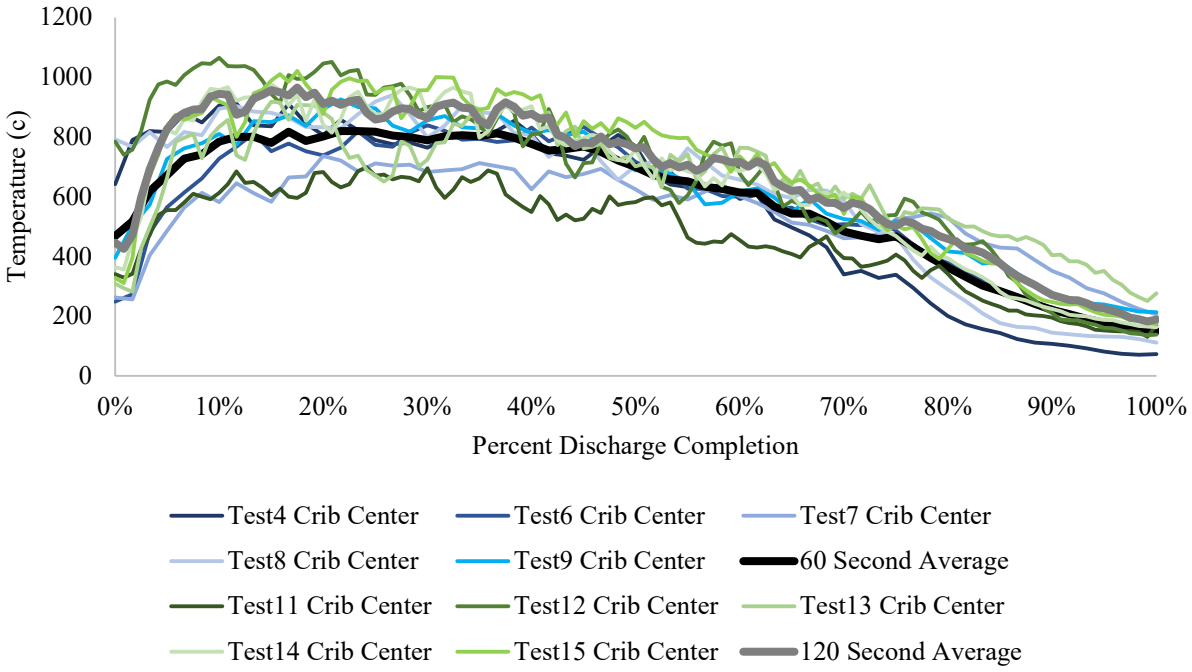

Figure 37: Reduced-scale central crib thermocouple corrected temperature for the 60-s discharges (blue shades) and 120-s discharges (green shades) with averaged values for each discharge period.

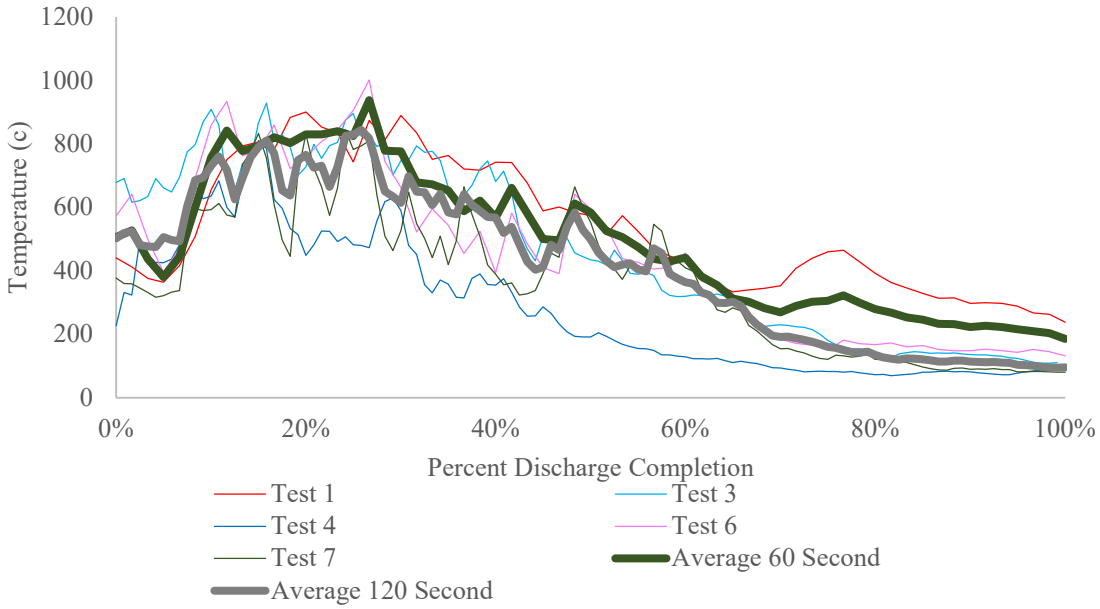

Figure 38: Full-scale central crib thermocouple corrected temperature for the 60-s discharges (red shades) and 120-s discharges (blue shades) with averaged values for each discharge period.

Each scale tracked a similar temperature curve regardless of the discharge period, shown below in Fig. 39.

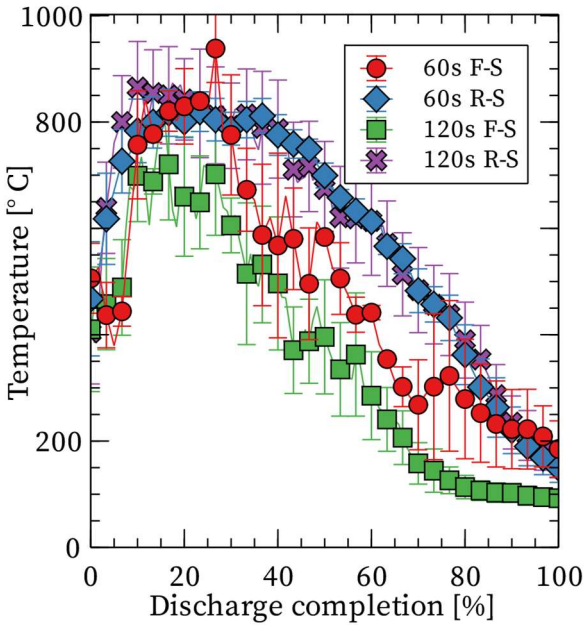

Figure 39: Full and reduced-scale average central crib thermocouple corrected temperature for the 60 s for both discharge periods.

The gradual decrease in temperature after 20% discharge is likely from the increasing amount of heat absorbed by the nitrogen gas and the reduction of the combustion reaction. Between scales, the reduced-scale cribs recorded higher temperatures than the full-scale. The discrepancy between scales is likely due to the location of the thermocouples as combustion temperatures scale according to the ambient temperature which remained unchanged [14]. Different locations in the crib do read different temperatures during discharge likely due to changes in the location of the hot pyrolysis gas and flame boundary. This boundary is where the combustion reaction takes place and is visually observed to move further into the crib during discharge as a result of bulk flow. The flame boundary transition follows the theory that as more agent and entrained air enter the crib base during discharge, the hot pyrolysis gas will need to diffuse a shorter distance before reaching a suitable amount of oxygen to combust. Future testing should locate thermocouples in areas that are eighter consistently in the flame zone or hot pyrolysis gas zone.

The increase in temperature at the start of discharge arises from the increase in the crib burning rate as a response to two phenomena: the concurrent bulk flow through the crib and the location change of the flame and hot gas boundary in the crib. The increase in burning rate was observed by McAllister & Finney over a variety of flows at ambient concentrations of oxygen and obtained similar results [19].

4.4.4 Mass During Discharge

The mass of the crib during discharge is of utmost importance as the MLR and HRR can define the combustion characteristics of the crib and provide additional clarity into extinction dynamics. Unfortunately, the effects of bulk flow prevented the direct extraction of the MLR from the mass balance assembly, which is shown below in Fig. 40.

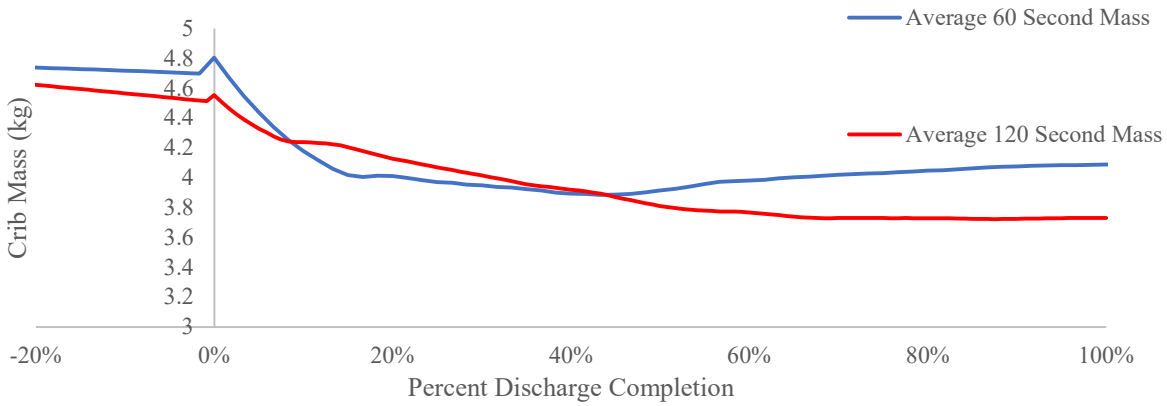

Figure 40: Full-scale averaged crib mass by discharge period.

Before discharge, the steady-state mass loss and heat release rate can be easily calculated. After the start of discharge, the effects of bulk flow push up on the crib assembly. This upward force created a rapid decrease in the recorded crib mass and apparent mass gain by the crib as the apparent strength of the bulk flow weakens and lowers the crib, shown in the MLR plots of Fig. 41.

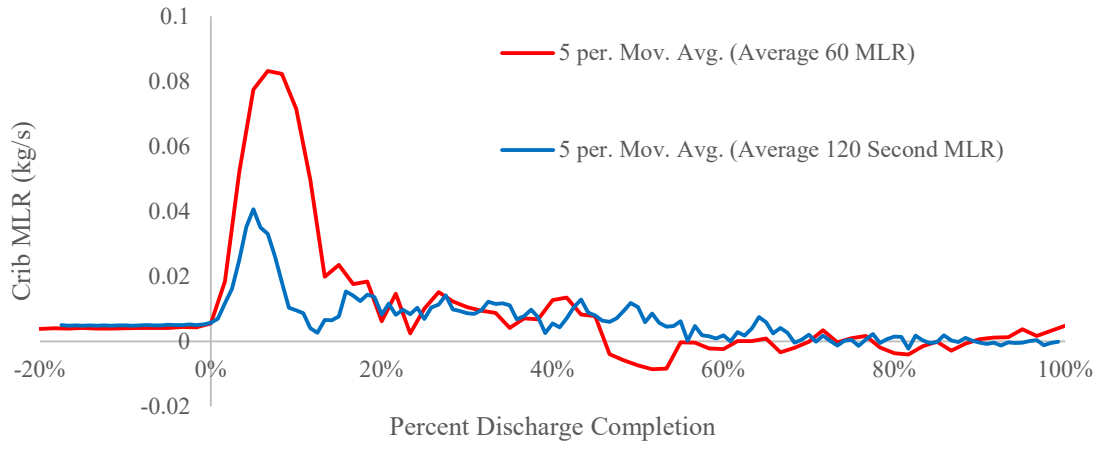

Figure 41: Full-scale averaged crib mass loss rate by discharge period with a 5-s moving average.

Periods where the crib mass loss rate is negative indicate that the crib is gaining mass, something that is known to be false as all observed cribs are still combusting halfway through the discharge period. The effects of bulk flow are much less apparent on the reduced-scale data, shown below in Fig. 42.

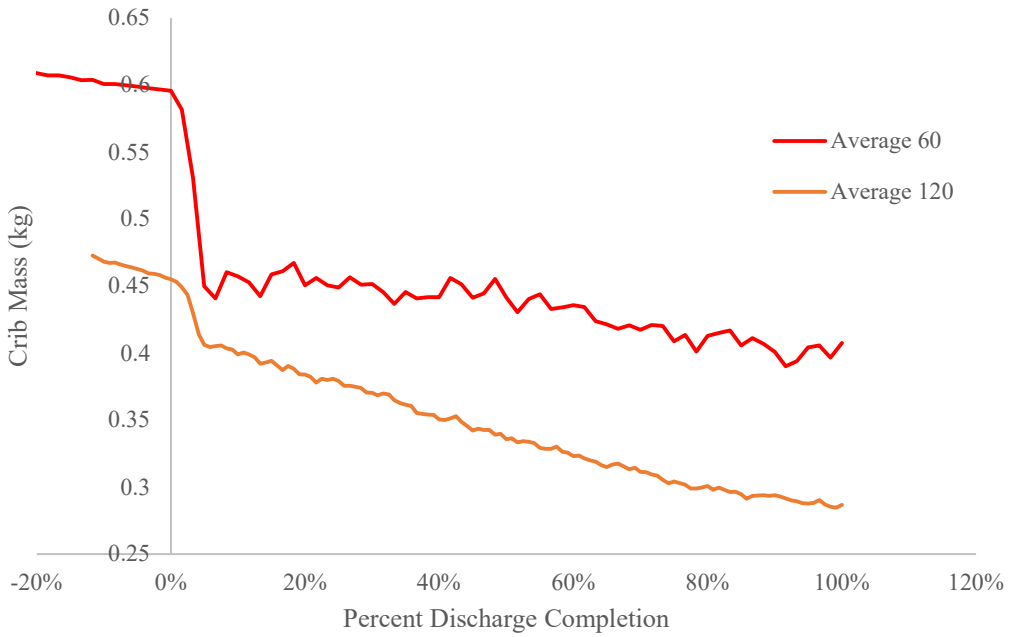

Figure 42: Reduced-scale averaged crib mass by discharge period.

The average mass plots are the perfect example of the changing effects of bulk flow during discharge. At the start of discharge, the effects are the strongest as the enclosure volume comes to a new steady state. During this period the increase of velocity through the crib and the upward force on the crib mass assembly is the highest, causing the apparent dip in crib mass and increase in MLR. After this peak, there is a relatively steady state between 20% and 40% of the discharge for both the MLR and velocity. After 50% of the discharge, the velocity through the crib starts to decrease because of weakening bulk flow effects and the suppression of the crib. At the time of crib suppression, the MLR of the crib still approaches zero as expected, but the bulk flow effects still are interacting with the assembly.

Filtering out the effects of bulk flow on the mass data proved difficult for two reasons. First, the effects of bulk flow vary greatly from the start of discharge to the end, as evident by the peaks in MLR at the start of discharge shown above in Fig. 42. Second, the relative amplitude of the effects of bulk flow are much larger than that of the desired MLR. At the start of discharge, the crib should still be burning at a similar MLR to the steady-state around 4.66 g/s. However, the 60-s discharge maxes out at 82 g/s, a 1700% increase. This removal of bulk flow effects while preserving the underlying mass loss rate of the crib requires additional measurements and correlations.

The currently proposed filtering method utilizes the changing dynamic pressure through the crib over time. Because no full-scale cold discharge tests, without a combusting crib, measured the dynamic pressures near the crib and resulting MLR, an empirical equation cannot be easily created. Several reduced scale cold discharge tests did record the velocity through a non-combusting crib, but the quality of these measurements is too inaccurate to account for the bulk flow.

Additional changes to the mass assembly can also help reduce the effects of bulk flow. The addition of a box or shield around the base of the balance should prevent any entrain agent-air mixture from pushing on the plate of the balance. Additionally, the stand assembly on which the crib is placed should be rebuilt such that the weight is reduced, and the surface area of the stand is minimized.

4.5 Extinction

UL 2127 requires that the crib be extinguished 600 s after the end of discharge and prevented from reignition when exposed to fresh air. In all cases, crib suppression is achieved and reignition did not occur. Crib extinction is quantified as the total disappearance of flame

from the wooden crib test article. Observations are made visually through a window in the enclosure and checked against the variety of cameras station around and in the enclosure.

During discharge, the flames rising from the crib became erratic, and would gradually decrease in the second half of discharge. At the full scale, the edges of the crib would extinguish first, and a wavelike movement of extinguishing would move to the center of the crib until the entire crib is extinguished. Typically, the last member to extinguish would be in the center of the crib. Similar behavior is observed at the reduced scale. However, if a stick member broke across the stick grain, combustion would be supported in that location the longest, likely due to reradiation effects of the two new parallel surfaces.

The extinguishing concentration is the average enclosure oxygen concentration recorded at the time of extinguishment, shown below for all experiment in Fig. 43.

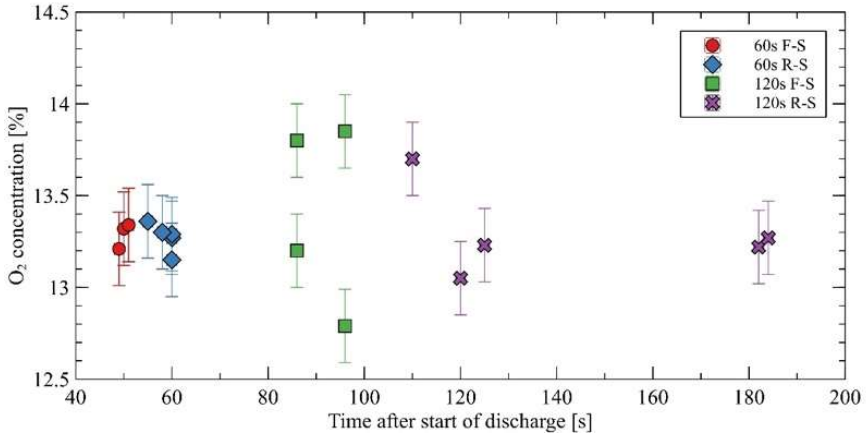

Figure 43: Average Enclosure Oxygen concentration at extinguishment versus time of extinguishment.

The average extinguishing concentrations for the full and reduced-scale tests are 13.35% O_2 and 13.33% O_2 oxygen, respectively. Both oxygen concentrations correspond to 36% agent. The extinguishing content is slightly larger than the 33.4% target agent concentration, possibly due to the overdesign of the systems which lead to additional agent discharged into the enclosure.

While 33.4% agent may have been enough to eventually extinguish the cribs in the allowed timeframe, the experimental concentration of agent increased too rapidly to observe this.

The most interesting outcome of crib extinguishment is the range in extinguishment times, and the fact that several cribs can support combustion after the end of discharge in environments with low oxygen concentrations. The range of extinguishment times at the full-scale is 2 and 5 s for the 60 and 120-s discharges respectively. The range of extinguishment times at the reduced scale is 5 and 72 s for the 60 and 120-s discharges respectively. The range in extinguishment times fits into the bulk flow hypothesis such that larger bulk flow effects reduce the range in extinguishment times, possibly due to additional effects such as blowout of the crib at the higher gas velocities of stronger bulk flow effects.

While the validity of the reduced scale enclosure in accomplishing the design goals is clear, additional errors may have been introduced in the construction of the reduced-scale enclosure. While the entire enclosure is sealed by expanding foam, the floor of the enclosure is raised, and cracks allowed for the exchange of gasses after the foam is pushed out. While this meant that pressure relief venting during discharge is not required, it also created a pathway for oxygen to enter the enclosure post-discharge. This oxygen stream may have been able to supply the test article with enough oxygen to support the combustion of the crib, resulting in extraordinarily longer times to extinguishment. The future reduced-scale enclosure should also be placed on a laboratory floor and sealed similarly to the full-scale.

4.6 Soak Period Results

After the end of discharge, the average oxygen concentration in the enclosure rapidly approaches its lowest value. However, without the mixing effects brought on by the bulk flow, stratification due to gaseous density differences occur within the enclosure. For inert gasses, the

difference in density can arise from the temperature difference between the agent-gas mixture in the enclosure and ambient air that leaks into the enclosure or from differences in atomic densities. Since the atomic density of nitrogen at STP is very close to that of air, the density difference that drives stratification is likely that of temperature difference.

The response of the oxygen sensors at the full-scale demonstrate stratification well, as seen in Fig. 44 below for the exemplary full-scale test 1. After discharge, the concentration of oxygen continues to fall 0.1% to 0.3% oxygen on average for 10 s due to residual mixing and transport in the oxygen analysis systems. From there, natural leakage begins to occur and the average oxygen concentration in the enclosure will begin to rise.

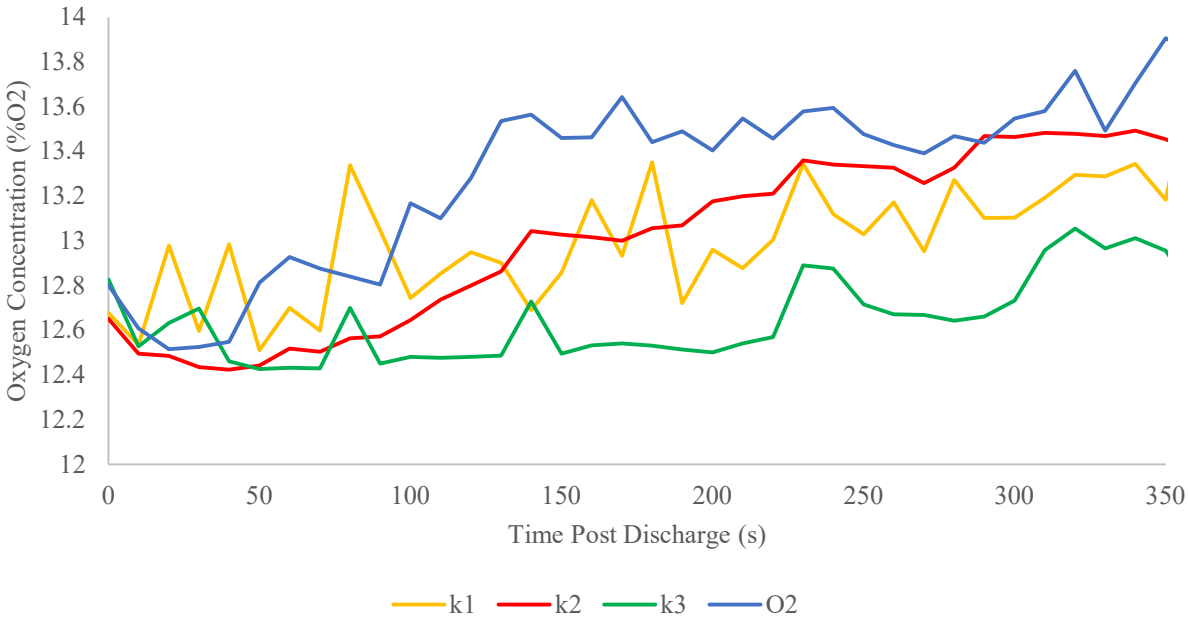

Figure 44: Ful Scale Test 1 oxygen concentration at various enclosure locations post-discharge.

In general, for all the full-scale tests, there is minimal oxygen concentration rise at the top of the enclosure, k3. The oxygen sensors at the bottom of the enclosure, k1, and at the crib, O_2,

recorded the highest increase in oxygen concentration as reflected in Table 10. This is due to the colder ambient air settling at the bottom as the air leaks into the enclosure.

Table 10: Average leakage rate at each full-scale oxygen sensor location

	K1	K2	K3	O_2
Averages (%O_2)	2.87E-03	2.38E-03	1.39E-04	2.46E-03

Instrumentation could not record the entire 10-minute soak period due to complications with data acquisition memory and function. Some tests only record short periods of the post-discharge soak period. Visual observations of the oxygen sensors confirmed oxygen concentration rise throughout the entire soak period. Using the same method as the average concentration during discharge, the average leakage rate can be calculated for each test through the averaging of oxygen concentration at each sensor location, as shown in Fig. 45 below.

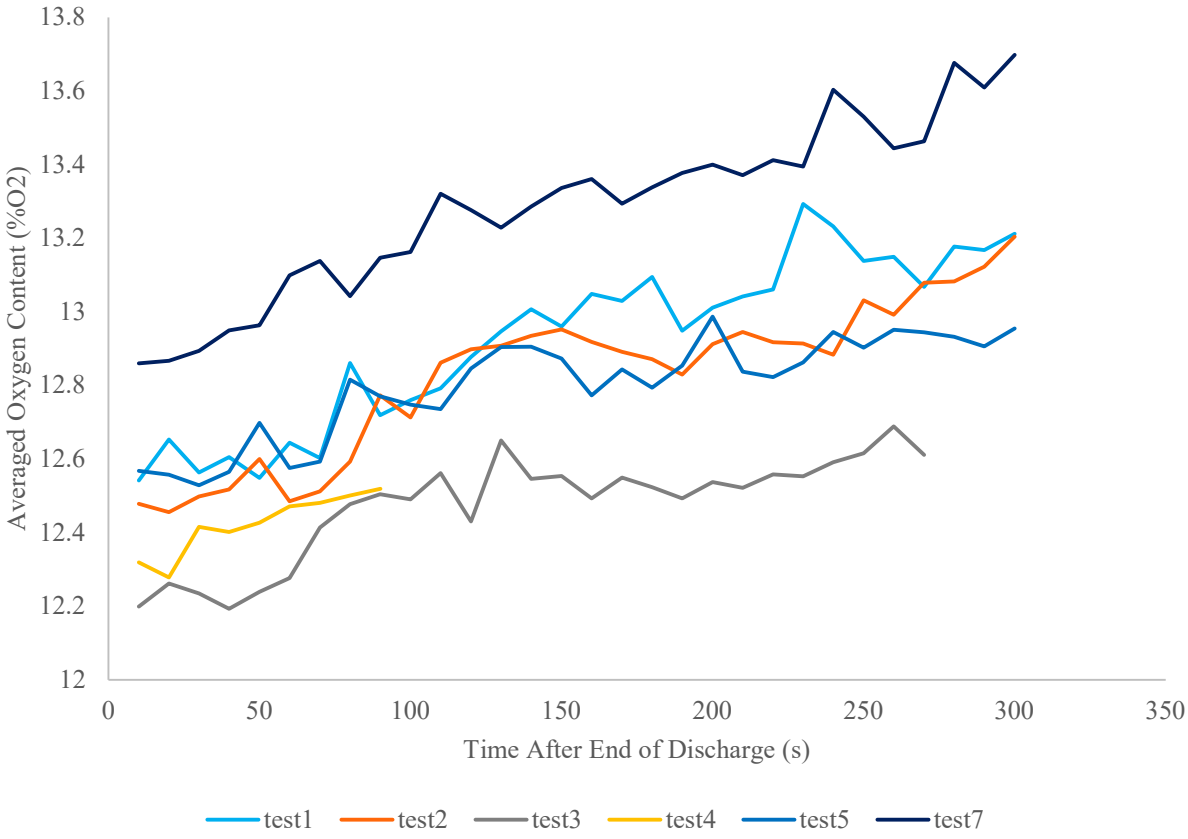

Figure 45: Ful scale average enclosure oxygen concentration post-discharge.

Averaging each available leakage value, the large-scale enclosure leakage rate can be quantified as 0.002225 % O_2/s, which correlates to an average increase of 1.34 % O_2 over the whole 10-minute soak period.

At the reduced scale, higher average leakage rates are observed due to the construction of the enclosure. Interestingly, the upper layer of constant agent concentration extended down to the second highest far-field oxygen sensor, k2 and k3, shown in Fig. 46. This change from the full-scale is likely due to the relative location of the k2 sensors. At both scales, the k2 sensor is at a height equivalent to the crib base. However, the distance between the ceiling and the crib base is significantly larger at the full-scale, which would explain a change in the stratified layered location.

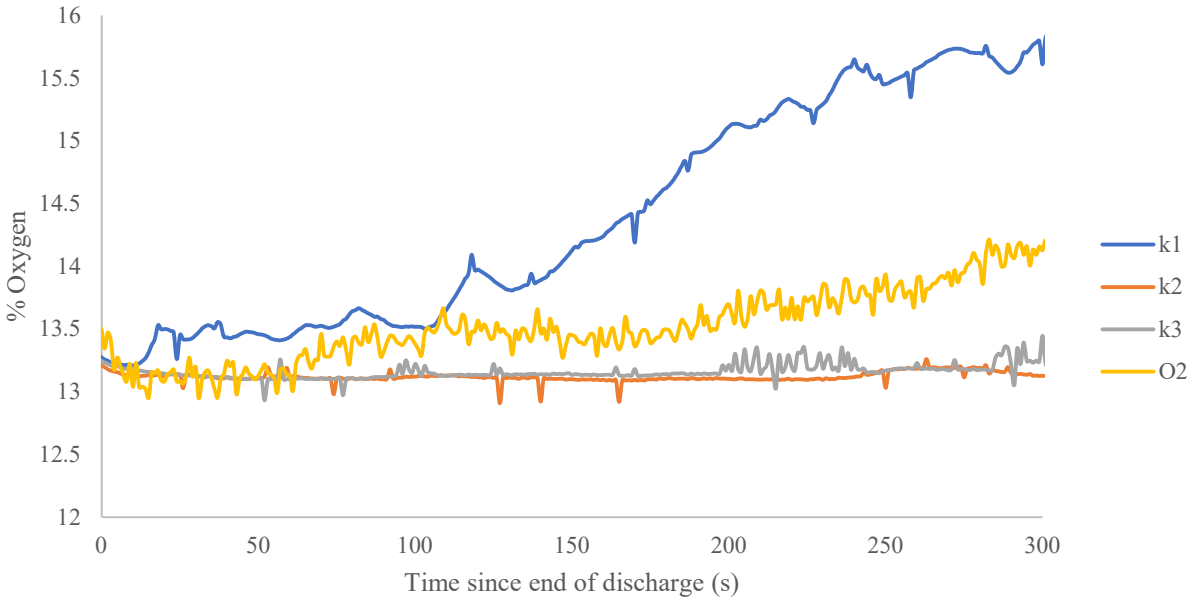

Figure 46: Reduced-scale test 15 post-discharge oxygen concentrations at the four oxygen sensor locations.

Various mixing effects are shown on the figure above which are visible as dips or peaks on the oxygen concentration. Again, the average oxygen concentration for all four sensors per time step is used to characterize the leakage of the enclosure for each test, shown below in Fig. 47.

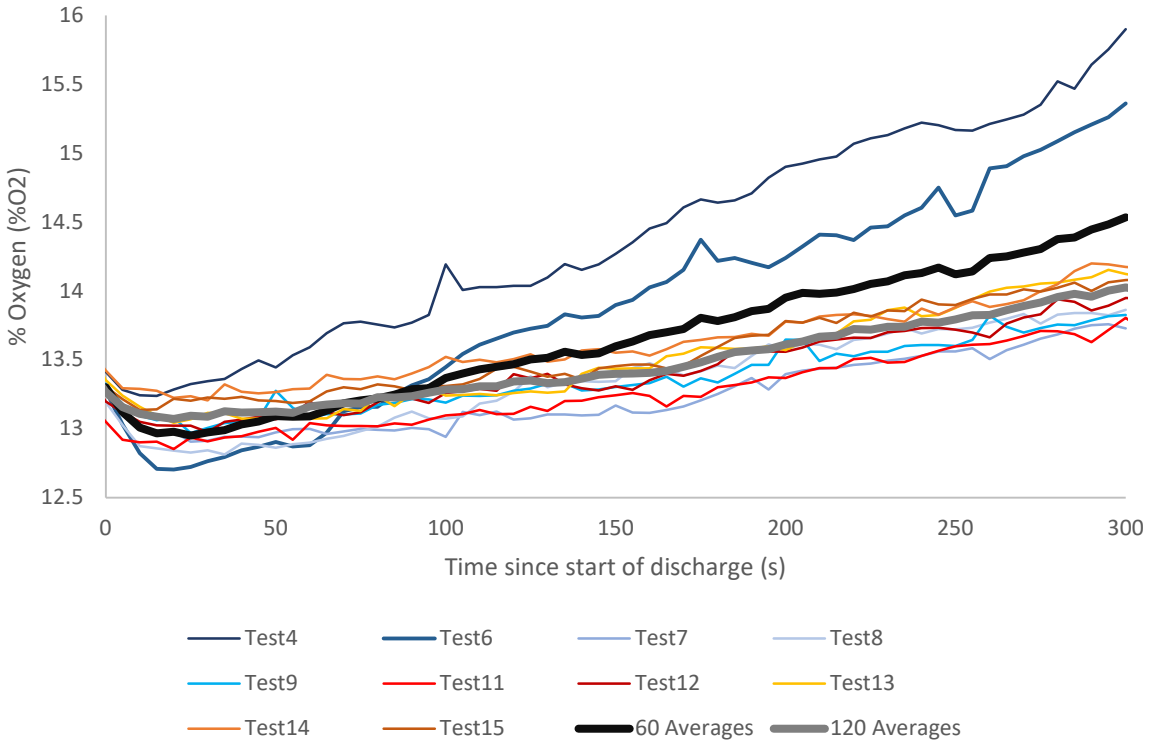

Figure 47: Reduced-scale post discharge leakage rates, averaged oxygen concentrations.

Reduced-scale Tests 4 and 6 has significantly higher leakage than originally intended. After these tests, the enclosure received another layer of expanding foam sealant, which reduced the leakage of the enclosure post-discharge significantly. Average leakages are calculated for each test once oxygen concentration levels reach their minimum roughly 30 s after the end of discharge. The average enclosure leakage is taken to be the average of each test leakage, excluding tests 4 and 6, and is calculated to be 3.39 E-3 % O_2 ± 6.43 E-4 % O_2. This leakage would create an average loss of 2.03 % O_2 over the entire 10-minute soak period, which is slightly larger than that of the full-scale. The differences in leakages arise from differences in leakage area to enclosure surface area ratios between the scales where smaller leakage areas at the reduced scale have significantly larger impacts than at the full-scale.

Future characterization of enclosure leakage may utilize a pressurization method to define leakages between scales. Construction of the reduced-scale enclosure should be on a solid floor, not on a raised wooden platform. While this platform did allow for pressure relief during discharge, it is hypothesized to have a significant impact on post-discharge leakage.

Experience has shown that utilizing two layers of expanding foam on the outside of the enclosure to cover all sheeting joints followed by a single heavy layer on the inside of the enclosure creates a good seal. A layer of foam should also be applied at the bottom of the enclosure where it joins with the floor.

5.0 Conclusions

Wood crib fire suppression over a 60-s and 120-s discharge period was examined using full-scale and reduced-scale experiments modeled after the UL 2127 and FM 5600 extinguishment test methodologies for the inert gas agent IG-100. The change in discharge time from 60 to 120 s had a negligible effect on the average agent extinguishment concentration of 36% for both scales. No crib at either scale or discharge period reignited after suppression or when exposed to fresh air after the prescribed 10-minute soak period.

The constant agent extinguishing concentration results indicate that any differences between approved and listed MEC are likely not related to the discharge period selection. While the choice of extinguishment period may not affect the extinguishing concentration, it does change the extinguishment dynamics. A requirement to identify the chosen discharge period on the official test results would significantly reduce any confusion around this issue and assist in identifying the source of any differences in MEC.

The differences in extinguishment dynamics are a result of the bulk flows of agent and entrained air within the enclosure. The effects of bulk flow include an increase in gas velocity through the crib, higher temperatures at the center of the crib, and measurable forces on the mass balance assembly during discharge compared to the free burning period before discharge. The effects of bulk flow were found to be dependent on the amount of agent discharged and the discharge period. The effects of bulk flow are weakest at longer discharge periods and smaller scales due to the reduced rate of agent discharge. Inert gas system designers should consider these bulk flow effects when selecting the discharge period.

While the UL 2127 extinguishment test is efficient at approving design concentration for inert gas extinguishing systems, additional instrumentation is shown to be required to fully study

the suppression dynamics of the test article within the enclosure. A mass balance was added to quantify the mass loss of the wood crib during the test, and several thermocouples and velocity probes were used to measure the bulk flow effects at each scale and discharge period. This additional volume of data collected allowed the evaluation of agent concentration and temperature profiles during discharge which supports the use of the reduced-scale testing methodology in replicating the full-scale test results at both the 60 s and 120 s discharge periods. Furthermore, agent concentrations and the average extinguishment concentration obtained through the reduced-scale tests replicate those of the average full-scale test results.

The results presented in this thesis are promising and entice the further study of extinction dynamics specifically at the two specified discharge periods and scales. As the extinguishing concentrations for both discharge periods are the same, there must be some additional extinction mechanism that effects the listed MEC. Additionally, the reduced scale crib and enclosure have the potential to become a useful tool in the study of inert gas and other clean agent extinguishing systems.

6.0 Recommendations

At the beginning of the project, it was decided that only wood cribs would be studied to observe any changes in reignition potential at the longer discharge time. As such, the reduced scale enclosure was scaled around the wood crib and its burning rate. Further testing is still required to adopt the three UL plastic sheet arrays to the reduced-scale enclosure. While these sheet arrays were not originally selected, the extinguishing dynamics of the arrays is still important to the UL 2127 test. Additionally, these sheet arrays utilize a baffle to block the direct flow of gasses onto the sheets which may change the interactions of agent with the test article.

From this work, it is known that the enclosure leaks agent in two ways; through pressure relief vents during discharge and through small gaps in the enclosure construction during discharge and the 10-minute soak period. These leakages should be better characterized in support of completing the agent mass balance and identifying where the discharged agent goes during and after discharge with the intent of identifying how much agent interacts with the wood crib before extinction. Further, the mass of agent and air extracted for oxygen sensors during the soak period should be accounted for and less invasive oxygen measurement methods should be utilized or developed.

References

[1] P.J. di Nenno, E.W. Forssell, Clean agent total flooding fire extinguishing systems, SFPE Handbook of Fire Protection Engineering, Fifth Edition. (2016) 1483–1530. https://doi.org/10.1007/978-1-4939-2565-0_44.

[2] T. Moore, N. Yamada, Nitrogen gas as a halon replacement, Nist.Gov. (n.d.). https://www.nist.gov/system/files/documents/el/fire_research/R0000296.pdf (accessed January 27, 2022).

[3] European Aviation Safety Agency Certification Specifications for Large Aeroplanes (CS-25), 2012.

[4] J. Gałaj, T. Drzymała, Assessment of extinguishing efficiency of hybrid system using water mist and inert gas during class A fires, Matec-Conferences.Org. (n.d.). https://doi.org/10.1051/matecconf/201824700013.

[5] X. Zhou, Y. Xin, S. Dorofeev, Evaluation of an oxygen reduction system (ORS) in large-scale fire tests, Fire Safety Journal. 106 (2019) 29–37. https://doi.org/10.1016/J.FIRESAF.2019.03.013.

[6] I.S. Organization, ISO 14520-1, Gaseous Fire Extinguish Systems (2006), (n.d.).

[7] NFPA 2001: Standard on Clean Agent Fire Extinguishing Systems, 2018 Edition, (n.d.). https://codesonline.nfpa.org/code/61bf4122-7b68-4751-877d-043cdc7564e8/ (accessed January 27, 2022).

[8] J.A. Senecal, Flame extinguishing in the cup-burner by inert gases, Fire Safety Journal. 40 (2005) 579–591. https://doi.org/10.1016/J.FIRESAF.2005.05.008.

[9] UL 2127, Inert Gas Clean Agent Extinguishing System Units, (n.d.). https://standardscatalog.ul.com/ProductDetail.aspx?productId=UL2127 (accessed January 27, 2022).

[10] FM Approvals, Examination Standard for Clean Agent Extinguishing Systems Class Number 5600, 2021.

[11] V. Gupta, J.L. Torero, J.P. Hidalgo, Burning dynamics and in-depth flame spread of wood cribs in large compartment fires, Combustion and Flame. 228 (2021) 42–56. https://doi.org/10.1016/j.combustflame.2021.01.031.

[12] P.H. Thomas, Behavior of fires in enclosures-Some recent progress, Symposium (International) on Combustion. 14 (1973) 1007–1020. https://doi.org/10.1016/S0082-0784(73)80091-8.

[13] D. Gross, Experiments on the burning of cross piles of wood, Journal of Research of the National Bureau of Standards, Section C: Engineering and Instrumentation. 66C (1962) 99. https://doi.org/10.6028/JRES.066C.010.

[14] J.G. Quintiere, Fundamentals of fire phenomena, John Wiley, Place of publication not identified, 2006.

[15] G. Heskestad, Modeling of enclosure fires, Symposium (International) on Combustion. 14 (1973) 1021–1030. https://doi.org/10.1016/S0082-0784(73)80092-X.

[16] W.L. Fons, H.B. Clements, P.M. George, Scale effects on propagation rate of laboratory crib fires, Symposium (International) on Combustion. 9 (1963) 860–866. https://doi.org/10.1016/S0082-0784(63)80092-2.

[17] M.A. Delichatsios, Fire growth rates in wood cribs, Combustion and Flame. 27 (1976) 267–278. https://doi.org/10.1016/0010-2180(76)90028-6.

[18] P.A. Croce, Y. Xin, Scale modeling of quasi-steady wood crib fires in enclosures, Fire Safety Journal. 40 (2005) 245–266. https://doi.org/10.1016/j.firesaf.2004.12.002.

[19] S. McAllister, M. Finney, The effect of wind on burning rate of wood cribs, Springer. 52 (2016). https://doi.org/10.1007/s10694-015-0536-4.

[20] S. McAllister, M. Finney, Burning Rates of Wood Cribs with Implications for Wildland Fires, Fire Technology. 52 (2016) 1755–1777. https://doi.org/10.1007/s10694-015-0543-5.

[21] P.H. Thomas, D.L. Simms, H.G. Wraight, Fire Spread in Wooden Cribs Part II Heat Transfer Experiments in Still Air, Fire Safety Science. 599 (1965) 1.

[22] J.G. Quintiere, B.J. McCaffrey, The Burning of Wood and Plastic Cribs in an Enclosure: Volume I and II, Nbsir. (1980).

[23] F. Folk, Experiments in Fire Extinguishment, Quarterly of the National Fire Protection Association. 31 (1937) 115–126.

[24] V. Babrauskas, Free burning fires, 11 (1986) 33–51.

[25] Q. Xu, G.J. Griffin, Y. Jiang, C. Preston, A.D. Bicknell, G.P. Bradbury, N. White, Study of burning behavior of small scale wood crib with cone calorimeter, Journal of Thermal Analysis and Calorimetry. 91 (2008) 787–790. https://doi.org/10.1007/s10973-007-8338-7.

[26] J.A. Block, A theoretical and experimental study of nonpropagating free-burning fires, Symposium (International) on Combustion. 13 (1971) 971–978. https://doi.org/10.1016/S0082-0784(71)80097-8.

[27] NFPA 13: Standard for the Installation of Sprinkler Systems, 2022 Edition, (n.d.). https://codesonline.nfpa.org/code/ff23db20-cc0f-46d1-8c39-7bcc396d1203/ (accessed January 27, 2022).

[28] NFPA 502: Standard for Road Tunnels, Bridges, and Other Limited Access Highways, 2017 Edition, (n.d.). https://codesonline.nfpa.org/code/49dafd1b-c48b-43bc-9a0a-e03b43da5593/ (accessed January 27, 2022).

[29] NFPA 251: Standard Methods of Tests of Fire Resistance of Building Construction and Materials , 2006 Edition, (n.d.). https://codesonline.nfpa.org/code/fe1efac0-4548-4154-b5c0-911a6907a97e/ (accessed January 27, 2022).

[30] NFPA 285: Standard Fire Test Method for Evaluation of Fire Propagation Characteristics of Exterior Wall Assemblies Containing Combustible Components, 2019 Edition, (n.d.). https://codesonline.nfpa.org/code/fe1efac0-4548-4154-b5c0-911a6907a97e/ (accessed January 27, 2022).

[31] UL 711, Rating and Fire Testing of Fire Extinguishers, (n.d.). https://standardscatalog.ul.com/ProductDetail.aspx?productId=UL711_8_S_20180806 (accessed January 27, 2022).

[32] UL 1626, Residential Sprinklers for Fire Protection Service, (n.d.). https://standardscatalog.ul.com/ProductDetail.aspx?productId=ULC1626_1_O_20031101 (accessed January 27, 2022).

[33] UL 1715, Fire Test of Interior Finish Material, (n.d.). https://standardscatalog.ul.com/ProductDetail.aspx?productId=UL1715 (accessed January 27, 2022).

[34] M.J. Hurley, D.T. Gottuk, J.R. Hall Jr., Kazunori. Harada, E.D. Kuligowski, Milosh. Puchovsky, J.L. Torero, J.M. Watts Jr., C.J. WIECZOREK, SFPE Handbook of Fire Protection Engineering, (2016).

[35] M. Obach, E. Weckman, Comparing the heat release rate and heat flux of uniformly constructed wood cribs, Researchgate.Net. (2010). https://www.researchgate.net/profile/E-Weckman-2/publication/284158399_Comparing_the_Heat_Release_Rate_and_Heat_Flux_of_Uniformly_Constructed_Wood_Cribs/links/564ca8bb08aedda4c1343331/Comparing-the-Heat-Release-Rate-and-Heat-Flux-of-Uniformly-Constructed-Wood-Cribs.pdf (accessed January 27, 2022).

[36] Y.Z. Li, H. Ingason, Scaling of wood pallet fires Scaling of wood pallet fires, 88 (2014) 96–103.

[37] Loss Prevention Council, Halon alternatives: a report on the fire extinguishing performance characteristics of some gaseous alternatives to Halon 1301, 1996.

[38] E. Forssell, personal communication. March 31, 2021, (n.d.).

[39] Inc.) Peter Stokes (Kidde Fenwal, personal communication. March 24, 2021, (n.d.).

[40] D. Drysdale, An introduction to fire dynamics, John Wiley & sons, 2011.

[41] The Wood Database, (n.d.). https://www.wood-database.com/ (accessed January 27, 2022).

[42] D.J. Rasbash, B. Langford, Burning of wood in atmospheres of reduced oxygen concentration, Combustion and Flame. 12 (1968) 33–40. https://doi.org/10.1016/0010-2180(68)90006-0.

[43] ISO - ISO 14520-13:2015 - Gaseous fire-extinguishing systems — Physical properties and system design — Part 13: IG-100 extinguishant, 2015.

[44] J.A. Senecal, personal communication. March 24, 2021, (n.d.).

[45] NOVA Analytical Systems, 320 Series: Portable Flue Gas Analyzer for Oxygen, n.d. www.nova-gas.com.

[46] K. Fire Systems, Kidde Fire Systems Inert Gas Engineered Fire Suppression System Design, Installation, Operation, and Maintenance Manual with FM Approval, 2020. www.fia.uk.com.

[47] Kidde Fenwal Inc., Kidde Fire Systems ® Nitrogen Engineered Systems, (2016) 2015–2016.

[48] B.J. McCaffrey, G. Heskestad, A robust bidirectional low-velocity probe for flame and fire application, Combustion and Flame. 26 (1976) 125–127. https://doi.org/10.1016/0010-2180(76)90062-6.

[49] L. Kent, M. Schneider, The design and application of bi-directional velocity probes for measurements in large pool fires, Instrument Society of America Transactions. 26 (1987). https://ui.adsabs.harvard.edu/abs/1987isa..symp...11K/abstract (accessed January 27, 2022).

[50] Engineeringtoolbox.com., Engineering Tool Box. (2016).

[51] C. Shaddix, Correcting thermocouple measurements for radiation loss: a critical review, (1999). https://www.osti.gov/biblio/20002672 (accessed January 27, 2022).

[52] C. Shaddix, A new method to compute the proper radiant heat transfer correction of bare-wire thermocouple measurements., (2017). https://www.osti.gov/servlets/purl/1456686 (accessed January 27, 2022).

[53] A. v. Singh, M.J. Gollner, A methodology for estimation of local heat fluxes in steady laminar boundary layer diffusion flames, Combustion and Flame. 162 (2015) 2214–2230. https://doi.org/10.1016/J.COMBUSTFLAME.2015.01.019.

[54] S. Whitaker, Forced convection heat transfer correlations for flow in pipes, past flat plates, single cylinders, single spheres, and for flow in packed beds and tube bundles, AIChE Journal. 18 (1972) 361–371. https://doi.org/10.1002/AIC.690180219.

[55] B. Messerschmidt, P. van Hees, Inuence of Delay Times and Response Times on Heat Release Measurements, FIRE AND MATERIALS Fire Mater. 24 (2000) 121–130. https://doi.org/10.1002/1099-1018(200003/04)24:2.

[56] M.J. Didomizio, E.J. Weckman, An evaluation of methodologies for determining delay times in the cone calorimeter fire test, Journal of Testing and Evaluation. 44 (2016) 1050–1063. https://doi.org/10.1520/JTE20140401.

Annex A: Kidde Statement of Work

Subject: Effects of Inert Gas Discharge Time on Class A Fires

Introduction

This document briefly describes critical aspects of conducting Class A fire tests for inert gas agent fire extinguishing systems. Passing such tests in the most efficient manner possible, i.e., using the least amount of agent, while still satisfying the performance requirements of the prevailing safety standards, is important to the commercial success of the product. There is little or no published research on the Class A fire test methodology and effects of parameter variance, namely in total system discharge time, on system performance.

Background

Agency approval of total flooding fire extinguishing systems includes establishment of a minimum extinguishing concentration (MEC) of a gaseous agent, as developed by the specific manner of agent discharge, including nozzle performance, that meets the extinguishing criteria of a specified Class A fire test protocol.[1] The Class A fire tests are conducted in a test enclosure having a volume of at least 100 m^3 and that meets certain dimensional requirements. There are four different test articles: a wood crib and three arrays of plastic sheets made from either polypropylene, PMMA, or ABS resin. The construction and preparation of the test articles are described in the standards. Each test sets afire a test article using prescribed protocol for ignition and pre-burn after which the gaseous agent fire extinguishing is "actuated," initiating discharge of agent in the intended manner. See Annex A. The test is successful if there is no evidence of combustion when the test article is moved from the test chamber and into ambient air ten-minutes after the end of discharge. The plastic sheet arrays must also meet the additional

requirement of not having lost more than 15 grams of mass "between 10 s and 600 s after the end of discharge."

The Class A fire test protocol is largely unchanged since it was first introduced in the first edition of UL 2127 (and UL-2166 for halocarbon agents) in 1997. At that time inert gas fire extinguishing systems were required to fully discharge in 1 minute, as required by the then current edition of NFPA 2001.

The 2012 and subsequent editions of NFPA 2001 allow for two-minute discharge time for inert gas systems when the fire hazard was Class A (or C), but not Class B. The use of two-minute discharge over one-minute discharge has some operational cost advantages including reduced-size enclosure pressure relief vents and smaller diameter distribution pipe.

Effect of discharge time on Class A fire test performance

At the end of the pre-burn time, the inert gas extinguishing system is actuated, beginning the discharge of inert gas agent. During the discharge period the mean concentration of agent in the agent-air mixture rises steadily. It is to the advantage of the system manufacturer to pass the test while having discharged the smallest quantity of agent possible. As such, the total quantity of agent needed to just meet the extinguishing criteria would only have

[1]See agency standards UL 2127 (STANDARD FOR SAFETY / ANSI/CAN/UL/ULC 2127, Inert Gas Clean Agent Extinguishing System Units, May 2017) and FM 5600 (Approval Standard for Clean Agent Fire Extinguishing Systems, Class 5600, April 2013) been discharged at the very end of the allowed discharge time. That is, the

extinguishing concentration is not attained in the enclosure until after the last of the agent has been discharged.

Questions related to the foregoing include, but are not limited to:

1. How does fire development occur on the
    a. Wood crib?
    b. Plastic sheet array?
2. How does the discharge event and its duration affect rate of fire growth on a test article due to a. Turbulence induced in the enclosure air?
    b. Rate of increase of agent concentration?
    c. Uniformity of agent concentration throughout the enclosure at the end of discharge?
3. What is the state of combustion of a test article at the onset of discharge
    a. Heat release rate?
    b. Depth of char penetration in the wood crib?
    c. Temperature of as yet unburned Class A fuel in the flame zone?
    d. Agent concentration needed to extinguish flames?
4. How are the parameters noted in (3) affected by
    a. Rate of agent discharge?
        i. During the period of 0 to 25 % of agent discharge?
        ii. During the period of 25 to 50 % of agent discharge?
        iii. During the period of 50 to 755 % of agent discharge?
        iv. During the period of 75 to 100 % of agent discharge?
    b. Extending the duration of discharge from one-minute to two-minutes?

c. Variance in rate of gas discharge

i. Case 1: Discharge valve fully open at start of flow?

ii. Case 2: Discharge valve acts in a regulating manner, limiting the agent flow rate or pressure developed in at its outlet (at the beginning of a simple single-cylinder pipe system, or in the manifold of a multi-cylinder system.

Testing Materials

University shall source and purchase wood cribs and plastic sheet array using funds from the fixed fee under this Agreement. Sponsor shall provide filled cylinders containing fire suppression agent. As it conducts research, the University shall return empty cylinders to Sponsor for refills as needed and will return all Sponsor cylinders upon the Termination or expiration of this Agreement. University shall provide all other laboratory space and materials needed to conduct the Project.

Deliverables

Specific project schedule and milestones shall be agreed in writing between Sponsor and University, and shall correlate to the University's Fall 2020, Spring 2021, and Summer 2021 academic calendar.

Deliverables shall be shared with Sponsor on at least a monthly basis, and shall include, but not be limited to

1. Photographs and videos of different burn/pre-burn scenarios as discussed by Sponsor and University.

2. Raw data outputs around oxygen levels, test chamber atmospheric conditions (air temperature, pressure, etc.), agent concentrations, burn specimen mass, and other critical parameters as needed in Microsoft Excel, Access or other modifiable applications.

3. Statistical analysis and regression of different burn/pre burn scenarios.

    a. Error margin calculations

4. Analysis of raw data including graphical representations and conclusions

5. Final report at the conclusion of the 2020-2021 academic year providing detailed summary of findings, that answer the questions raised above in the section titled, “Effect of discharge time on Class A fire test performance.” Report shall include:

    a. All raw data underlying final report conclusions shall be traceable and included

    b. Names, contact information and curriculum vitae for all students and academic faculty involved

Any notes, drawings, data, or base materials prepared in the creation of the Deliverables shall be considered to be Sponsor Sole Intellectual Property, as defined in Section 7.0 of the Agreement.

Review Cadence

Throughout the duration of the project, bi-weekly review cadence is expected where personnel from Sponsor will have the opportunity to review the progress and results of the project.

Methodology

Class A test article ignition and pre-burn scenarios

Wood crib tests

UL 2127 / 35.2.2.3 The heptane is to be ignited and the crib is to burn freely for 6 min outside the test enclosure or equivalent provisions are to be provided to insure adequate venting. The heptane fire is to burn for at least 3 min, with 0.40 gallons of heptane providing a 3 to 3-1/2 min burn time. Less than 15 s before the end of the total pre burn period of 6 min, the crib is to be moved into the test enclosure and placed on a stand such that the bottom of the crib is 60 – 70 cm (24 – 30 inches) above the floor. The time required to position the burning crib within the test enclosure and the initiation of system discharge shall not exceed 15 s. Except for the pressure relief, the vents are to be closed and the system is to be actuated. At the time of actuation, the percent oxygen within the enclosure at the level of the crib shall be within 0.5 units of the normal oxygen level at atmospheric conditions.

Polymeric fuel tests

UL 2127 / 35.2.3.7 The heptane pan is to be ignited and is to burn freely for 90 s. The agent is then to be discharged 210 s after ignition of the heptane and observations made for extinguishment. The enclosure is to remain sealed for 10 min after the end of discharge.

The requirements of FM 5600 are the same as UL 2127.

Annex B: Instrumentation Calibrations and Corrections

The following subsections describe the calibration and or the correction of data recorded during experimentation.

B.1 Bidirectional Probes

Bidirectional velocity probes work on the principle that if a known pressure difference across the probe is recorded, the velocity of the fluid can be calculated [48]. Typically, the length of the probe will be 2 times the diameter, as shown in the example probe in Fig. B1 below, and the probe will be mounted in line with the direction of flow. Each probe is connected with lengths of flexible tubing to Omega® Differential Pressure Transmitters with a set range of 0.25 in H20, 62 Pa, and an accuracy of 0.01 in H20, or 2.5 Pa.

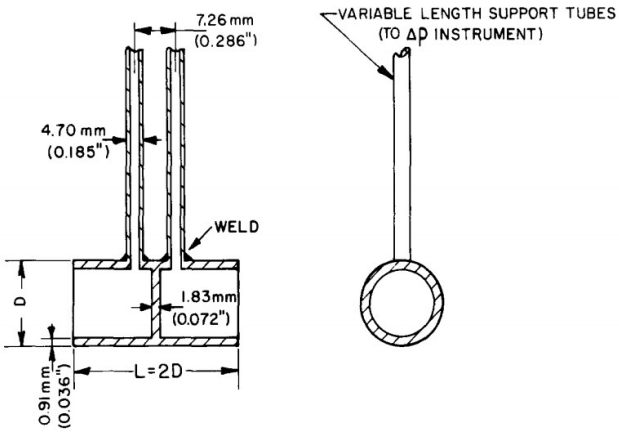

Figure B1: Example bi-directional probe construction and dimension [44]

The pressure transducers record a voltage that relates to a calibrated dynamic pressure, ΔP. The pressure difference can be used to calculate gas phase velocity through Eq. B1 below.

$$v = \left(\frac{\Delta P}{\frac{1}{2}\rho C^2} \right)^{\frac{1}{2}} \qquad Eq.\ B1$$

In the above Eq. B1, ρ is the density of the gas, C is a proportional constant, and v is the velocity of the gas in m/s. Often, the probes will be calibrated with some constant, C, relative to a piezo tube [49]. This constant is dependent on the probe construction and Reynolds number and is often within 5% of 1.05 for the expected crib fire buoyant flows. The calibration with a piezo tube is intended to provide a cleaner calibration of the pressure transducer which would in turn provide better results. However, the probes used through this study are calibrated directly with their differential pressure transducers and therefore do not require a constant.

All pressure transducers are calibrated with a paired bidirectional probe in a conditioned wind tunnel over a velocity range of 0 to 4.25 m/s. A hot-wire anemometer with an accuracy of ± 0.01 m/s is used to define the reference flows. 18 data points over a 60-s calibration average are used while at room temperature, 21 ºC. Eq. B1 above is used to calculate the differential pressure from the hot wire velocity output. From there, the slope of the voltage versus differential pressure can be calculated. The voltage to differential pressure slope is used as it is a straight line and can be used at different temperatures and gas densities. Because of the trends in the differential pressure transducer and probes, two separate calibrations are made for under and over 1 pa, presented below in Fig. B2.

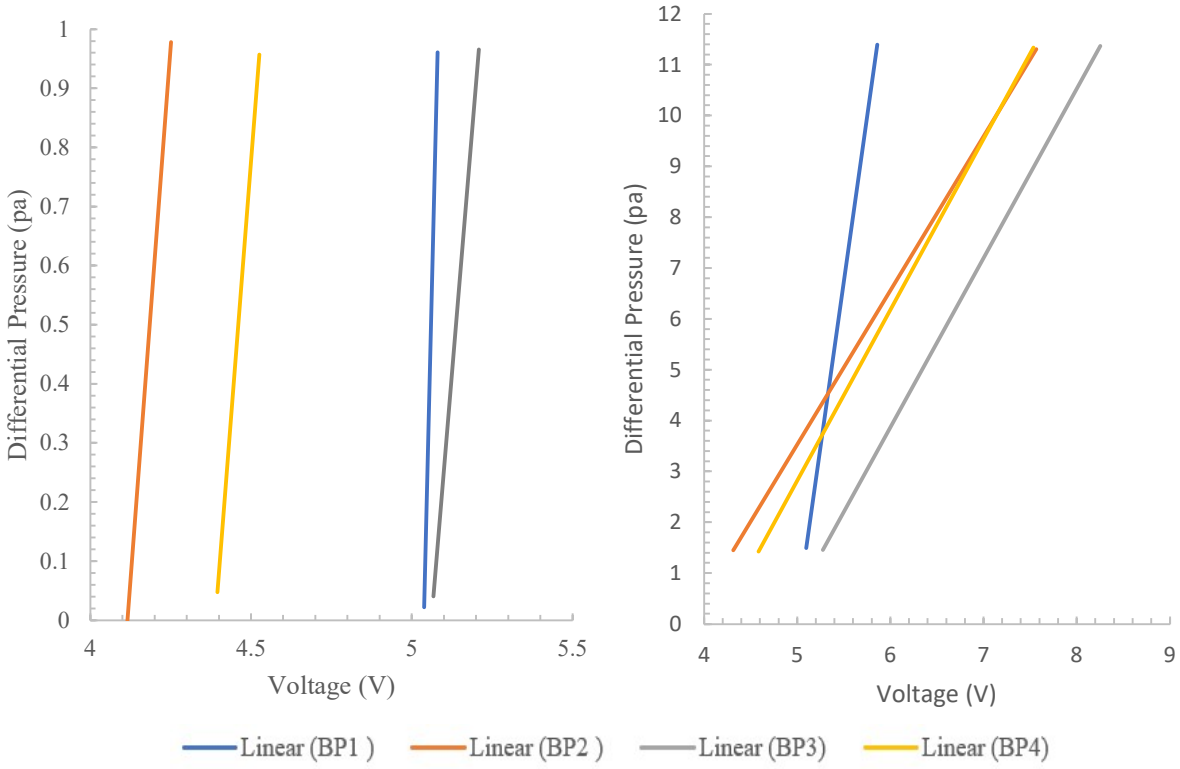

Figure B2: Bidirectional probe and pressure transducer calibrations for under 1 Pa, left, and over 1 Pa, right for the 4 sensors used through testing.

The tabulated slopes for the probe-transducer combinations are below in Table B1.

Table B1: Bidirectional probe and pressure transducer calibrations slopes in Pa/volt.

	V 1	V 2	V 3	V 4
0 to 1 Pa	22.00	7.24	6.56	6.99
1 to 11 Pa	13.01	3.03	3.33	3.36

Additionally, bi-directional probes have good angular sensitivity compared to piezo tubes and can accurately record data when not completely aligned with the flow direction. This sensitivity is within 10 percent of the mean velocity when within 50 degrees of offset with the probe, shown below in Fig. B3 [48].

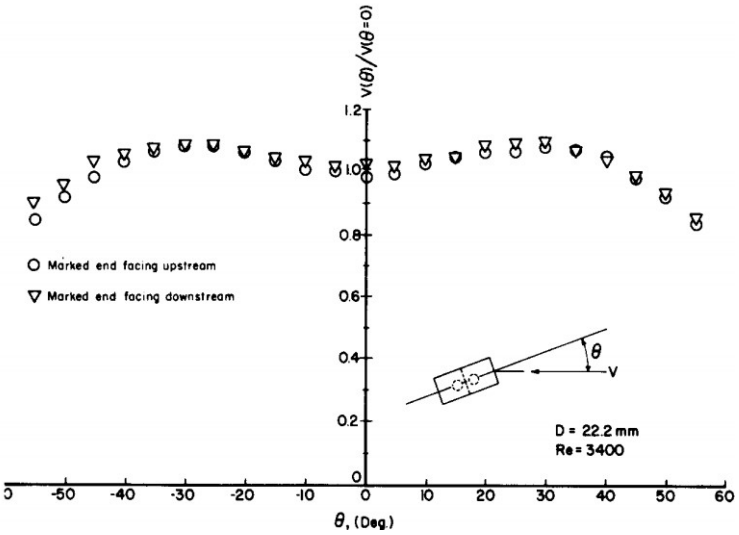

FIGURE B3: Example probe angular sensitivity under constant flow for variable offset angles [4]

An angular sensitivity study is conducted on the bidirectional probes used for experimentation, shown below in Fig. B4. The angular study demonstrates that changing flow direction will only have minor impacts on the measured velocity up to a 40-degree offset from the parallel flow.

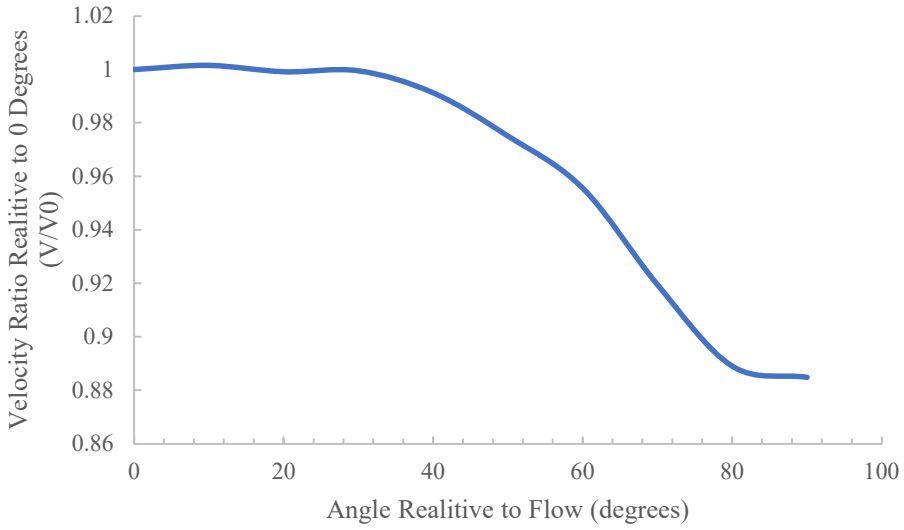

FIGURE B4: Angular sensitivity of bidirectional probe and pressure transducer V 2 at 1.3 m/s

The flow was provided by a conditioned wind tunnel at 1.3 m/s in an ambient temperature at 21 ^{o}C. The results of the test indicate that the chosen bidirectional probes and transducers share similar levels of angular sensitivity as the literature. As such, any angular distortion of the bi-direction probes or variation in flow direction during testing are ignored, and the direction of flow around the probes is always assumed to be parallel to the bi-directional probe openings.

At the start of every day, the differential pressure transducers are zeroed, and a zero-shift voltage is calculated to account for any voltage drift since calibration. After each testing day, the bidirectional probe orifices are cleaned with compressed air to remove any soot buildup. Periodically throughout testing, the tubes connecting the probes and transducers are also cleared with compressed gas to dislodge any particulates.

Since it is necessary to know the density of the gas when calculating the velocity, thermocouples are used in parallel to sample the temperature and calculate the air density. It is assumed that the gases interacting with the probes have the same density properties of air at 1 atm. Eq. B2, below, is used to calculate the density of air derived from publicly available data [5].

$$\rho = \frac{101325}{287.058*(273+\ )} \qquad \textit{Eq. B2}$$

B.2 Thermocouples

In general, the thermocouples chosen provided accurate temperatures for analysis. However, thermocouples lose heat due to radiation at high temperatures and the thermal inertia of the thermocouple must be accounted to obtain accurate measurements. Eq. B3, below, provides a method to correct for these trends [51–53].

$$T_{gas} = T_{TC} + \tau \frac{dT_{TC}}{dt} + \varepsilon_{TC}\, \sigma({T^4}_{TC} - {T^4}_{W}) \frac{d}{k*Nu} \qquad \textit{Eq. B3}$$

In the above Eq., TC is the subscript for thermocouple and gas is the subscript for the measured gas. Ambient temperature in the lab is assumed to be constant at 21 °C. The second term, $\tau \frac{dT_{TC}}{dt}$, represents the thermal inertia correction of the thermocouple in relation to the forced convection flow of gasses and thermocouple properties. The third term represents the emissivity correction for the radiation energy lost by the thermocouple. To calculate the temperature correction, both the original thermocouple temperature and velocity need to be known.

The characteristic response time for a thermocouple, τ, can be calculated through the below Eq. [51–53].

$$\tau = \frac{p_{tc} c_p d^2}{6Nuk} \qquad \textit{Eq. B4}$$

p_{tc} is the density of the thermocouple junction and is assumed to be 0.49665 kg/K for K type thermocouples. c_p is the isobaric specific heat constant, calculated through an empirical correlation from publicly available date, below in Fig. B5. d is the diameter of the thermocouple junction. Nu is the Nusselt number and k is the thermal conductivity of air.

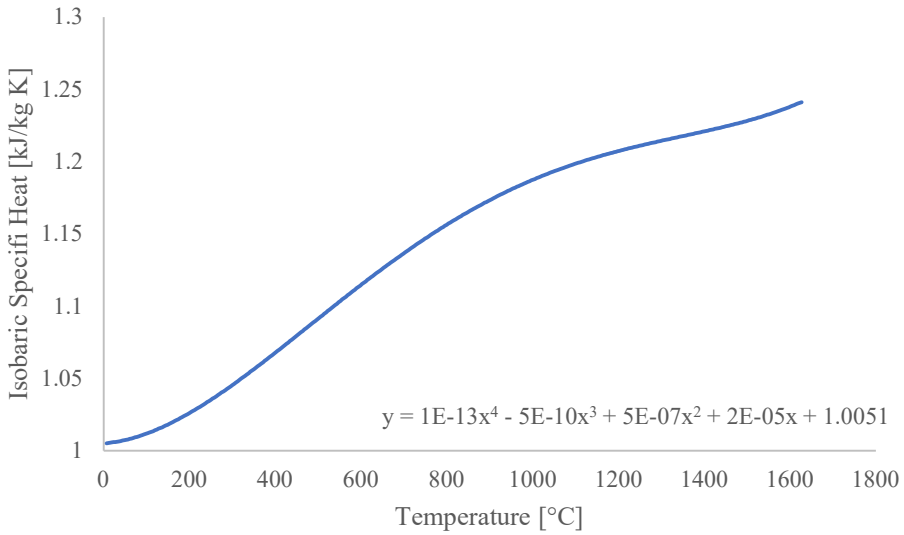

FIGURE B5: Isobaric specific heat constant, Cp, for air from publicly available data [5]

The Nusselt number, Nu , is needed for both the second and third terms in the thermocouple correction. Nu for low flow spherical geometries can be calculated through the below Eq. B5[54].

$$Nu = 2 + \left(.4Re^{\frac{1}{2}} + .06Re^{\frac{2}{3}}\right) * Pr^{.4} * \left(\frac{\mu_\infty}{\mu_s}\right)^{1/4} \qquad Eq.\ B5$$

The prandial number, Pr, was assumed to be 0.7, and can be calculated through the below equation.

$$Pr = \frac{\mu cp}{k} \qquad Eq.\ B6$$

Several data points are chosen to confirm the assumption that *Pr* is equal to 0.7 across a multitude of values, and all calculations fall within a range of 0.01. The Reynolds number, *Re*, can be calculated below.

$$\mathrm{Re} = \frac{v\,\mathrm{d}}{u} \qquad Eq.\ B7$$

When calculating the Reynolds number, v is the gas velocity and d is the diameter of the thermocouple bead. The dynamic viscosity, u, can be calculated below through an empirical correlation derived from publicly available data shown below in Fig. B6.

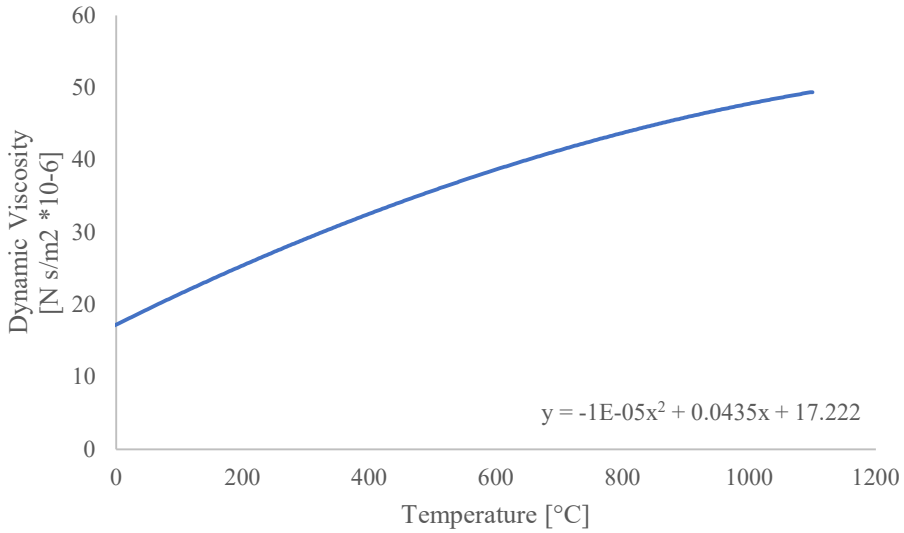

FIGURE B6: Dynamic viscosity of air at different temperatures from publicly available data [5]

The term $(\frac{\mu_\infty}{\mu_s})^{1/4}$ in the Nusselt number correlation represents the ratio of gas viscosities at the ambient temperature conditions versus thermocouple bead conditions. Under most circumstances, the entire term is assumed to be one. In the third term of the thermocouple correction, the thermal conductivity of the thermocouple, k_{tc}, is dependent on the temperature and can be found with units of W/mk with the below empirical equation from publicly available data [5].

$$k_{tc} = \frac{(-0.00002*T\text{^}2 + 0.073*T + 24.1)}{1000} \qquad Eq.\ B8$$

The heat transfer coefficient, h, can then be calculated below in units of W/m^2k.

$$h = k_{tc} * Nu/d \qquad Eq.\ B9$$

Values for ε_{TC} and σ are assumed to be 0.25 and the Stefan–Boltzmann constant of $5.670\times10{-}8$ $W\cdot m^{-2}\cdot K^{-4}$, respectively.

The temperature correction is not necessary for relatively low temperatures, as visible through the exemplary test data presented below in Fig. B7. However, at the 800 ºC peak, there is a 13.5% increase in absolute temperature needed to accurately represent the true temperature.

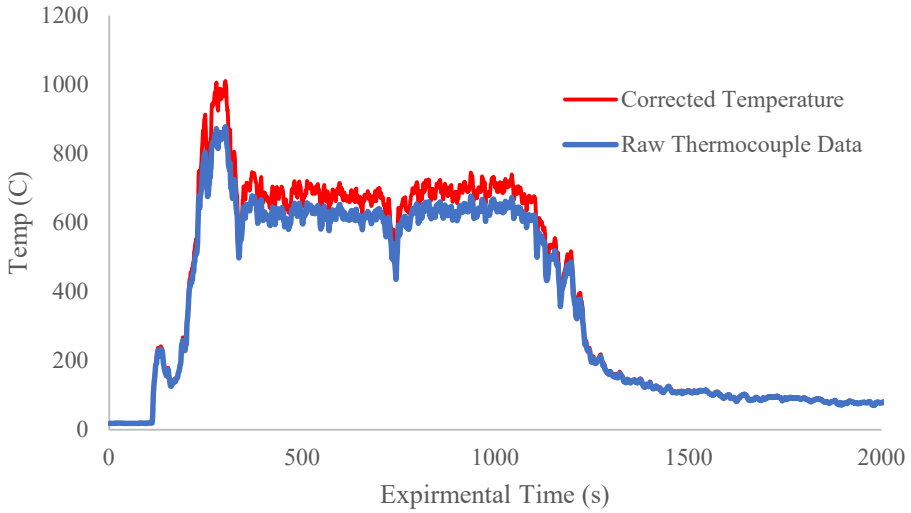

FIGURE B7: Example temperature corrected, red, and thermocouple output temperature, blue, data for a free-burning UL 2127 scale crib sampled one ft above the center of the crib

Where velocity profiles are unavailable to calculate the temperature shift, it is assumed that the temperature correction is equal to the same percent increase between the thermocouple reading and the adjusted temperature of the nearest thermocouple.

B.3 Gas Sensors

It is necessary to synchronize each individual gas sampler with the other instrumentation and experimental timeline, commonly called the delay time, t_d. This delay time accounts for both the transport time to the analyzer including the time it takes for the sample to go through conditioning such as cooling, drying, and filtering, t_t, and the response time of the sensor itself, t_R, as shown below in Eq. B10 [55].

$$t_D = t_t + t_R \qquad \textit{Eq. B10}$$

Three different methods are used to calculate the delay time, and an average of all the methods was taken to be the actual delay time. A method using the period between a 10%, t_{10}, and 90%, t_{90}, or t_{10}-t_{90} of a normalized step signal change has been shown to provide a good approximation of the delay time [55]. This method utilized pure nitrogen flowing through each running sensor to create a step-change from 0% oxygen to ambient conditions, as shown below in Fig. B8.

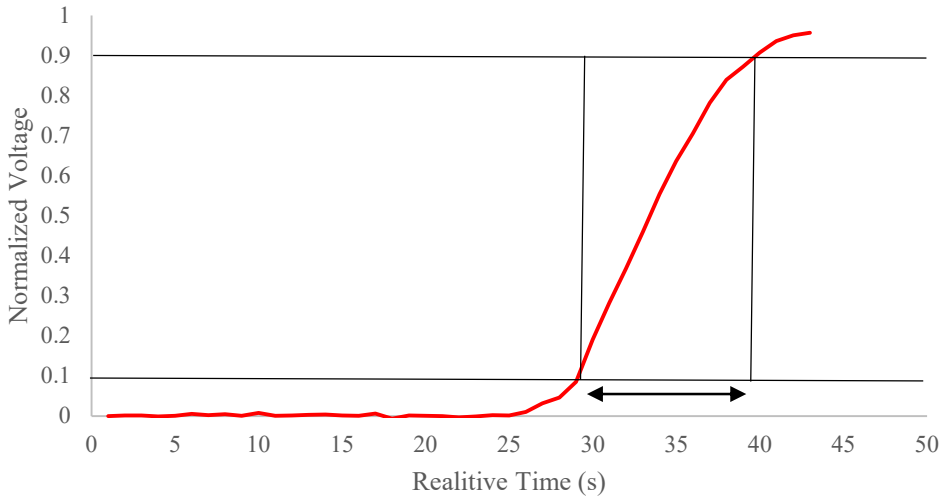

Figure B8: t_{10}-t_{90} delay time calculation method for sensor K2.

In the above Fig. B8, the black lines represent 10% and 90% of the signal change, respectively. Each test is repeated three times to yield an average for this method.

The second method utilizes the time from an input change to 50% of signal response, t_{50} [47]. This method accounts for the transport time and assumes the response time is best approximated as the time to 50% step change, as shown below in Fig. B9.

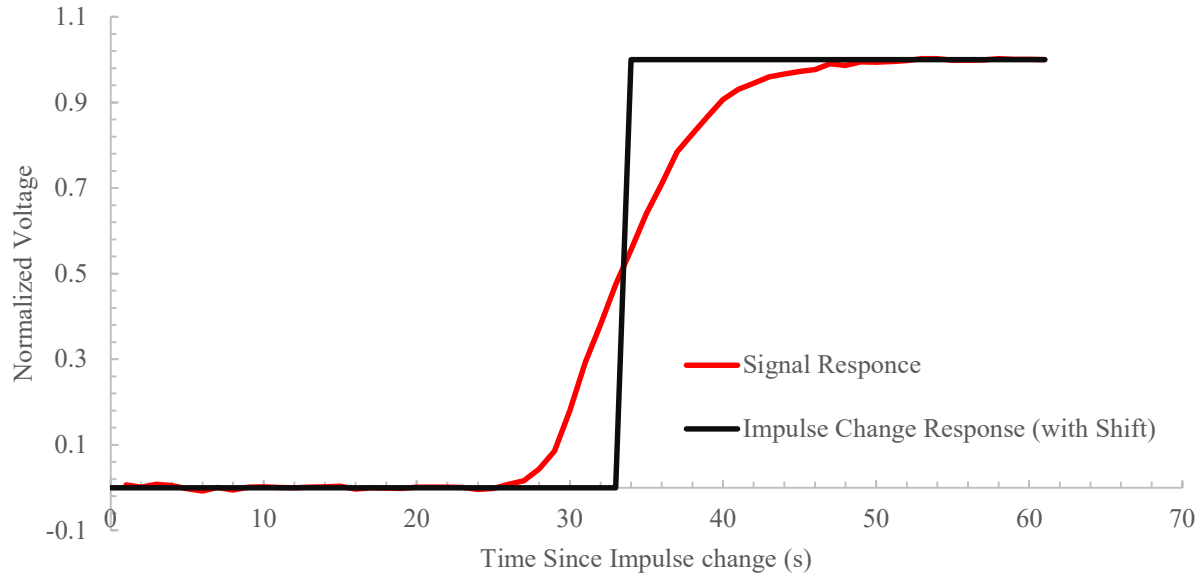

FIGURE B9: Servo-Mex® signal response, red, to an input step change, black, shifted by the calculated delay time to T_{50}

In the above Fig. B9, the red line is the signal, and the black line is the time event adjusted profile represented by removing the source of pure nitrogen from the sampling port. The time adjustment, t_{50}, is equal to the delay time through this method. At least two trials are conducted for each sensor and averaged.

The third method utilized the first derivative of the signal during the suppression testing for each oxygen sensor to identify the experimental time at which the sensor responded to a discharge event. The delay time is calculated as the time difference between the known and recorded start and end of discharge. The first zero and nonzero values of the smoothed signal derivative are used to calculate the time to respond to the end of suppression and the onset of the suppression event, respectively. The experimental time these events should have occurred at, 360 s for the start of discharge or 360 s plus the discharge time, is then subtracted to measure the sensor response to testing conditions, as shown in the example below, Fig. B10.

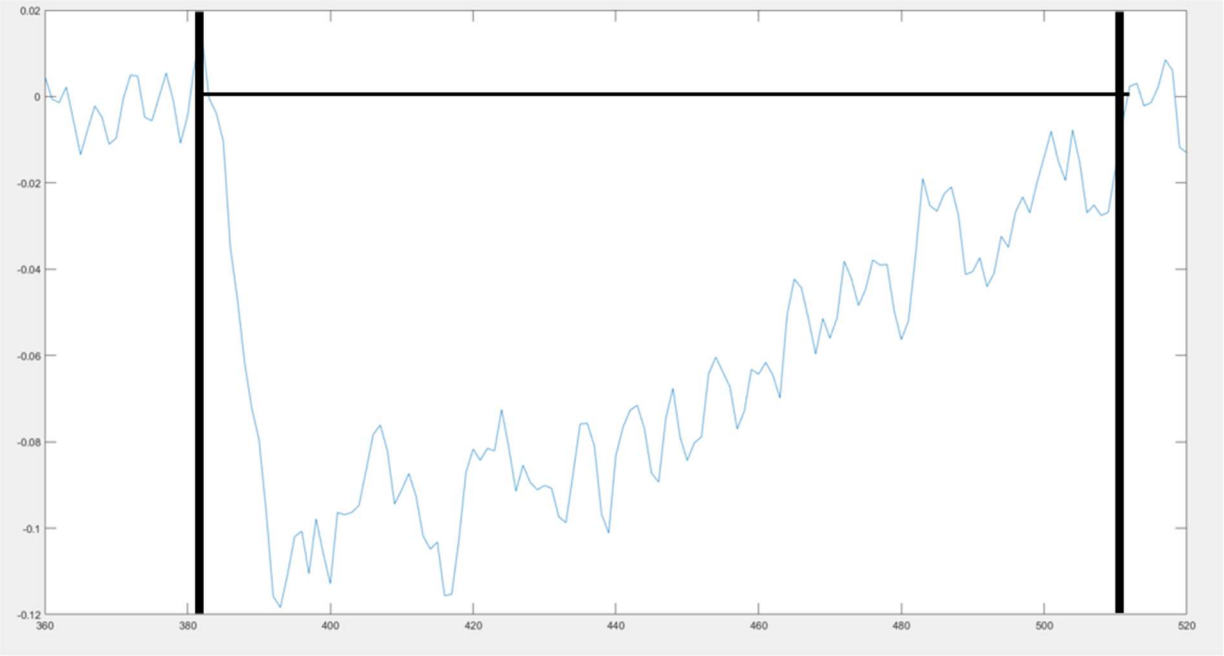

Figure B10: The first derivative of the smoothed Servo-Mex® signal for test 7. Each black line represents the times for onset, left, and end, right, of the 120-s suppression event

The response of each sensor for all the 7 large-scale tests is averaged to yield an average signal response time for each sensor, rounded to the nearest second for both the start and end of the suppression event.

Tabulated average delay times for each of the four methods are presented below in Table B2. Delay times are calculated through the average of the 4 values from the three methods.

Table B2: Average response times for gas sensors, s.

Sensor	T_{10}-T_{90}	T_{50}	The first derivative, onset of suppression	The first derivative, end of suppression	Average value ± uncertainty
K1	15	17	7	21	15 ± 1
K2	15	15	7	22	15 ± 1
K3	13	15	11	24	16 ± 1
O2	11	33	23	36	29 ± 2

Annex C: Identification of the Crib Member Least Likely to Extinguish

There are 12 stick members that comprise of the reduced -scale crib and 24 in the full-scale. Each of these stick members is subject to similar ignition, burn period, and suppression events but at different location in the crib.

Figure C1: Picture of full-scale crib ignition from alcohol pan.

At the point right before crib suppression, there will be a single stick member that is most resilient to the suppression event and therefor at the most risk to not extinguish, potentially causing a failure of the UL 2127 requirements. The intent in identifying the stick member most at risk is to better understand how the ignition, burn, and suppression events interact with the crib, where the member at most risk to failure is located, and identify the point in the crib most resistant to a suppression event. This methodology is built upon the understanding that the thinnest member will have undergone the most combustion and therefor have the deepest set fire and be the hardest to extinguish.

Full-scale stick members were measured in the center of the member, the typical thinnest part of the stick member, by a digital caliper to 4 significant figures. Each of the six stick member thicknesses per crib level were averaged with a counterpart on the other side of the crib and then ranked in order from thickest to thinnest such that each level had an average dimension for ranking and diameter for each horizontal location. The horizontal locations included the two members on the outside, middle, and center of the crib, shown below in Fig. C2.

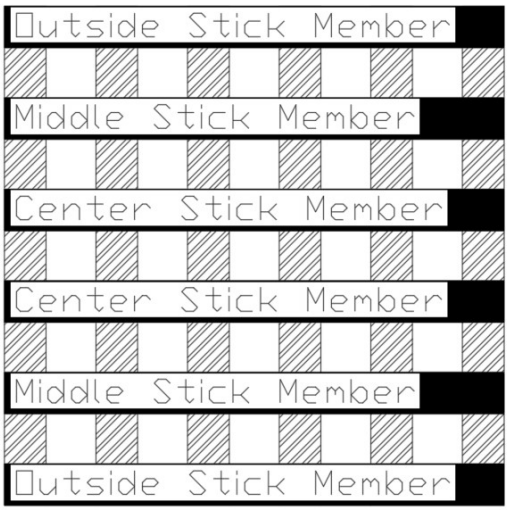

FIGURE C2: Stick member location names for a full-scale crib.

The thicknesses of each layer were then averaged and ranked in comparison to the 3 other layers of the crib. The rankings and diameters for both the levels and horizontal locations were averaged for all 7 full-scale cribs, regardless of discharge timeline.

The above method was intended to be replicated on the reduced-scale experiments as well, however the degradation of the crib during testing prevented accurate measurements to be taken. Observation of cracked members and crib disintegration patterns during removal from the testing stand were instead used to identify the member at most risk.

90 stick member post test diameters from the 7 full-scale experiments were recorded and charted against their relative probability as shown below in Fig. C3.

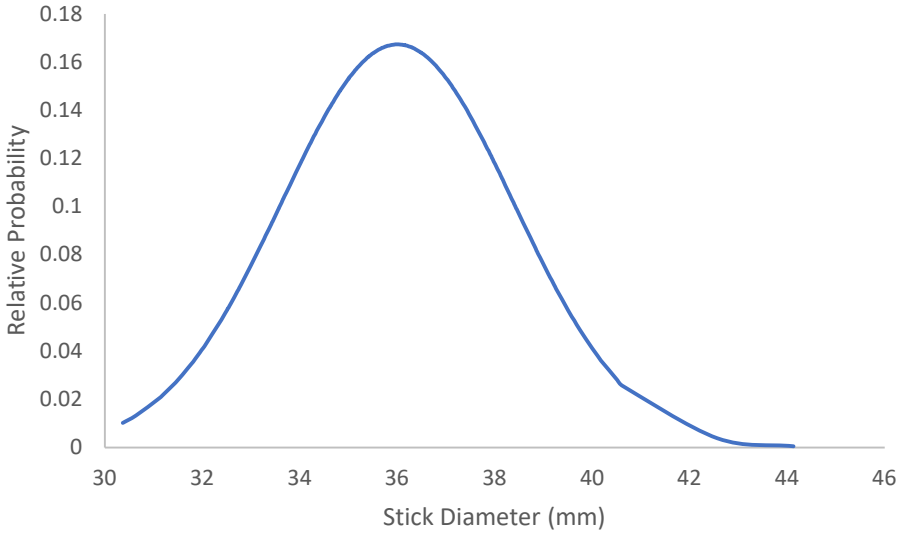

FIGURE C3: Full-scale stick member diameters normal distribution.

The center stick members on average burned more than outside members. The average diameter for the two members on the outside, middle, and center of the crib were 36.02 mm, 36.11 mm, and 35.88 mm respectively. The average stick member diameters from the top to bottom layers were 37.44 mm, 36.42 mm, 35.61 mm, and 34.50 mm respectively. When ranked against other members within the same crib, the top layer of stick members had an 87% probability of being the thickest layer. The thinnest members were constantly from the bottom layer, 91.5% of the time. For each layer regardless of height, the center members were consistently thinner than the middle members, which were consistently thinner than the outside members.

The initial variations in stick member thickness were not originally accounted for as it was assumed that all members were generally cut perfectly square at 1.5 inches or 3.8 cm. Slight variations in the initial stick member thickness and swelling during the test due to char layer accumulation likely contributed to the excess stick member diameter. While small variations

during the process of preparing the stick members likely existed, these variations would have been distributed evenly through the sampled cribs as each member was pulled randomly from a common stock when building the cribs.

As indicated above, the bottom center stick members are consistanly the thinnest. These center members additionally burned on average 12% more diameter than their exterior counterparts when assumed to start at exactly 38 mm, which supports the assumption that more combustion occurred in the center of the crib than the exterior. Additionally, the bottom layer stick member diameters were reduced 250% more than those on the top layer of the crib. This trend is likely a result of closer proximity to the lit alcohol pan during preburn.

Interestingly, the second and third layers of stick members for the 60-s discharge burned on average 36% more diameter compared to the 120 s discharges. This difference was not significant for the top layer, 4.6 %. However, the diameter of the bottom layer of stick members was reduced by more than a full centimeter, or 32.9% more in the 120-s discharge case compared to the 60-s discharge. The original hypothesis that the larger airflow over time transferred more oxygen into the crib and thus further assisted the combustion during the 60-s discharge is no longer congruent with the above trends, and more tests should be done to identify the cause of the discrepancy. Potential variables to better control include starting stick member diameter, moisture content, and wood source. While every effort was made to control these variables on the crib level, small variation may have caused additional errors on the stick member level.